Reexamining right-handed neutrino EFTs up to dimension six

Manimala Mitra,[1,2,*] Sanjoy Mandal,[3,†] Rojalin Padhan,[1,2,4,‡] Agnivo Sarkar,[1,2,§] and Michael Spannowsky[5,‖]

[1]*Institute of Physics, Sachivalaya Marg, Bhubaneswar 751005, India*
[2]*Homi Bhabha National Institute, BARC Training School Complex, Anushakti Nagar, Mumbai 400094, India*
[3]*Korea Institute for Advanced Study, Seoul 02455, Korea*
[4]*Pittsburgh Particle Physics, Astrophysics, and Cosmology Center, Department of Physics and Astronomy, University of Pittsburgh, Pittsburgh 15260, USA*
[5]*Institute for Particle Physics Phenomenology, Department of Physics, Durham University South Road, Durham DH1 3LE, United Kingdom*

(Received 21 November 2022; accepted 2 December 2022; published 29 December 2022)

The gauge singlet right-handed neutrinos (RHNs) are essential fields in several neutrino mass models that explain the observed eV scale neutrino mass. We assume RHN field to be present in the vicinity of the electroweak scale and all the other possible beyond the Standard Model fields arise at high energy scale $\geq\Lambda$. In this scenario, the beyond the Standard Model physics can be described using effective field theory (EFT) where the set of canonical degrees of freedoms consists of both RHN and SM fields. EFT of this kind is usually dubbed as N_R-EFT. We systematically construct relevant operators that can arise at dimension five and six while respecting underlying symmetry. To quantify the phenomenological implication of these EFT operators we calculate different couplings that involve RHN fields. We discuss the constraints on these EFT operators coming from different energy and precision frontier experiments. For pp, e^-p and e^+e^- colliders, we identify various channels which crucially depends on these operators. We analytically evaluate the decay widths of RHN considering all relevant operators and highlight the differences that arise because of the EFT framework. Based upon the signal cross section we propose different multilepton channels to search for the RHN at 14 TeV LHC as well as future particle colliders.

DOI: 10.1103/PhysRevD.106.113008

I. INTRODUCTION

The tremendous achievement of the Standard Model (SM) is that it can make precise numerical predictions about the particle dynamics up to the TeV scale. The Higgs boson's discovery [1,2] at the Large Hadron Collider (LHC) as well as precision frontier experiments favor the theoretical claims of this model with significant precision. Despite these experimental success, there are many compelling reasons correspond to nonzero neutrino mass, dark matter or the natural explanation behind the electroweak symmetry breaking (EWSB) etc. motivate us to construct beyond Standard Model (BSM) theories that can satisfactorily answer these questions. These BSM theories typically contain new degrees of freedom (d.o.f) that interact with the SM particles. Different experimental collaborations have extensively looked for these BSM particles decaying into various SM final states. The results obtained from these searches so far fail to provide any conclusive evidence in support of their existence or their corresponding properties. One of the plausible explanations behind these null results is that these BSM states are situated at a very large energy scale Λ and the center of mass energy of the present day colliders is not sufficient enough to produce them on shell. However the indirect effects of these particles can be detected while analyzing different low-energy observables [3]. In view of this, one can consider the effective field theory (EFT) [4,5] approach, which can serve as an efficient pathway to parametrize these indirect effects that can help us uncover the nature of BSM.

The construction of any EFT [6,7] typically requires two ingredients, the canonical d.o.f. that are present in low energy theory and the symmetries which manifestly dictate the interactions between these fundamental d.o.f. The Lagrangian corresponds to the EFT framework [8] is sum of both the $d = 4$ renormalizable part as well as

*manimala@iopb.res.in
†smandal@kias.re.kr
‡rojalin.p@iopb.res.in
§agnivo.sarkar@iopb.res.in
‖michael.spannowsky@durham.ac.uk

different higher dimensional operators that are allowed by the symmetry. We assume at the scale Λ, there exists a gauge theory that contains extra massive d.o.f. At this scale these fields get decoupled from the low-energy theory. The effects of these heavy states can be reinstated in forms of a tower of effective operators at each order of mass dimensions $n > 4$. These higher dimensional operators $\{\mathcal{O}_n\}$[1] are built upon canonical d.o.f of low energy theory while respecting space-time as well as the gauge and discrete symmetries. The decoupling theorem [9,10] guarantees that all measurable observables corresponding to the heavy scale physics are suppressed by inverse powers of cutoff scale Λ. As a corollary of the decoupling theorem one can establish the hierarchy between the operators that arise at each dimension. As a consequence, the measurable effects of the operators at dimension n in general dominant over the operators arise at dimension $n+1$. One can optimally use this framework to investigate the physics associated with neutrinos and establish their connection with the SM physics.

The absence of right-handed neutrinos (RHNs, N) in the SM field content, forbids us to generate neutrino mass similar to other SM fermions. However, the measurements from different neutrino oscillation experiments [11–15] strongly suggest nonzero masses for neutrinos thus encourages us to modify the existing SM. The simplest way to encounter this issue is to add RHNs to the SM particle contents and write down Yukawa interactions for neutrinos similar to other SM charged fermions. As these RHN fields are charge neutral and singlet under the SM gauge group $SU(3)_c \times SU(2)_L \times U(1)_Y$, one can include a Lepton-number-violating Majorana type mass term $M_N \bar{N}_R^c N_R$ in the Lagrangian in addition to the previously mentioned Yukawa interaction. The smallness of the neutrino mass can therefore be explained as the hierarchy between the electroweak scale v and the RHN mass scale M_N, which can be expressed as $M_\nu \sim \frac{y_\nu^2 v^2}{M_N}$. Here, y_ν stands for Yukawa coupling correspond to neutrinos. If we assume the value of y_ν to be $\mathcal{O}(1)$, one can see that the requirement for tiny neutrino mass set the value of M_N in the vicinity of grand unification regime (roughly around 10^{14}–10^{15} GeV). This simplistic setup for neutrino mass is in general known as a type-I seesaw mechanism [16–19]. The interaction strength between these heavy neutrinos and the SM particles is controlled by the active sterile mixing parameter θ, which is defined as $\theta \propto \frac{y_\nu v}{M_N}$. The above relation implies a small value of θ and leads to a small production cross section for the RHNs at different collider experiments.

The major disadvantage of the type-I setup is that the physics associated with the RHN fields become relevant at around the grand unified theory (GUT) scale, which the current experimental facilities fail to probe. One can alter this situation while assuming that at least one of these RHN fields is within the regime of the electroweak scale [20–22] while satisfying the existing experimental constraints. In this context one can describe the dynamics involving RHN using EFT. The EFT of this kind is denoted as N_R-EFT.

There are many works which encompass different aspects of N_R-EFT. References [23–26] and [27] present the nonredundant operator basis up to dimension seven and dimension nine of N_R-EFT, respectively. References [28–31] discuss the collider phenomenology of the dimension five N_R-EFT at future Higgs factories as well as LHC. Other studies [23,32–35] also looked into various subset of these higher dimensional operators and presented their phenomenological implication at LHC. If the total decay width of the light RHN is small, then it can give rise to interesting displaced decay signatures and detailed study regarding this can be found in Refs. [36–39]. References [40–42] focused on the interesting production modes that are invoked by the different four Fermi operators that one construct at dimension six. The study assume relevant decay modes for the N field to be $N \to \nu\gamma$ and $N \to 3f$ (where f is SM fermions). Reference [43] discusses the theoretical aspects of the dimension six operators that involve the Higgs doublet and discuss their sensitivity under various Higgs mediated processes. In addition to that, Refs. [44,45] study the sensitivity of different dimension six operators at LHC and lepton colliders.

In this work we present the complete phenomenological description of the N_R-EFT up to dimension six. In Sec. II we begin with the general setup and systemically construct different dimension five (see Sec. II A) as well as dimension six (see Sec. II B) operators along with highlighting their physics aspects. In Sec. III, we evaluate the constraints on different operators coming from precision frontier as well as direct search experiments. In Sec. IV, we calculate the cross section for RHN production at pp, e^-p, and e^+e^- colliders. Depending on the RHN mass, the N field can decay either to two body or to three body decay modes, respectively. In Sec. V, we present the detailed analytic calculations correspond to each of these decay modes and evaluate the branching ratios (BRs) for different benchmark scenarios. We also present expected number of signal events with multilepton final state for above mentioned colliders in Sec. VI. We summarize our findings along with few concluding remarks in Sec. VII.

II. GENERAL SETUP

We begin with a phenomenological Lagrangian that can be expressed as

$$\mathcal{L} \equiv \mathcal{L}_{\rm SM} + \bar{N}_R \not{\partial} N_R - \bar{L}_\ell Y_\nu \tilde{H} N_R - \frac{1}{2}\tilde{M}_N \bar{N}_R^C N_R + \sum_{n>4} \frac{\mathcal{O}_n}{\Lambda^{n-4}} + \text{H.c.}, \tag{2.1}$$

[1]The n stands for the mass dimension of these operators.

where $\tilde{H} = i\sigma^2 H^*$, $N_R^C = C\bar{N}_R^T$ with charge conjugation matrix $C = i\gamma^2\gamma^0$. The term $\tilde{M}_N$ stands for the Majorana bare mass term, which is a $\mathcal{N}\times\mathcal{N}$ matrix in the flavor space. L_ℓ is the SM lepton doublet and Y_ν is the Dirac-type Yukawa coupling. The terms $\bar{L}_\ell Y_\nu \tilde{H} N_R$ and $\frac{1}{2}\tilde{M}_N \bar{N}_R^C N_R$ contribute to the neutrino mass matrix. The $\mathcal{O}_n$ are the higher dimensional operators, which one can build at each dimension. The effect of these operators are suppressed by the cutoff scale Λ with appropriate power.

A. N_R-EFT operators at dimension five

With this general setup in mind, one can write down three possible N_R-EFT operators at dimension five. In Table I, we present the explicit form of these operators where $\alpha_i^{(5)}$ ($i = 1$ to 3) represent the Wilson coefficients corresponding to each of these operators. Considering the space time transformation rules, one can realize that the $\alpha_1^{(5)}$ and $\alpha_2^{(5)}$ are symmetric matrices in flavor space. In contrast to that, $\alpha_3^{(5)}$ is an antisymmetric matrix that arises if we only consider more than one N_R fields. The $\mathcal{O}_1^{(5)}$, which is famously known as the Weinberg operator [46], primarily contributes to active neutrino masses. This is the only operator one can construct in this dimension solely using SM fields. The renormalizable realization of this operator can be found in Refs. [47–49] and its phenomenological implications have been studied in Refs. [50,51]. On the other hand, operator $\mathcal{O}_2^{(5)}$ provides additional contributions to the Majorana mass term that is mentioned in Eq. (2.2). The operator $\mathcal{O}_3^{(5)}$ does not play any role in the neutrino mass matrix, but the presence of $B_{\mu\nu}$ in that term brings out nontrivial vertices between neutrinos and SM neutral vector boson fields. Assuming the full theory is a gauge theory one may predict that out of these three operators, $\mathcal{O}_1^{(5)}$ and $\mathcal{O}_2^{(5)}$ may be generated in tree level but the $\mathcal{O}_3^{(5)}$ would only appear via loop mediated processes. As a consequence, one can estimate a further $\frac{1}{16\pi^2}$ suppression to the $\alpha_3^{(5)}$ coefficient [52]. For a detailed discussion on this aspect the interested reader may follow Ref. [53].

TABLE I. All possible N_R-EFT operators that appear at dimension five. The $\sigma^{\mu\nu}$ is defined as $\sigma^{\mu\nu} = \frac{i}{2}[\gamma^\mu, \gamma^\nu]$, and $B_{\mu\nu}$ is the field strength tensor corresponding to the $U(1)_Y$ gauge group. Λ is the cutoff scale of underlying N_R-EFT.

$\mathcal{O}_1^{(5)}$	$\frac{\alpha_1^{(5)}}{\Lambda}(\bar{L}^c\tilde{H}^\dagger\tilde{H}L)$
$\mathcal{O}_2^{(5)}$	$\frac{\alpha_2^{(5)}}{\Lambda}(\overline{N_R}^c N_R)(H^\dagger H)$
$\mathcal{O}_3^{(5)}$	$\frac{\alpha_3^{(5)}}{\Lambda}(\overline{N_R}^c\sigma_{\mu\nu}N_R)B_{\mu\nu}$

1. Neutrino mass in dimension five

We will now define the neutrino mass matrix while considering all the relevant terms up to dimension five. In the basis $\{\nu_L, N_R^c\}$, the neutrino mass matrix will take the following form:

$$\mathcal{M}_{\nu N}^{(5)} = \begin{bmatrix} \frac{\alpha_1^{(5)}v^2}{\Lambda} & \frac{Y_\nu v}{\sqrt{2}} \\ \frac{Y_\nu^T v}{\sqrt{2}} & \left(\tilde{M}_N + \frac{\alpha_2^{(5)}v^2}{\Lambda}\right) \end{bmatrix}. \tag{2.2}$$

In the seesaw approximation (when $\nu - N$ blocks are smaller than the ones in the $N - N$ one), this leads to the following light and heavy neutrino mass matrix:

$$m_{\text{light}}^{(5)} \approx \frac{\alpha_1^{(5)}v^2}{\Lambda} - \frac{Y_\nu^T M_N^{-1} v^2 Y_\nu}{2}, \tag{2.3}$$

$$m_{\text{heavy}}^{(5)} \approx M_N = \tilde{M}_N + \frac{\alpha_2^{(5)}v^2}{\Lambda}. \tag{2.4}$$

The mass matrix in Eq. (2.2) can be diagonalized by a unitary matrix as

$$V^T \mathcal{M}_{\nu N}^{(5)} V = (\mathcal{M}_{\nu N}^{(5)})^{\text{diag}}. \tag{2.5}$$

Following the standard procedure of two step diagonalization V can be expressed as

$$V = \mathcal{U}W \quad \text{with} \quad \mathcal{U}^T \mathcal{M}_{\nu N}^{(5)} \mathcal{U} = \begin{pmatrix} m_{\text{light}}^{(5)} & 0 \\ 0 & m_{\text{heavy}}^{(5)} \end{pmatrix}. \tag{2.6}$$

Hence, $\mathcal{U}$ is the matrix that brings the neutrino mass matrix in the block diagonalized form, and further $W = \text{Diag}(U_{\text{PMNS}}, \kappa)$ diagonalizes the mass matrices in the light and heavy sector. One can approximately write the matrix V as follows:

$$\begin{aligned} V = \mathcal{U}W &\approx \begin{pmatrix} 1+\mathcal{O}(M_N^{-2}) & \theta \\ -\theta^T & 1+\mathcal{O}(M_N^{-2}) \end{pmatrix} \begin{pmatrix} U_{\text{PMNS}} & 0 \\ 0 & \kappa \end{pmatrix} \\ &\approx \begin{pmatrix} U_{\text{PMNS}} & \theta \\ -\theta^T & \kappa \end{pmatrix}, \end{aligned} \tag{2.7}$$

where $\theta = M_N^{-1}\frac{Y_\nu v}{\sqrt{2}}$ is the mixing angle between the active and sterile neutrinos, U_{PMNS} is the Pontecorvo-Maki-Nakagawa-Sakata (PMNS) matrix and κ is $\mathcal{O}(1)$ (for details see Ref. [54]). Following is the mixing relations between the gauge and mass eigenstates:

$$\begin{aligned} \nu_L &\simeq U_{\text{PMNS}}\nu_{L,m} + \theta N_{R,m}^c, \\ N_R^c &\simeq -\theta^T \nu_{L,m} + \kappa N_{R,m}^c, \end{aligned} \tag{2.8}$$

where the subscript "m" signifies the mass eigenstate.

TABLE II. Coupling from the three-point vertices that arise after taking into account both the dimension four and dimension five terms of the Lagrangian. Here U signifies $U_{\rm PMNS}$ matrix. The abbreviation "RT" stands for renormalizable term, which includes charge current, neutral current, as well as Yukawa term. The chirality projection matrix is denoted by P_L and P_R. The momentum factor p_ν in different vertices arise from field strength tensor $B_{\mu\nu}$ after transforming it into momentum space.

Couplings	Explicit form	Operator
$\mathcal{C}^{W_\mu}_{\ell\nu}$	$\frac{g\gamma_\mu U}{\sqrt{2}} P_L + \text{H.c.}$	RT
$\mathcal{C}^{W_\mu}_{\ell N}$	$\frac{g\gamma_\mu \theta}{\sqrt{2}} P_L + \text{H.c.}$	RT
$\mathcal{C}^{h}_{\bar{\nu}\nu}$	$\frac{Y_\nu}{\sqrt{2}} U^\dagger \theta^\dagger P_R + \frac{\alpha_1^{(5)} v}{\Lambda} U^T U P_L + \frac{\alpha_2^{(5)} v}{\Lambda} \theta^* \theta^\dagger P_R + \text{h.c.}$	RT, $\mathcal{O}_1^{(5)}$, $\mathcal{O}_2^{(5)}$
$\mathcal{C}^{h}_{\bar{N}N}$	$-\frac{Y_\nu}{\sqrt{2}} \theta^\dagger \kappa^* P_R + \frac{\alpha_1^{(5)} v}{\Lambda} \theta^\dagger \theta P_L + \frac{\alpha_2^{(5)} v}{\Lambda} \kappa^\dagger \kappa^* P_R + \text{h.c.}$	RT, $\mathcal{O}_1^{(5)}$, $\mathcal{O}_2^{(5)}$
$\mathcal{C}^{h}_{\bar{\nu}N+\bar{N}\nu}$	$\{-\frac{Y_\nu}{\sqrt{2}} U^\dagger \kappa^* P_R + \frac{\alpha_1^{(5)} v}{\Lambda} U^\dagger \theta P_L - \frac{\alpha_2^{(5)} v}{\Lambda} \theta^* \kappa^* P_R\} + \{\frac{Y_\nu}{\sqrt{2}} \theta^\dagger \theta^\dagger P_R + \frac{\alpha_1^{(5)} v}{\Lambda} \theta^\dagger U P_L - \frac{\alpha_2^{(5)} v}{\Lambda} \kappa^\dagger \theta^\dagger P_R\} + \text{h.c.}$	RT, $\mathcal{O}_1^{(5)}$, $\mathcal{O}_2^{(5)}$
$\mathcal{C}^{Z_\mu}_{\bar{\nu}\nu}$	$\frac{g\gamma_\mu}{2c_w} U^\dagger U P_L - 2i \frac{\alpha_3^{(5)} s_w}{\Lambda} \theta^* \theta p_\nu \sigma_{\mu\nu} P_R + \text{h.c.}$	RT, $\mathcal{O}_3^{(5)}$
$\mathcal{C}^{Z_\mu}_{\bar{N}N}$	$\frac{g\gamma_\mu}{2c_w} \theta^\dagger \theta P_L - 2i \frac{\alpha_3^{(5)} s_w}{\Lambda} \kappa^\dagger \kappa^* p_\nu \sigma_{\mu\nu} P_R + \text{h.c.}$	RT, $\mathcal{O}_3^{(5)}$
$\mathcal{C}^{Z_\mu}_{\bar{\nu}N+\bar{N}\nu}$	$\{\frac{g\gamma_\mu}{2c_w} U^\dagger \theta P_L + 2i \frac{\alpha_3^{(5)} s_w}{\Lambda} \theta^* \kappa^* p_\nu \sigma_{\mu\nu} P_R\} + \{\frac{g\gamma_\mu}{2c_w} U \theta^\dagger P_L + 2i \frac{\alpha_3^{(5)} s_w}{\Lambda} \kappa^\dagger \theta^\dagger p_\nu \sigma_{\mu\nu} P_R\} + \text{H.c.}$	RT, $\mathcal{O}_3^{(5)}$
$\mathcal{C}^{A_\mu}_{\bar{\nu}\nu}$	$2i \frac{\alpha_3^{(5)} c_w}{\Lambda} \theta^* \theta^\dagger p_\nu \sigma_{\mu\nu} P_R + \text{H.c.}$	$\mathcal{O}_3^{(5)}$
$\mathcal{C}^{A_\mu}_{\bar{N}N}$	$2i \frac{\alpha_3^{(5)} c_w}{\Lambda} \kappa^\dagger \kappa^* p_\nu \sigma_{\mu\nu} P_R + \text{H.c.}$	$\mathcal{O}_3^{(5)}$
$\mathcal{C}^{A_\mu}_{\bar{\nu}N+\bar{N}\nu}$	$\{-2i \frac{\alpha_3^{(5)} c_w}{\Lambda} \theta^* \kappa^* p_\nu \sigma_{\mu\nu} P_R\} - \{2i \frac{\alpha_3^{(5)} c_w}{\Lambda} \kappa^\dagger \theta^\dagger p_\nu \sigma_{\mu\nu} P_R\} + \text{H.c.}$	$\mathcal{O}_3^{(5)}$

2. *Interesting facets of the dimension five operators*

In Eq. (2.8), we show the relation between flavor and mass eigenstates between light (active) and heavy (sterile) neutrinos. In the subsequent discussion, we denote the Majorana mass eigenstate of RHN fields as $N = N_{R,m} + N^c_{R,m}$, while we use similar notation for light neutrino mass basis, $\nu = \nu_{L,m} + \nu^c_{L,m}$. With these definitions we now present various three point vertices that involve neutrino fields which are coming from renormalizable Lagrangian and dimension five operators. The details of the calculations have been included in Appendix B. In Table II, we illustrate the explicit form of all these couplings. One can notice that the coupling between the W_μ boson and neutrinos does not get any additional contributions from the dimension five operators. However, the situation alters in the case of Higgs as well as neutral gauge boson operators:

(i) The tree-level vertices that involve Higgs field do get modified due to the presence of $\mathcal{O}_1^{(5)}$, $\mathcal{O}_2^{(5)}$ operators. In view of Eq. (2.4), one can see that the operator $\mathcal{O}_1^{(5)}$ regulates the SM neutrino masses. The smallness of these mass values forces us to choose a tiny magnitude for $\frac{\alpha_1^{(5)}}{\Lambda}$, which is below the order of $\mathcal{O}(10^{-11})$ GeV for Λ to be in the order TeV. This is why, the effects coming from this operator cannot be studied in the present day experimental setup. Due to this, for all our analysis we will set $\alpha_1^{(5)}$ to be zero.

(ii) In contrast to that, a similar conclusion cannot be made for the $\frac{\alpha_2^{(5)}}{\Lambda}$ coefficient. Hence, one should critically analyze its role on a case by case basis.

(iii) The operator $\mathcal{O}_3^{(5)}$ changes the couplings that involve both massless and massive vector boson fields. However as we have mentioned before, the structure of this operator contains two important aspects. First, the $\alpha_3^{(5)}$ is an antisymmetric matrix in the flavor space and can only exist if we consider more than one flavor of RHN fields within the EFT framework. In addition to that, from a full theory point of view the vertices coming from this operators cannot possibly be realized in tree level graphs. Hence, the effects come from this operator must be further suppressed by the loop factor $(\frac{1}{16\pi^2})$.

(iv) The compelling facet of the operator $\mathcal{O}_3^{(5)}$ is to invoke a nontrivial coupling between the photon field and neutrinos that are not present in the SM counterpart. The presence of a $B_{\mu\nu}$ tensor in the $\mathcal{O}_5^{(3)}$ operator introduces an interaction term between the RHN fields and hypercharge gauge boson B_μ. After the symmetry breaking the B_μ field can be written as the linear combination of Z boson and photon $(B_\mu = -s_w Z_\mu + c_w A_\mu)$. As a consequence of the

TABLE III. List of all possible operators that appear in dimension six construction. The four Fermi operators can arise in this order as oppose to dimension five N_R-EFT. In this paper we would refrain ourselves from discussing the phenomenology that arises from operators mentioned in the last two rows.

Relevant operators in dim-6			
	$\mathcal{O}_6$	Explicit Form	n_f
ψ^2H^3	$\mathcal{O}_{LNH} :=$	$\frac{\alpha_{LNH}}{\Lambda^2}(\bar{L}N_R)\tilde{H}(H^\dagger H)+\text{H.c.}$	$2n_f^2$
ψ^2H^2D	$\mathcal{O}_{HN} :=$	$\frac{\alpha_{HN}}{\Lambda^2}(\bar{N}_R\gamma^\mu N_R)(H^\dagger i\overleftrightarrow{D}_\mu H)$	n_f^2
	$\mathcal{O}_{HNe} :=$	$\frac{\alpha_{HNe}}{\Lambda^2}(\bar{N}_R\gamma^\mu e_R)(\tilde{H}^\dagger iD_\mu H)+\text{H.c.}$	$2n_f^2$
ψ^2H^2X	$\mathcal{O}_{LNB} :=$	$\frac{\alpha_{LNB}}{\Lambda^2}(\bar{L}\sigma_{\mu\nu}N_R)\tilde{H}B_{\mu\nu}+\text{H.c.}$	$2n_f^2$
	$\mathcal{O}_{LNW} :=$	$\frac{\alpha_{LNW}}{\Lambda^2}(\bar{L}\sigma_{\mu\nu}N_R)\tau^I\tilde{H}W^{I\mu\nu}+\text{H.c.}$	$2n_f^2$
$(\bar{L}R)(\bar{R}L)$	$\mathcal{O}_{QuNL} :=$	$\frac{\alpha_{QuNL}}{\Lambda^2}(\bar{Q}u_R)(\bar{N}_R L)+\text{H.c.}$	$2n_f^4$
$(\bar{R}R)(\bar{R}R)$	$\mathcal{O}_{NN} :=$	$\frac{\alpha_{NN}}{\Lambda^2}(\bar{N}_R\gamma^\mu N_R)(\bar{N}_R\gamma_\mu N_R)$	$\frac{n_f^2(n_f+1)^2}{4}$
	$\mathcal{O}_{eN} :=$	$\frac{\alpha_{eN}}{\Lambda^2}(\bar{e}_R\gamma^\mu e_R)(\bar{N}_R\gamma_\mu N_R)$	n_f^4
	$\mathcal{O}_{uN} :=$	$\frac{\alpha_{uN}}{\Lambda^2}(\bar{u}_R\gamma^\mu u_R)(\bar{N}_R\gamma_\mu N_R)$	n_f^4
	$\mathcal{O}_{dN} :=$	$\frac{\alpha_{dN}}{\Lambda^2}(\bar{d}_R\gamma^\mu d_R)(\bar{N}_R\gamma_\mu N_R)$	n_f^4
	$\mathcal{O}_{duNe} :=$	$\frac{\alpha_{duNe}}{\Lambda^2}(\bar{d}_R\gamma^\mu u_R)(\bar{N}_R\gamma_\mu e_R)+\text{H.c.}$	$2n_f^2$
$(\bar{L}L)(\bar{R}R)$	$\mathcal{O}_{LN} :=$	$\frac{\alpha_{LN}}{\Lambda^2}(\bar{L}\gamma^\mu L)(\bar{N}_R\gamma_\mu N_R)$	n_f^4
	$\mathcal{O}_{QN} :=$	$\frac{\alpha_{QN}}{\Lambda^2}(\bar{Q}\gamma^\mu Q)(\bar{N}_R\gamma N_R)$	n_f^4
$(\bar{L}R)(\bar{L}R)$	$\mathcal{O}_{LNLe} :=$	$\frac{\alpha_{LNLe}}{\Lambda^2}(\bar{L}N_R)\epsilon(\bar{L}e_R)\,\text{H.c.}$	$2n_f^4$
	$\mathcal{O}_{LNQd} :=$	$\frac{\alpha_{LNQd}}{\Lambda^2}(\bar{L}N_R)\epsilon(\bar{Q}d_R)+\text{H.c.}$	$2n_f^4$
	$\mathcal{O}_{LdQN} :=$	$\frac{\alpha_{LdQN}}{\Lambda^2}(\bar{L}d_R)\epsilon(\bar{Q}N_R)+\text{H.c.}$	$2n_f^4$
$\underline{L}\cap B$	$\mathcal{O}_{NNNN} :=$	$\frac{\alpha_{NNNN}}{\Lambda^2}(N_R C N_R)(N_R C N_R)+\text{H.c.}$	$\frac{n_f^2(n_f^2-1)}{6}$
$\underline{L}\cap\underline{B}$	$\mathcal{O}_{QQdN} :=$	$\frac{\alpha_{QQdN}}{\Lambda^2}\epsilon_{ij}\epsilon_{\alpha\beta\sigma}(Q^i_\alpha C Q^j_\beta)(d_{R\sigma}C N_R)+\text{H.c.}$	$n_f^3(n_f+1)$
	$\mathcal{O}_{uddN} :=$	$\frac{\alpha_{uddN}}{\Lambda^2}\epsilon_{\alpha\beta\sigma}(u^\alpha_R C d^\beta_R)(d^\sigma_R C N_R)+\text{H.c.}$	$2n_f^4$

field redefinition, RHN fields would couple to photon. These couplings would have a direct impact to neutrino magnetic moment [53]. Using XENON data [55] one can determine the size of the associated Wilson coefficient $\frac{\alpha_3^{(5)}}{\Lambda}$. Here we conclude our discussion on dimension five operators and in the next section, we discuss $d=6$ operators.

B. N_R-EFT operators at dimension six

In the last section we have presented various aspects of dimension five operators. We will now turn our attention to the details of the dimension six operators. In Table III, we enlist all possible operators in systematic manner. For a methodical construction of these operators, one may read through Ref. [26].

1. Neutrino mass in dimension six

Before engaging ourselves into an extensive discussion on these operators, we like to point out possible modification that happens in the neutrino mass matrix when one considers dimension six operators. The operator that falls under the class of ψ^2H^3, where ψ^2 represents two fermionic fields, contributes towards the neutrino mass matrix as this operator would give additional contribution towards the off-diagonal Dirac elements of the matrix mentioned in Eq. (2.2). The updated form of this matrix can be illustrated in the following fashion:

$$\mathcal{M}_{\nu N}^{(6)}=\begin{bmatrix}\frac{\alpha_1^{(5)}v^2}{\Lambda} & \frac{Y_\nu v}{\sqrt{2}}+\left(\frac{\alpha_{LNH}v^3}{2\sqrt{2}\Lambda^2}\right)\\ \frac{Y_\nu^T v}{\sqrt{2}}+\left(\frac{\alpha_{LNH}^T v^3}{2\sqrt{2}\Lambda^2}\right) & \left(\tilde{M}_N+\frac{\alpha_2^{(5)}v^2}{\Lambda}\right)\end{bmatrix}. \tag{2.9}$$

Our next task is to obtain the correct form of eigenvalues and eigenvectors corresponds to the light and heavy neutrinos, respectively. To do so, we would consider the following redefinition of the off-diagonal element of the above matrix:

$$\tilde{Y}_\nu=Y_\nu+\left(\frac{\alpha_{LNH}v^2}{2\Lambda^2}\right). \tag{2.10}$$

We use this parametrization to write down the light neutrino mass. To evaluate the eigenvalues of the above matrix we choose the limit $M_N \gg \frac{\alpha_{LNH} v^3}{\Lambda^2}, \frac{\alpha_1^{(5)} v^2}{\Lambda}$. In this limit, the light and heavy mass eigenvalue will take the following matrix form:

$$m_{\text{light}}^{(6)} \approx \frac{\alpha_1^{(5)} v^2}{\Lambda} - \frac{\tilde{Y}_\nu^T (\tilde{M}_N^{-1}) v^2 \tilde{Y}_\nu}{2},$$
$$m_{\text{heavy}}^{(6)} \approx M_N. \tag{2.11}$$

Looking at the above form of the neutrino mass matrices one can appreciate the rational behind the parametrization mentioned in Eq. (2.10). The inclusion of the dimension six contribution does not alter the form of the mass eigenvalues as compared to Eq. (2.4). The mass matrix in the dimension six setup can also be diagonalized using the prescription discussed in the last section. To do so we need to redefine the mixing angle between active and sterile neutrino. The matrix V of Eq. (2.7) will take the following form:

$$V \approx \begin{pmatrix} U_{\text{PMNS}} & \tilde{\theta} \\ -\tilde{\theta}^T & \kappa \end{pmatrix}, \tag{2.12}$$

where $\tilde{\theta}$ is

$$\tilde{\theta} = \theta^{(5)} + \theta^{(6)} = M_N^{-1} \frac{\tilde{Y}_\nu v}{\sqrt{2}}, \quad \text{and} \quad \theta^{(5)} = M_N^{-1} \frac{Y_\nu v}{\sqrt{2}},$$
$$\theta^{(6)} = M_N^{-1} \frac{\alpha_{LNH} v^3}{2\sqrt{2}\Lambda^2}.$$

With this new definition of the mixing angle one can obtain the corresponding mass eigenstates for the neutrinos. We illustrate these results in Eq. (2.13)

$$\nu_L \simeq U_{\text{PMNS}} \nu_{L,m} + \tilde{\theta} N_{m,R}^c,$$
$$N_R^c \simeq -\tilde{\theta}^T \nu_{L,m} + \kappa N_{m,R}^c, \tag{2.13}$$

where the orthonormality between these two states dictate $U_{\text{PMNS}} \simeq \kappa$.

2. Interesting facets of the dimension six operators

With this setup, we now point out various aspect of the dimension six operators that are tabulated in Table III. We have categorized these operators based upon their Lorentz structure as well as the field contents that are present:

(i) $\mathcal{O}_{LNH}$: In dimension six, the only possible operator which can come under the class of $\psi^2 H^3$ is $\mathcal{O}_{LNH}$ where ψ denotes the charged as well as neutral fermionic fields present in that operator. Apart from modifying the neutrino mass matrix, this operator also contributes toward the Higgs neutrino couplings. The modification of these couplings are explicitly presented in Table IV that we will discuss in detail in the later part of this section. Before that we like to highlight interesting aspects of other classes of dimension six operators.

(ii) $\mathcal{O}_{HN}$ & $\mathcal{O}_{HNe}$: Two operators $\mathcal{O}_{HN}$ and $\mathcal{O}_{HNe}$ fall in the class of $\psi^2 H^2 D$, where D represents the covariant derivative corresponds to $SU(2)_L \times U(1)_Y$ gauge group. Upon expanding $H^\dagger i\overleftrightarrow{D}_\mu H^2$ and $\tilde{H}^\dagger i D_\mu H$, one can see both active and sterile neutrinos couple to Z boson via $\mathcal{O}_{HN}$ operator, and not via $\mathcal{O}_{HNe}$. On the other hand, $\mathcal{O}_{HNe}$ only contributes to the $\mathcal{C}_{\ell\nu}^{W_\mu}$ and $\mathcal{C}_{\ell N}^{W_\mu}$ couplings. If we expand this operator explicitly, one can see the W boson couple to right-handed chiral leptons via this operator. This is indeed a striking departure from the existing SM theory. The SM is a $SU(2)_L$ theory that forbids the coupling between charged gauge bosons and right-handed fermions. The present experimental bounds on the respective coupling can be translated to estimate the current limit on this operator.

(iii) $\mathcal{O}_{LNW}$ & $\mathcal{O}_{LNB}$: The dimension six allows us to write two operators that involve the field-strength tensor, i.e., $W_{\mu\nu}^I$ and $B_{\mu\nu}$ corresponding to $SU(2)_L$ and $U(1)_Y$, respectively. Similar to the operator $\mathcal{O}_3^{(5)}$, both these operators would be suppressed by an extra $\frac{1}{16\pi^2}$ as these can only be realized in a full theory via loop mediated processes. In case of dimension five, the operator $\mathcal{O}_5^{(3)}$ is an antisymmetric tensor in the flavor space, which is not the same for the dimension six case.

(iv) Four Fermi: The dimension six case allows us to construct various kind of four Fermi operators. Considering the chirality of different fermions these operators can be categorized into four separate classes: $(\bar{L}R)(\bar{R}L)$, $(\bar{R}R)(\bar{R}R)$, $(\bar{L}L)(\bar{R}R)$, and $(\bar{L}R)(\bar{L}R)$. In addition to that, one can write three more operators that violate either lepton number or lepton-baryon number. The operator $\mathcal{O}_{QuNL}$ that comes under the $(\bar{L}R)(\bar{R}L)$ class would contribute toward the neutral as well as charged four-point contact interaction terms. Considering the underlying Lorentz structure, one can see in the full theory that this operator can be realized via the charged scalar mediated process. In contrast to that, the operator, $\mathcal{O}_{duNe}$, would also give rise to the charged four-point contact interaction. Moreover, the presence of γ^μ matrices in this interaction vertex suggest that it can be incorporated in a possible non-Abelian gauge extended theory. These operators lead to the

[2]Where the explicit form of $H^\dagger i\overleftrightarrow{D}_\mu H$ is $i(H^\dagger D_\mu H - (D_\mu H)^\dagger H)$. Replacing H field with the SM Higgs doublet one can see the terms which contain Z-boson field would only survive.

TABLE IV. The explicit modification of three point couplings after the inclusion of the dimension six operator contributions. The couplings up to dimension five is embedded in the $\mathcal{C}^{S}_{ff'}$ term where S is SM bosons and f and f' can be the charged as well as neutral leptons. The column three highlights the dimension six operators that participate in each of these couplings.

Couplings	Explicit form	Operator
$\mathcal{C}^{6}_{W_\mu \ell_\nu}$	$\mathcal{C}^{W_\mu}_{\ell_\nu} + \{\frac{g\alpha_{HNe}v^2}{2\sqrt{2}\Lambda^2}\tilde{\theta}^\dagger\gamma^\mu P_R - 2ip_\nu \frac{v\alpha_{LNW}}{\sqrt{2}\Lambda^2}\tilde{\theta}^\dagger\sigma_{\mu\nu}P_R\} + \text{H.c.}$	$\mathcal{O}_{HNe}$, $\mathcal{O}_{LNW}$
$\mathcal{C}^{6}_{W_\mu \ell N}$	$\mathcal{C}^{W_\mu}_{\ell N} + \{-\frac{g\alpha_{HNe}v^2}{2\sqrt{2}\Lambda^2}\kappa^*\gamma^\mu P_R + 2ip_\nu \frac{v\alpha_{LNW}}{\sqrt{2}\Lambda^2}\kappa^*\sigma_{\mu\nu}P_R\} + \text{H.c.}$	$\mathcal{O}_{HNe}$, $\mathcal{O}_{LNW}$
$\mathcal{C}^{6}_{h\bar{\nu}\nu}$	$\mathcal{C}^{h}_{\bar{\nu}\nu} + \{-\frac{3v^2\alpha_{LNH}}{2\sqrt{2}\Lambda^2}U^\dagger\tilde{\theta}^\dagger P_R\} + \text{H.c.}$	$\mathcal{O}_{LNH}$
$\mathcal{C}^{6}_{h\bar{N}N}$	$\mathcal{C}^{h}_{\bar{N}N} + \{\frac{3v^2\alpha_{LNH}}{2\sqrt{2}\Lambda^2}\tilde{\theta}^\dagger\kappa^* P_R\} + \text{H.c.}$	$\mathcal{O}_{LNH}$
$\mathcal{C}^{6}_{h(\bar{\nu}N+\bar{N}\nu)}$	$\mathcal{C}^{h}_{(\bar{\nu}N+\bar{N}\nu)} + \{\frac{3v^2\alpha_{LNH}}{2\sqrt{2}\Lambda^2}U^\dagger\kappa^* P_R - \frac{3v^2\alpha_{LNH}}{2\sqrt{2}\Lambda^2}\tilde{\theta}^\dagger\tilde{\theta}^\dagger P_R\} + \text{H.c.}$	$\mathcal{O}_{LNH}$
$\mathcal{C}^{6}_{Z_\mu\bar{\nu}\nu}$	$\mathcal{C}^{Z_\mu}_{\bar{\nu}\nu} + \{-\frac{\alpha_{HN}vm_Z}{\Lambda^2}\tilde{\theta}\tilde{\theta}^\dagger\gamma^\mu P_R + 2is_w p_\nu \frac{v\alpha_{LNB}}{\sqrt{2}\Lambda^2}U^\dagger\tilde{\theta}^\dagger\sigma_{\mu\nu}P_R - 2ic_w p_\nu \frac{v\alpha_{LNW}}{\sqrt{2}\Lambda^2}U^\dagger\tilde{\theta}^\dagger\sigma_{\mu\nu}P_R\} + \text{H.c.}$	$\mathcal{O}_{HN}$, $\mathcal{O}_{LNB}$, $\mathcal{O}_{LNW}$
$\mathcal{C}^{6}_{Z_\mu\bar{N}N}$	$\mathcal{C}^{Z_\mu}_{\bar{N}N} + \{-\frac{\alpha_{HN}vm_Z}{\Lambda^2}\kappa^\dagger\kappa^*\gamma^\mu P_R - 2is_w p_\nu \frac{v\alpha_{LNB}}{\sqrt{2}\Lambda^2}\tilde{\theta}^\dagger\kappa^*\sigma_{\mu\nu}P_R + 2ic_w p_\nu \frac{v\alpha_{LNW}}{\sqrt{2}\Lambda^2}\tilde{\theta}^\dagger\kappa^*\sigma_{\mu\nu}P_R\} + \text{H.c.}$	$\mathcal{O}_{HN}$, $\mathcal{O}_{LNB}$,$\mathcal{O}_{LNW}$
$\mathcal{C}^{6}_{Z_\mu(\bar{\nu}N+\bar{N}\nu)}$	$\mathcal{C}^{Z_\mu}_{(\bar{\nu}N+\bar{N}\nu)} + \{\frac{\alpha_{HN}vm_Z}{\Lambda^2}\tilde{\theta}\kappa^*\gamma^\mu P_R - 2is_w p_\nu \frac{\alpha_{LNB}v}{\sqrt{2}\Lambda^2}U^\dagger\kappa^\dagger\sigma_{\mu\nu}P_R$ $+2ic_w p_\nu \frac{\alpha_{LNW}v}{\sqrt{2}\Lambda^2}U^\dagger\kappa^\dagger\sigma_{\mu\nu}P_R\} + \{\frac{\alpha_{HN}vm_Z}{\Lambda^2}\kappa^T\theta^\dagger\gamma^\mu P_R + 2is_w p_\nu \frac{\alpha_{LNB}v}{\sqrt{2}\Lambda^2}\tilde{\theta}^\dagger\tilde{\theta}^\dagger\sigma_{\mu\nu}P_R$ $-2ic_w p_\nu \frac{\alpha_{LNW}v}{\sqrt{2}\Lambda^2}\tilde{\theta}^\dagger\tilde{\theta}^\dagger\sigma_{\mu\nu}P_R\} + \text{H.c.}$	$\mathcal{O}_{HN}$, $\mathcal{O}_{LNB}$, $\mathcal{O}_{LNW}$
$\mathcal{C}^{6}_{A_\mu\bar{\nu}\nu}$	$\mathcal{C}^{A_\mu}_{\bar{\nu}\nu} + \{-2ic_w p_\nu \frac{\alpha_{LNB}v}{\sqrt{2}\Lambda^2}U^\dagger\tilde{\theta}^\dagger\sigma_{\mu\nu}P_R + 2is_w p_\nu \frac{\alpha_{LNW}v}{\sqrt{2}\Lambda^2}U^\dagger\tilde{\theta}^\dagger\sigma_{\mu\nu}P_R\} + \text{H.c.}$	$\mathcal{O}_{LNB}$, $\mathcal{O}_{LNW}$
$\mathcal{C}^{6}_{A_\mu\bar{N}N}$	$\mathcal{C}^{A_\mu}_{\bar{N}N} + \{2ic_w p_\nu \frac{\alpha_{LNB}v}{\sqrt{2}\Lambda^2}\tilde{\theta}^\dagger\kappa^*\sigma_{\mu\nu}P_R + 2is_w p_\nu \frac{\alpha_{LNW}v}{\sqrt{2}\Lambda^2}\tilde{\theta}^\dagger\kappa^*\sigma_{\mu\nu}P_R\} + \text{H.c.}$	$\mathcal{O}_{LNB}$, $\mathcal{O}_{LNW}$
$\mathcal{C}^{6}_{A_\mu(\bar{\nu}N+\bar{N}\nu)}$	$\mathcal{C}^{A_\mu}_{(\bar{\nu}N+\bar{N}\nu)} + \{2ic_w p_\nu \frac{\alpha_{LNB}v}{\sqrt{2}\Lambda^2}U^\dagger\kappa^*\sigma_{\mu\nu}P_R + 2is_w p_\nu \frac{\alpha_{LNW}v}{\sqrt{2}\Lambda^2}U^\dagger\kappa^\dagger\sigma_{\mu\nu}P_R$ $-2ic_w p_\nu \frac{\alpha_{LNB}v}{\sqrt{2}\Lambda^2}\tilde{\theta}^\dagger\tilde{\theta}^\dagger\sigma_{\mu\nu}P_R - 2is_w p_\nu \frac{\alpha_{LNB}v}{\sqrt{2}\Lambda^2}\tilde{\theta}^\dagger\tilde{\theta}^\dagger\sigma_{\mu\nu}P_R\} + \text{H.c.}$	$\mathcal{O}_{LNB}$, $\mathcal{O}_{LNW}$

single production of RHN, which is not mixing suppressed. The other operators $\mathcal{O}_{eN}$, $\mathcal{O}_{uN}$, and $\mathcal{O}_{dN}$ would also invoke the pair production of the RHN fields in the lepton and hadron colliders, respectively. The corresponding production cross section is independent of the active-sterile mixing angle. The operators that come under the $(\bar{L}L)(\bar{R}R)$ class would also give rise to pair production processes similar to the operators $\mathcal{O}_{eN}$, $\mathcal{O}_{uN}$, and $\mathcal{O}_{dN}$. The operator $\mathcal{O}_{LN}$ would also invoke an additional contact interaction term $(\bar{\nu}_L\gamma^\mu\nu_L)(\bar{N}_R\gamma_\mu N_R)$. Nevertheless, one can neglect this term for further discussion as it is phenomenologically imprudent.

(v) $(\bar{L}R)(\bar{L}R)$: In case of $(\bar{L}R)(\bar{L}R)$ scenario, one can write three operators $\mathcal{O}_{LNLe}$, $\mathcal{O}_{LNQd}$, and $\mathcal{O}_{LdQN}$ where ϵ stands for 2×2 antisymmetric matrices. From the structure of these operators one can interpret their effects with heavy scalar mediated processes. The terms arise from these operators would contribute to both neutral as well as charged four-point vertices. Furthermore, the Lorentz structure of these vertices can possibly be incorporated in a full theory that contains both neutral and charged scalar d.o.f.

(vi) $\mathcal{O}_{NN}$ & $\mathcal{O}_{NNNN}$: Dimension six also allows us to build two operators $\mathcal{O}_{NN}$ and $\mathcal{O}_{NNNN}$, which involve four N fields. The differences between these two are many folds. From the standpoint of the Lorentz structure, one can see that $\mathcal{O}_{NN}$ invokes a vectorlike process in contrast to the scalarlike $\mathcal{O}_{NNNN}$ operator. On the other hand $\mathcal{O}_{NNNN}$ explicitly violates the lepton number as opposed to $\mathcal{O}_{NN}$. In addition to that, the Wilson coefficient α_{NNNN} is antisymmetric in flavor space, whereas α_{NN} is symmetric. However, the explicit computation of the operators suggest that the coupling of N with SM neutrinos coming from these operators would be $\tilde{\theta}^3$ suppressed (see Table V for the explicit form). As a result, both these operators remain inaccessible from present day collider experiments.

(vii) $\mathcal{O}_{QQdN}$ & $\mathcal{O}_{uddN}$: We conclude our discussion while presenting two lepton $\oplus$ baryon numbers violating operators: $\mathcal{O}_{QQdN}$ and $\mathcal{O}_{uddN}$. Both these operators invoke a nontrivial decay mode of N such as $N_i \to d_\alpha u_\alpha d_\beta$. These operators also play an important role in physics involving $B-L$ asymmetry. However in the current paper, we refrain ourselves to discussing the aspects of these operators.

TABLE V. The four point coupling arise from different four Fermi operators. Here we have only presented those couplings which are relevant for the three body decay calculation for N. The other four point couplings that involve more than one heavy neutrino fields are presented in Appendix C. We represent these couplings while adopting a generic structure $\mathcal{G}^N_{f_1 f_2 f_3}$, where f_1, f_2, and f_3 represent the SM fermions. The greek indices α, β and latin indices i, j, k describe the underlying flavor of the quarks and leptons, respectively.

Couplings	Explicit form	Operator
$\mathcal{G}^N_{\ell_j \ell_k \nu_k}$	$\frac{\alpha_{LNLe}}{\Lambda^2}\{U^\dagger \kappa^* (\bar{\nu}_m P_R N_m)(\bar{e}_m P_R e_m) - \kappa^* U^\dagger (\bar{e}_m P_R N_m)(\bar{\nu}_m P_R e_m)\}$ $+ \frac{\alpha_{eN}}{\Lambda^2}(\bar{e}_m \gamma^\mu P_R e_m)\{-\kappa^T \tilde{\theta}^\dagger (\bar{N}_m \gamma^\mu P_R \nu_m) - \tilde{\theta}\kappa^* (\bar{\nu}_m \gamma^\mu P_R N_m)\}$ $+ \frac{\alpha_{LN}}{\Lambda^2}(\bar{e}_m \gamma^\mu P_L e_m)\{-\kappa^T \tilde{\theta}^\dagger (\bar{N}_m \gamma^\mu P_R \nu_m) - \tilde{\theta}\kappa^* (\bar{\nu}_m \gamma^\mu P_R N_m)\}$ + H.c.	$\mathcal{O}_{LNLe}$, $\mathcal{O}_{eN}$, $\mathcal{O}_{LN}$
$\mathcal{G}^N_{\nu_k \ell_k \ell_k}$	Same as above	Same as above
$\mathcal{G}^N_{\nu_j \ell_k \ell_k}$	Same as above	Same as above
$\mathcal{G}^N_{\ell_j u_\alpha d_\beta}$	$\frac{\alpha_{duNe}}{\Lambda^2}(\bar{d}_m \gamma^\mu P_R u_m)(\kappa^T \bar{N}_m \gamma^\mu P_R e_m) + \frac{\alpha_{QuNL}}{\Lambda^2}(\bar{d}_m P_R u_m)(\kappa^T \bar{N}_m P_L e_m)$ $-[\frac{\alpha_{LNQd}}{\Lambda^2} + \frac{\alpha_{LdQN}}{\Lambda^2}]\kappa^\dagger (\bar{e}_m P_R N_m)(\bar{u}_m P_R d_m)$ + H.c.	$\mathcal{O}_{duNe}$, $\mathcal{O}_{QuNL}$ $\mathcal{O}_{LNQd}$, $\mathcal{O}_{LdQN}$
$\mathcal{G}^N_{\nu_j u_a u_\alpha}$	$\frac{\alpha_{QuNL}}{\Lambda^2}\kappa^T U(\bar{u}_m P_R u_m)(\bar{N}_m P_L \nu_m) - \frac{\alpha_{uN}}{\Lambda^2}\kappa^T \tilde{\theta}(\bar{u}\gamma^\mu P_R u_m)(\bar{N}_m \gamma^\mu P_R \nu_m)$ $-\frac{\alpha_{QN}}{\Lambda^2}\kappa^T \tilde{\theta}^\dagger (\bar{u}_m \gamma^\mu P_L u_m)(\bar{N}_m \gamma^\mu P_R \nu_m)$ + H.c.	$\mathcal{O}_{QuNL}$, $\mathcal{O}_{uN}$ $\mathcal{O}_{QN}$
$\mathcal{G}^N_{\nu_j d_a d_\alpha}$	$\frac{\alpha_{LdQN}}{\Lambda^2}(U^\dagger \kappa^* \bar{\nu}_m P_R d_m \bar{d}_m P_R N_m) + \frac{\alpha_{LNQd}}{\Lambda^2}(U^\dagger \kappa^* \bar{\nu}_m P_R N_m \bar{d}_m P_R d_m)$ $-\frac{\alpha_{dN}}{\Lambda^2}(\kappa^T \tilde{\theta}^\dagger \bar{d}_m \gamma^\mu P_R d_m \bar{N}_m \gamma^\mu P_R \nu_m) - \frac{\alpha_{QN}}{\Lambda^2}(\kappa^T \tilde{\theta}^\dagger \bar{d}_m \gamma^\mu P_R d_m \bar{N}_m \gamma^\mu P_R \nu_m)$ + H.c.	$\mathcal{O}_{LNQd}$, $\mathcal{O}_{LdQN}$ $\mathcal{O}_{dN}$, $\mathcal{O}_{QN}$
$\mathcal{G}^N_{\nu_j \nu \nu}$	$\frac{\alpha_{NNNN}}{\Lambda^2}(\tilde{\theta}^* \tilde{\theta}^\dagger \kappa^\dagger \tilde{\theta}^\dagger)(\bar{\nu}_m P_R \nu_m \bar{N}_m P_R \nu_m) - \frac{\alpha_{NN}}{\Lambda^2}(\tilde{\theta}\tilde{\theta}^\dagger \kappa^T \tilde{\theta}^\dagger)(\bar{\nu}_m P_R \nu_m \bar{N}_m P_R \nu_m)$ + H.c.	$\mathcal{O}_{NNNN}$ $\mathcal{O}_{NN}$

Our next step is to discuss the modifications as well as emergence of various three-point couplings that involve RHNs in the dimension six setup. The detail calculation to determine the explicit form of these couplings are illustrated in Appendix C. In the beginning of this section we have shown how the mass eigenstates of both the active and sterile neutrinos evolve due to the inclusion of the operator $\mathcal{O}_{LNH}$. This change can be incorporated by redefining the mixing parameter from θ to $\tilde{\theta}$.

One can divide all the relevant couplings into two subcategories. In Table IV, we also include those couplings that one can already find in the dimension five N_R-EFT. We write different couplings as $\mathcal{C}^6_{Sff'}$, where $\mathcal{C}^6_{Sff'}$ includes the sum of a dimension five contribution $C^S_{ff'}$ and the $\mathcal{O}(\frac{1}{\Lambda^2})$ corrections[3]:

(i) Unlike dimension five, the coupling between W and $\ell\nu/N$ receives additional correction due to both $\mathcal{O}_{HNe}$ and the loop-suppressed $\mathcal{O}_{LNW}$ (which has in general small value) operators. As mentioned earlier, the operator $\mathcal{O}_{HNe}$ invokes right handed coupling between SM leptons and the W boson. The upshot of this coupling is that it would modify the branching ratios as well as total decay width of W bosons. The precision measurements on this charged gauge boson can be used to place meaningful bounds on the Wilson coefficient $\frac{\alpha_{HNe}}{\Lambda^2}$. A recent article [56] proposed a similar kind of right handed couplings between SM fermions and W boson on the verge of solving the W-boson mass tension (see Ref. [57]).

(ii) The Z-boson coupling gets addition corrections both from tree-level mediated operators $\mathcal{O}_{HN}$ as well as loop-mediated operators $\mathcal{O}_{LNB}$ and $\mathcal{O}_{LNW}$, respectively. The last two operators also generate an appropriate alteration to photon neutrino couplings via neutral gauge state mixing. We like to reiterate that the terms coming from these would be $\frac{1}{16\pi^2}$ suppressed. Processes induced from these operators receive appropriate constraints from the different precession measurements such as Z-boson total width [58] measurement, $\mathcal{BR}(Z \to \nu N)$ [59] etc.

(iii) Apart from the gauge bosons, the Higgs-neutrino couplings also get modified in the underlying EFT setup due to the operator $\mathcal{O}_{LNH}$. In the beginning of this section we have shown how this operator enters into the off-diagonal elements of the mass matrix. From the parametrization that is displayed in Eq. (2.10), one can see that this operator also redefines the active-sterile mixing angles $\tilde{\theta}$.

The compelling ingredient of the dimension six N_R-EFT setup is the emergence of various four Fermi operators. As an upshot, one can write down the four-point contact interactions that involve at least one RHN field. Couplings like these play a crucial role in the production as well as decay of the right-handed neutrinos. Few of these operators would contribute to various pair production processes in lepton and hadron colliders with an appreciable cross section. In parallel to that, these operators have the capacity

[3]In the notation $\mathcal{C}^6_{Sff'}$ and $C^S_{ff'}$ the S denotes $W/Z/\gamma/h$, f stands for either charged or neutral leptons, and f' corresponds to either active or sterile neutrinos.

TABLE VI. Constraints on $\alpha_{LNB/W}$ and α_{HN} from Z-width measurement [58,60] for $\mathrm{BR}(N \to \nu\gamma) = 1$ (0.1).

	$\Lambda = 4$ TeV	$\Lambda = 1.5$ TeV	$\Lambda = 500$ GeV
$\mathcal{B}(Z \to \nu N \to 2\nu + \gamma)$	$\alpha_{LNB/W} \leq 1.88$ (5.9)	$\alpha_{LNB/W} \leq 0.26$ (0.84)	$\alpha_{LNB/W} \leq 0.029$ (0.09)
$\mathcal{B}(Z \to NN \to 2\nu + 2\gamma)$	$\alpha_{HN} \leq 1.04$ (10.4)	$\alpha_{HN} \leq 0.14$ (1.4)	$\alpha_{HN} \leq 0.01$ (0.16)

to participate into the three body decay modes of N. Up to dimension five, the RHN fields can decay to three body leptonic/semileptonic final states, where decay is mediated via off shell W/Z bosons. These can serve as dominant channels if mass of the N is below M_W. The four Fermi operators instead give rise to relevant four-point contact interactions which contribute towards these three body decay modes. In Sec. V, we present the analytic expression of these decay modes and the relevance of four Fermi operators in this context.

In Table V, we present some of these couplings with its explicit structure. Here we restrict ourselves to the couplings which only involve RHN field and SM fermions as they are relevant for our later discussion on the three body decay modes. In addition to that, we have chosen the mass of various flavor of heavy neutrinos to be same. As a result the decay from N_i to N_j states with $i \neq j$ are kinematically forbidden. Out of these seven couplings, three of them would be purely leptonic and other three would be an admixture of hadronic and leptonic state. There exists one coupling that involves only the active and sterile neutrinos:

(i) The couplings $\mathcal{G}^N_{\ell_j \ell_k \nu_k} (j \neq k)$, $\mathcal{G}^N_{\nu_k \ell_k \ell_k}$, and $\mathcal{G}^N_{\nu_j \ell_k \ell_k}$ are controlled by the same operators. However, the label of the SM leptons suggests that one cannot treat them on an equal footing. The contribution coming from $\mathcal{O}_{LNLe}$ operator only depends on the associated Wilson coefficient and the effect coming from it would be prominent. On the other hand, the operators $\mathcal{O}_{eN}$ and $\mathcal{O}_{LN}$ have an additional dependence on the mixing angle. As a consequence, their phenomenological implications are difficult to probe.

(ii) Apart from the leptonic channels, the N can couple to quarks via four point interactions. Noticeably, all the operators that furnish the coupling $\mathcal{G}^N_{\ell_j u_\alpha d_\beta}$ are phenomenologically viable as their impact is not suppressed by the smallness of mixing angle. Along with that, two other couplings $\mathcal{G}^N_{\nu_j u_\alpha u_\alpha}$ and $\mathcal{G}^N_{\nu_j d_\alpha d_\alpha}$ are also possible, which can provide addition signatures for the collider study of N_R-EFT. The operators' $\mathcal{O}_{uN}$, $\mathcal{O}_{QN}$, and $\mathcal{O}_{dN}$ contributions in these couplings face an additional $\tilde{\theta}$ suppression, while $\mathcal{O}_{QuNL}$, $\mathcal{O}_{LdQN}$ are unsuppressed. The vertex $\mathcal{G}^N_{\ell_j u_\alpha d_\beta}$ is not accompanied with any such suppression.

(iii) The coupling $\mathcal{G}^N_{\nu_j \nu\nu}$ is mediated via $\mathcal{O}_{NNNN}$ and $\mathcal{O}_{NN}$ operators, but its magnitude is proportional to the cubic order of $\tilde{\theta}$.

III. CONSTRAINTS ON RELEVANT N_R-EFT PARAMETERS

The EFT operators discussed above can contribute to the processes that has already been searched at the LHC and hence receive constraints from these experimental searches. Further these operators lead to BSM decay modes of the SM particles, and hence there are constraints from their branching ratios measurements. In the following we briefly discuss that:

(i) Constraints from decay of **Z**: The operators $\mathcal{O}_{LNB}$ and $\mathcal{O}_{LNW}$ can enhance the decay width of Z boson for nonzero α_{LNB} and α_{LNW} through the decay mode $Z \to \nu N$, which is

$$\Gamma(Z \to N\nu) = \frac{3M_Z^3 v^2}{12\pi\Lambda^4} (c_w \alpha_{LNW} - s_w \alpha_{LNB})^2 \times (1 - M_N^2/M_Z^2)^{3/2}. \quad (3.1)$$

The decay mode $Z \to \nu N$ and subsequent decay of N to $\nu\gamma$ (which can come from operators such as $\mathcal{O}_3^{(5)}$, $\mathcal{O}_{LNW,LNB}$) leads to $Z \to 2\nu + \gamma$. There exist experimental limit on $\mathrm{BR}(Z \to 2\nu + \gamma) < 3.2 \times 10^{-6}$ [60] that restricts the values of α_{LNB} and α_{LNW} for a given Λ. This limit has been presented in Table VI assuming $\alpha_{LNB} = \alpha_{LNW}$. To calculate this we consider $\mathrm{BR}(N \to \nu\gamma) = 1(0.1)$ and $\Lambda = 4$ TeV, 500 GeV. Similarly, $\mathcal{O}_{HN}$ leads to the decay mode $Z \to NN$, with decay width

$$\Gamma(Z \to NN) = \frac{m_Z^3 v^2 \alpha_{HN}^2}{8\pi\Lambda^4} (1 - 4M_N^2/M_Z^2)^{3/2}. \quad (3.2)$$

The subsequent decay of $N \to \nu\gamma$ can lead to the decay mode $Z \to 2\nu + 2\gamma$, whose branching ratio is bounded as $\mathrm{BR}(Z \to 2\nu + 2\gamma) < 3.1 \times 10^{-6}$ [58]. The upper limit on α_{HN} obtained from this observation is presented in Table VI.

(ii) Constraints from decay of **h**: In our framework, SM Higgs can have BSM decay modes such as $h \to \nu N/NN/\nu\gamma N$, where $\nu\gamma$ arises due to N decay. If N is stable at the detector length scale, then these decay modes lead to the invisible decay of Higgs, which is constrained as $\mathrm{Br}(h \to \text{invisible}) \leq 0.13$ [61]. This in turn limits the couplings $\alpha_2^{(5)}$, α_{LNH}, and

TABLE VII. Constraints on α_2^5, α_{LNH}, and $\alpha_{LNB/W}$ and from invisible Higgs decay [61].

$(\alpha_2^{(5)}, \alpha_{LNH}, \alpha_{LNB/W})$	$\Lambda = 4$ TeV	$\Lambda = 1.5$ TeV	$\Lambda = 500$ GeV
(c, c, c)	$c \leq 0.115$	$c \leq 0.043$	$c \leq 0.014$
$(0, c, c)$	$c \leq 1.93$	$c \leq 0.5$	$c \leq 0.242$
$(c, 0, c)$	$c \leq 0.115$	$c \leq 0.043$	$c \leq 0.0144$

$\alpha_{LNB/W}$, which is given in Table VII. We consider the values of these parameters as per Table VII for the evaluation of cross section in Sec. IV.

(iii) $pp \to \ell + N$: RHN has been searched for at the LHC by both the CMS [62] and ATLAS [63] collaborations through the process $pp \to W^{\pm} \to \ell + N$. These searches put bounds on the active-sterile neutrino mixing ($\tilde{\theta}$) as a function of RHN mass. The limit on $\tilde{\theta}$ can be translated into the limit on $\sigma(pp \to W^{\pm} \to \ell^{\pm} + N)$. In the EFT framework the production of $N + \ell^{\pm}$ can occur dominantly via a four fermion interaction ($pp \to \ell + N$) [42] along with the s-channel W-mediated process. As the kinematic feature of $pp \to \ell + N$ is not similar to that of $pp \to W^{\pm} \to \ell^{\pm} + N$ for all RHN mass, the above-mentioned constraints cannot be used in our case without the proper recasting of the CMS analysis. We check that the $p_T(\ell)$ distributions for both the processes are similar for $M_N \simeq 800$ GeV. However, for $M_N < 800$ GeV, the distributions are different and hence inappropriate to apply the limit directly. Without going into the detail recasting, we comment on the bounds for $M_N \geq 800$ GeV. The 95% C.L. limit on active-sterile mixing $\tilde{\theta} \leq 0.387$ for $M_N = 800$ GeV [62] leads to the limit on cross section $\sigma(pp \to \ell^{\pm} + N) \leq 0.8$ fb, which can be translated to the limit on the relevant couplings. For $M_N \geq 800$ GeV, the total cross section is dominated by the four Fermi interaction, which is mainly controlled by α_{duNe}, α_{LdQN}, α_{LNQd}, and α_{QuNL}. We assume all these couplings to be equal to α. Considering $\sigma(pp \to \ell^{\pm} + N) \leq 0.8$ fb for $M_N \simeq 800$ GeV, we obtain constraint on $\alpha \leq 0.28(0.04)$ for $\Lambda = 4$ TeV (1.5 TeV). As this is the strongest constraint on α_{duNe}, α_{LdQN}, α_{LNQd}, and α_{QuNL}, we consider this for the cross section calculation in Sec. IV.

(iv) $pp \to \ell + \gamma + MET$: Production of RHN with one associated lepton occurs via two processes, one is the four Fermi interaction and the other $pp \to W \to N\ell$ via s-channel W-mediated process. The decay mode of RHN $N \to \nu\gamma$ leads to the final state $\ell + \gamma + MET$, which has been searched by the CMS collaboration [64]. The couplings α_{duNe}, α_{LdQN}, α_{LNQd}, α_{QuNL}, α_{LNW}, and α_{HNe} that are involved in the above process receive constraints from the CMS result. This search has been recasted in [65] and limits have been set on the four-Fermi operators. Using the 95% C.L. limit on BSM events $\lesssim 9.7$ calculated in Ref. [65], we calculate constraints on the coefficient (α_{duNe}, α_{LdQN}, α_{LNQd}, α_{QuNL}) assuming all equal to α and $\mathrm{BR}(N \to \nu + \gamma) = 0.1$. For $M_N = 800$ GeV and $\sigma(pp \to \ell N) = 9.7$ fb, we obtain $\alpha \leq 0.5(0.07)$ for $\Lambda = 4$ TeV (1.5 TeV). For $M_N = 200$ GeV and $\sigma(pp \to \ell N) = 30$ fb, we obtain $\alpha \leq 0.28(0.04)$ for $\Lambda = 4$ TeV (1.5 TeV). For these masses the total cross section is dominated by the four fermion interaction, and the contribution from the W-mediated channel can be ignored.

(v) $pp \to 2\gamma + MET$: This signature can be obtained via the process $pp \to NN$ and subsequent decay $N \to \nu + \gamma$. Both the four Fermi interaction and the Higgs production via gluon fusion process lead to a pair of RHNs. For $M_N \geq 100$ GeV, the RHN production occurs primarily via a four Fermi interaction. The Wilson coefficients that are involved in this process are α_{dN}, α_{QN}, α_{uN}, α_{LNQd}, α_{LdQN}, α_{QuNL}, which we assume to be equal. However, one must note that contributions coming from the respective operators cannot be treated equally. From Eqs. (C13), (C14), and (C8), one can notice that the relevant coupling coming from the operators $\mathcal{O}_{LNQd}$, $\mathcal{O}_{LdQN}$, and $\mathcal{O}_{QuNL}$ receives additional $\tilde{\theta}^2$ suppression. Hence we can ignore their individual effect for present constraint calculation. There exists a search by the CMS collaboration for $2\gamma + MET$ signature [66], which sets limits on the BSM contribution to the $2\gamma + MET$ events. We adopt the 95% C.L. limit on observed $2\gamma + MET$ events $\lesssim 9.6$ for $\mathcal{L} = 35.9/\mathrm{fb}$, from Ref. [65], where the CMS analysis has been recasted. Considering this limit we obtain $\alpha \leq 1.49(0.209)$ for $\Lambda = 4$ TeV (1.5 TeV), assuming $M_N \geq 800$ GeV and $\mathrm{BR}(N \to \nu + \gamma) = 0.1$.

(vi) $pp \to \nu + N$: Production of one RHN in the process $pp \to \nu + N$ leads to $\gamma + MET$ signature for $N \to \nu + \gamma$ decay mode. This process involves Drell-Yan production ($pp \to \gamma^* \to \nu + N$), Higgs production ($pp \to h \to \nu + N$), and a four Fermi ($pp \to \nu + N$) interaction. The process $pp \to h \to \nu + N(\to \nu + \gamma)$ is not constrained as the photon is comparatively soft than for the process $pp \to \gamma^* \to \nu + N$ [43]. The relevant couplings α_{dN}, α_{QN}, α_{uN}, α_{LNQd}, α_{LdQN}, α_{QuNL}, and $\alpha_{LNW/B}$ are assume to be equal. The CMS analysis [67] for the $\gamma + MET$ signature sets limits on the BSM contribution. We consider a 95% C.L. limit on observed $\gamma + MET$ events $\lesssim 16$ from Ref. [43], where the CMS analysis

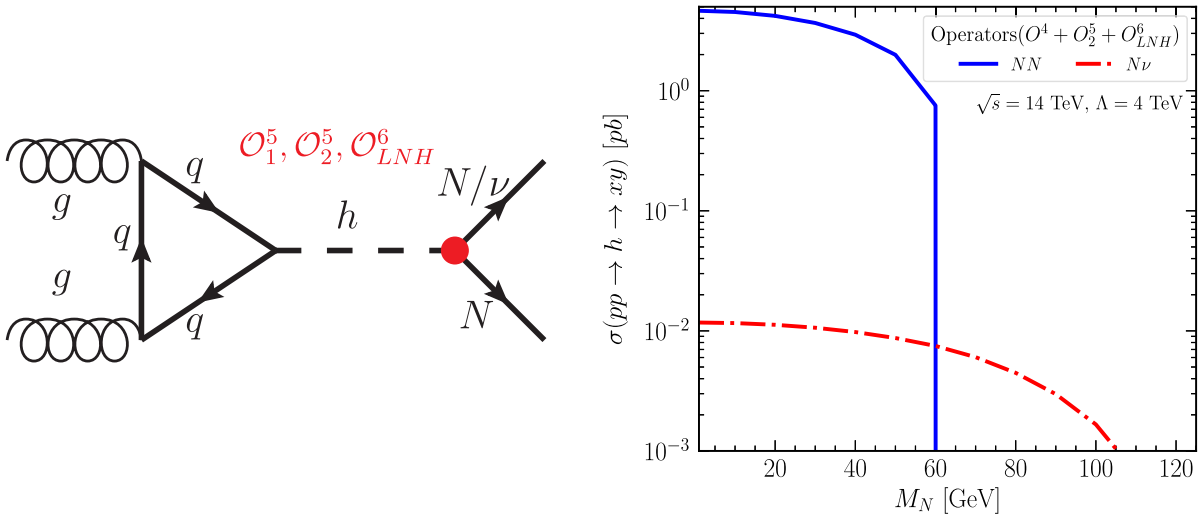

(a) (b)

FIG. 1. Left panel: the Feynman diagram and the relevant operator for the process $pp \to NN/\nu$. Right panel: the variation of cross section for the process $\sigma(gg \to h \to NN/\nu)$ with M_N for center-of-mass energy $\sqrt{s} = 14$ TeV and cutoff scale $\Lambda = 4$ TeV. $\sigma(gg \to h \to NN)$ is shown with the blue solid line and $\sigma(gg \to h \to N\nu)$ is shown with the red dashed-dot line. See text for details.

has been recasted. We obtain $\alpha \leq 8.67(1.28)$ for $\Lambda = 4$ TeV (1.5 TeV) assuming $M_N \geq 800$ GeV and $\mathrm{BR}(N \to \nu + \gamma) = 0.1$ For the considered mass leading contribution to the $\sigma(pp \to \nu + N)$ is from four Fermi operators that involve only one RHN (α_{LNQd}, α_{LdQN}, α_{QuNL}).

In view of the above discussion, to estimate the production rate in the next section we consider the values of the Wilsonian coefficient as follows. For $\Lambda = 4(1.5)$ TeV, we assume $\alpha_{HN}=1(1)$, $\alpha_{HNe}=1(1)$, $\alpha_{LNH} = 0.1(0.04)$, $\alpha_{LNW}=0.1(0.04)$, $\alpha_{LNB}=0.1(0.04)$, $\alpha_2^{(5)} = 0.1(0.04)$, $\alpha_{dN} = \alpha_{QN} = \alpha_{uN} = \alpha_{LNQd} = \alpha_{LdQN} = 0.5(0.04)$.

IV. POSSIBLE PRODUCTION MECHANISM

In order to calculate the cross section, we build this dimension six N_R-EFT using FeynRules(v2.3) [68] and generate corresponding Universal FeynRules Output (UFO) file. This UFO file can then use to evaluate the parton level cross section via Monte Carlo simulator MadGraph5_aMC@NLO(v2.6) [69].

A. Proton proton collider

The LHC is the machine that has the capability to probe the physics that possibly lies at high energies. Currently the LHC is going through an upgrade, and after that it will run at the c.m. energy $\sqrt{s} = 14$ TeV with a higher luminosity that will achieve the potential to collect 3000 fb^{-1} data by the year 2030. The detailed plan for the high-luminosity LHC (HL-LHC) is presented in Refs. [70–72]. In this paper, we will use 14 TeV LHC to propose various production processes for the RHNs.

1. $gg \to h \to NN/\nu$

At LHC, SM Higgs boson is dominantly produced via gluon-gluon fusion. The RHN field couples to the Higgs via Yukawa term at the renormalizable level. This coupling receives extra contribution via the operators $\mathcal{O}_1^{(5)}$, $\mathcal{O}_2^{(5)}$, and $\mathcal{O}_{LNH}$ at dimension five and dimension six, respectively. These operators along with the $d = 4$ term allow the Higgs to decay into νN and NN modes if kinematically admissible.

In Fig. 1(a) we present the Feynman diagram for this process. The vertices $\mathcal{C}^6_{h(\bar{\nu}N+\bar{N}\nu)}$ and $\mathcal{C}^6_{h\bar{N}N}$ are governed by the EFT parameters $\frac{\alpha_1^{(5)}}{\Lambda}$, $\frac{\alpha_2^{(5)}}{\Lambda}$, $\frac{\alpha_{LNH}}{\Lambda^2}$ along with the mixing angle. The smallness of the neutrino mass forces us to fix the $\alpha_1^{(5)}$ at zero. As mentioned in Sec. III the coupling $\alpha_2^{(5)}$ and α_{LNH} are considered to be 0.1 for $\Lambda = 4$ TeV while respecting the current experimental bounds. To calculate the production cross section we have considered $\tilde{\theta} = 10^{-3}$, which is allowed by the recent electroweak precision data [73]. In Fig. 1(b), we present the production cross section for the process $gg \to h \to NN$ by the blue solid line. As expected the cross section steeply falls at the mass around $\frac{m_h}{2}$ beyond which the Higgs decaying to a pair of on shell N fields is kinematically disallowed. At renormalizable level ($\mathcal{O}^4$) the coupling under consideration is controlled by the mixing angle $\tilde{\theta}$ and the smallness of this parameter leads to negligible cross section. The result significantly alters once we include the operator $\mathcal{O}_2^{(5)}$ that enhances the total cross section up to $\mathcal{O}(10$ pb) order. The cross section of this process does not substantially change once we include the

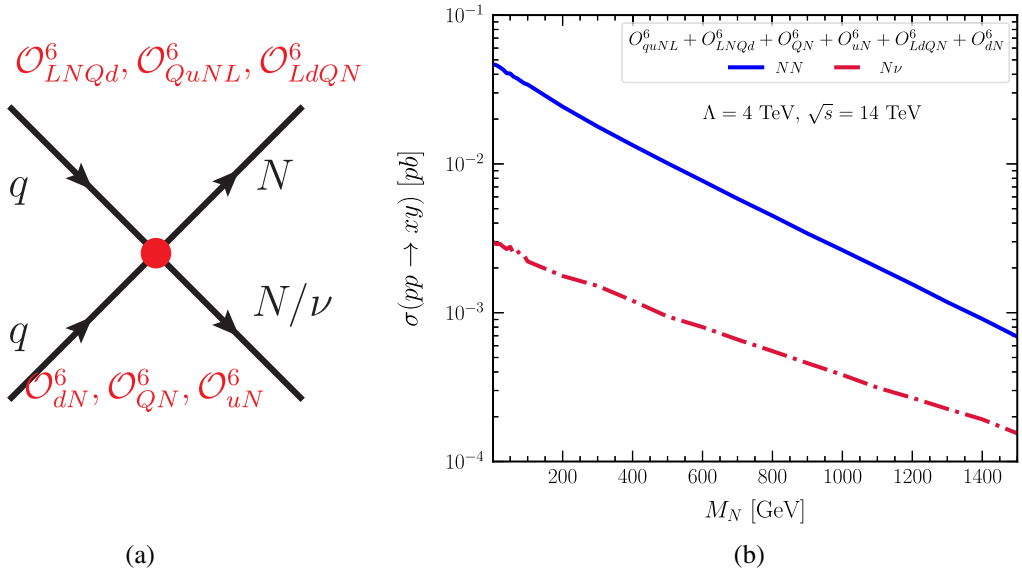

(a) (b)

FIG. 2. Left panel: the Feynman diagram and the relevant operators for the process $pp \to NN/\nu$. Right panel: the variation of cross section with M_N for center-of-mass energy $\sqrt{s} = 14$ TeV and cutoff scale $\Lambda = 4$ TeV. $\sigma(pp \to NN)$ is shown with the blue solid line and $\sigma(pp \to N\nu)$ is shown with the red dashed-dot line.

contribution coming from dimension six operator as this contributions depends on both the mixing angle and $\frac{\alpha_{LNH}}{\Lambda^2}$. We represent the cross section for $gg \to h \to N\nu$ in Fig. 1(b) by the red dashed-dotted line. Interestingly, the cross section due to the $\mathcal{O}^4$ term is comparable with the effect coming from $\mathcal{O}^{(5)}_2$. On the other hand the contribution coming from dimension six operator is independent of the mixing angle and enhances the total cross section by an order of magnitude. We would like to point out that the difference in the cross section between the $h \to NN$ and $h \to \nu N$ also arises due to the difference in associated kinematic factors.

2. $pp \to NN$ via four Fermi operators

We have discussed the pair production of the heavy neutrinos via Higgs decay. The problem with this production mode is that one can only probe a certain range of M_N owing to phase space suppression. In dimension six one can construct various four Fermi operators, which can produce these heavy neutral leptons with an appreciable cross section for a wider mass range of M_N. In proton proton collider these operators are $\mathcal{O}_{QN}$, $\mathcal{O}_{uN}$, $\mathcal{O}_{dN}$, and $\mathcal{O}_{QuNL}$, which can produce single as well as a pair of RHN fields [41]. In Fig. 2(a), we present the corresponding Feynman diagram of this process. To explicitly see how different operators participate in these process, we refer the readers to look into Appendix B. The contributions from $\mathcal{O}_{QN}$, $\mathcal{O}_{uN}$, and $\mathcal{O}_{dN}$ are independent of the mixing angle. Contrary to that, the cross section that is generated from $\mathcal{O}_{QuNL}$ depends on $\tilde{\theta}$ and hence will be suppressed.

In Fig. 2(b), blue line represents the pair production cross section generated via four Fermi operators at 14 TeV LHC. Lower parton density at high energy leads to decrease in the cross section as M_N increases. The contribution of the $\mathcal{O}_{uN}$ is larger than the $\mathcal{O}_{dN}$ due to the difference in their corresponding parton distribution function (pdf). Moreover the total cross section of this process is primarily governed by the $\mathcal{O}_{QN}$ as it involves both u and d quarks in the initial state. The operators ($\mathcal{O}_{QuNL}$, $\mathcal{O}_{LNQd}$, $\mathcal{O}_{LdQN}$) involving one RHN do not contribute substantially due to mixing suppression. We also present the cross section associated with the single N with the red dashed-dotted line, where the operators ($\mathcal{O}_{QuNL}$, $\mathcal{O}_{LNQd}$, $\mathcal{O}_{LdQN}$) involving one RHN are dominant.

3. RHN production via vector boson fusion process

The vector boson fusion (VBF) process remains one of the intriguing channels which one can study at the LHC. Here we specify a few VBF signals that are relevant for N production. Apart from being one of the golden channels for the Higgs discovery, VBF provides an excellent window to look for the unitarity of the underlying EWSB mechanism. Along with the Higgs, the W and Z can also be produced via this process. The large pseudorapidity ($\Delta\eta$) between the two leading jets helps to devise suitable cuts that can provide a relatively cleaner environment to search for the heavy neutrinos.

$pp \to hjj \to NN/\nu jj$.—In Fig. 3(a), we show the Feynman diagram for single and pair production of the sterile neutrinos via the VBF channel. The operator dependence remain same as the gluon-gluon fusion scenario. In Fig. 3(b) we display the cross section of $pp \to NNjj$ and $pp \to N\nu jj$ with the blue solid line and red

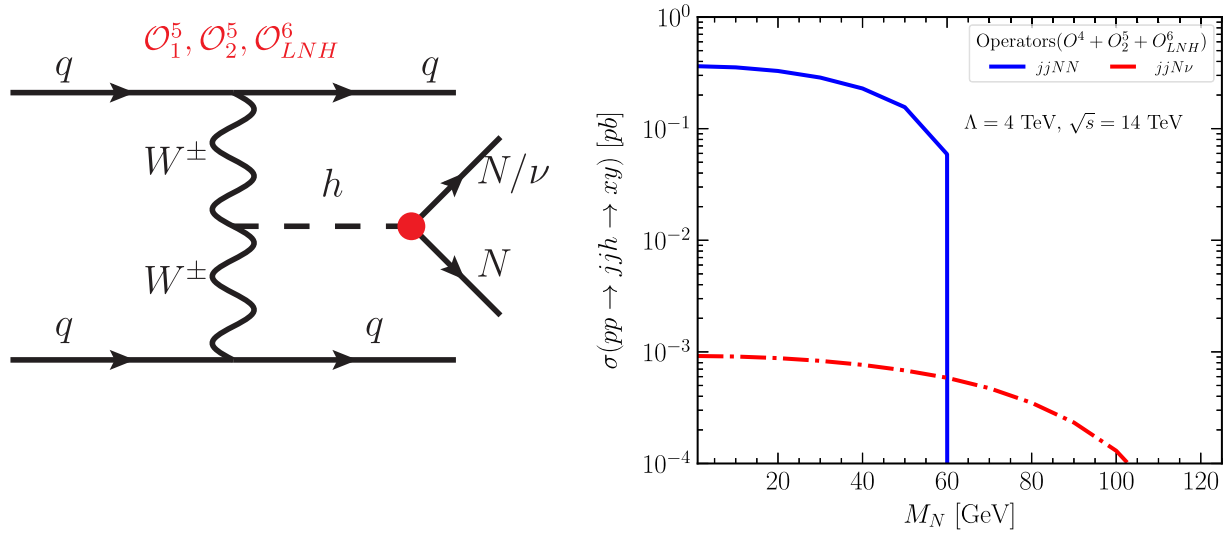

(a) (b)

FIG. 3. Left panel: the Feynman diagram with the corresponding relevant EFT operators that contribute to the processes $pp \to NNjj$ and $pp \to N\nu jj$. Right panel: the variation of a cross section with M_N. $\sigma(pp \to jjNN)$ is shown with the blue solid line and $\sigma(pp \to jjN\nu)$ is shown with the red dashed-dot line.

dashed-dotted line, respectively. Although the operator dependence remains same as of Fig. 1(b), the overall yield of the VBF Higgs production is lower than the gluon-gluon fusion Higgs production. This is reflected in the total cross section for this processes. The combine measurements in both these channels facilitate us to put suitable bounds on the EFT parameters.

$pp \to Zjj \to NN/\nu jj$.—Apart from the Higgs boson, the Z boson can also be produced in VBF mode and its subsequent decay can give rise to identical final states, i.e., $jjNN$ and $jjN\nu$. The Feynman diagram corresponding to these processes are shown in Fig. 4(a), where we mark the EFT operators that contribute to these processes. Along with the renormalizable neutral current, dimension five operator $\mathcal{O}_3^{(5)}$, dimension six operators such as $\mathcal{O}_{NH}$, $\mathcal{O}_{LNW}$, and $\mathcal{O}_{LNB}$ participate in these processes. However, the operator $\mathcal{O}_3^{(5)}$ is in general antisymmetric in the flavor space that vanishes if we consider Z-boson decay into the same flavor leptons.

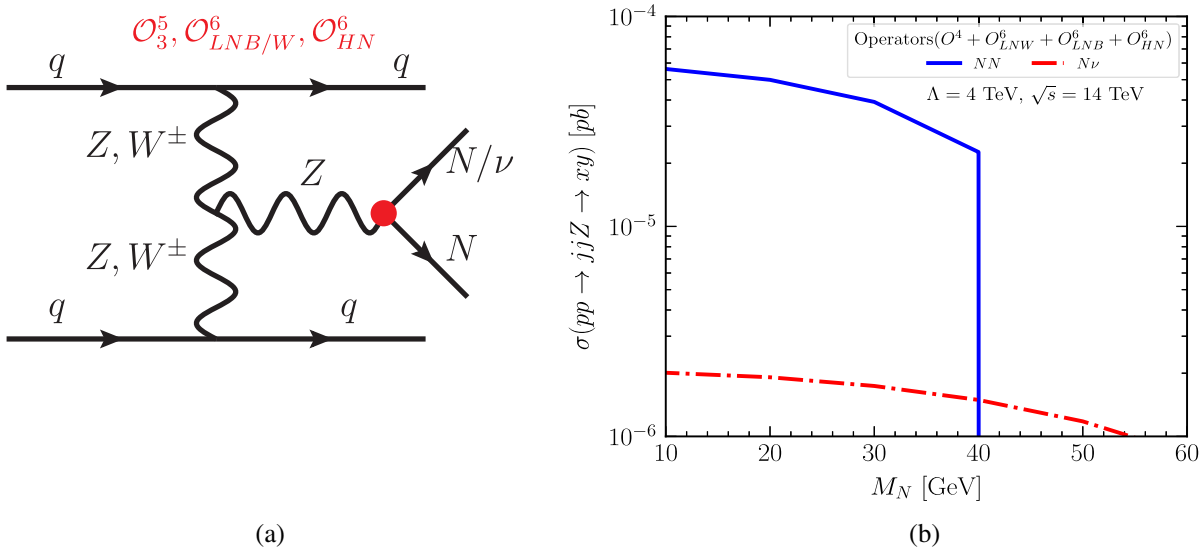

(a) (b)

FIG. 4. Left panel shows the Feynman diagram with the relevant contributing EFT operators for the VBF process $pp \to jjN\nu/jjNN$. Right panel shows the variation of cross section with RHN neutrino mass M_N. The blue and red lines represent $\sigma(pp \to jjNN)$ and $\sigma(pp \to jjN\nu)$, respectively.

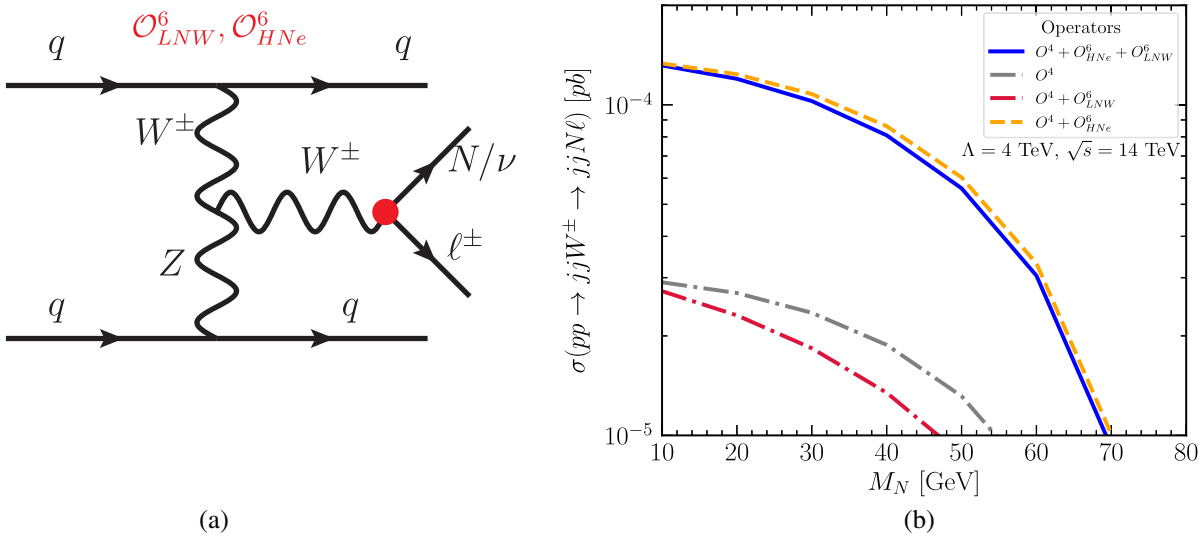

FIG. 5. Left panel shows the Feynman diagram with the relevant contributing operators for the VBF process $pp \to \ell^\pm Njj$. The right panel stands for variation of $\sigma(pp \to W^\pm jj \to \ell^\pm Njj)$ with M_N. The gray dot dashed, red dot dashed, orange dashed, and thick blue line stands for the contribution to this cross section coming from mixing only, mixing + $\mathcal{O}_{LNW}$, mixing + $\mathcal{O}_{HNe}$, and combining all the operators.

In Fig. 4(b), we demonstrate the corresponding cross sections. In case of $Z \to NN$, shown by the blue line, the cross section sharply falls down at the mass $\frac{M_Z}{2}$ after which the channel becomes kinematically forbidden. At dimension four the coupling $\mathcal{C}^Z_{\tilde{N}N}$ is primarily controlled by the quadratic power of mixing angle which is chosen to be 10^{-3}. Hence, with the renormalizable dimension four coupling, the cross section is highly suppressed $\mathcal{O}(10^{-18})$ pb. For $\mathcal{O}_{LNW}$ and $\mathcal{O}_{LNB}$, the Z boson couples to heavy neutrino pair via the gauge state W^3_μ and B_μ, respectively [see Eqs. (C4) and (C7) for details]. From Table IV one can observe a relative minus sign between the Wilson coefficient corresponding to these operators. This leads to destructive interference if we combine their effects in the cross section calculation. We like to point out that the cross section is larger if we consider only $\mathcal{O}_{LNB}$ or $\mathcal{O}_{LNW}$ instead of both $\mathcal{O}_{LNW}$ and $\mathcal{O}_{LNB}$ together. The $\mathcal{O}_{HN}$ operator significantly enhances the number of signal production as the vertex dependency coming from the $\mathcal{O}_{HN}$ operator is $\tilde{\theta}$ independent. The red dashed-dotted line of Fig. 4(b) highlights the cross section associated with the νNjj final state production via Z decay. Here also, the interference between the $\mathcal{O}_{LNB}$ and $\mathcal{O}_{LNW}$ exist similar to the case of $NNjj$. Finally the inclusion of $\mathcal{O}_{HN}$ increases the total cross section, but not much as the coupling coming from $\mathcal{O}_{HN}$ also has a mixing angle dependence.

$pp \to Wjj \to \ell Njj$.—The W boson is another SM field that can be produced via VBF process and leads to a single N production. The advantage of this process is that the RHN is produced along with a lepton that can be used to demarcate the signal from pure QCD events that in general appear during hadron collision. In Figs. 5(a) and 5(b), we present the Feynman diagram and the associated cross section for this process, respectively. At dimension four, the RHN production is only controlled by the mixing angle, and for $\tilde{\theta} = 10^{-3}$ one cannot achieve any appreciable cross section as represented by the gray dot-dashed line. As we include $\mathcal{O}_{LNW}$, the relative sign difference between $\mathcal{O}^4$ and $\mathcal{O}_{LNW}$ coupling leads to a destructive interference, which is shown by the red dot-dashed line. This situation significantly improves once we consider $\mathcal{O}_{HNe}$ instead of $\mathcal{O}_{LNW}$ as shown by the orange dashed line in Fig. 5(b). The contribution of $\mathcal{O}_{LNW}$ is suppressed by a factor $1/16\pi^2$ mentioned in Sec. II B, which leads to a lower contribution compared to that for the $\mathcal{O}_{HNe}$. Finally, the total contribution from all these three operators has been indicated by the blue line. The total contribution is slightly lower than that for $\mathcal{O}_{HNe} + \mathcal{O}^4$ due to the destructive interference as discussed above.

4. Drell-Yan production mechanism

The Drell-Yan process can serve as a viable production mode for N fields. Both the W and Z can be created in the s channel via parton parton collision. These s-channel heavy states will further decay and generate RHN fields. Coupling of N fields to Z boson is primarily regulated by the choice of mixing angle except for the $\mathcal{O}_{HN}$. Further there exists an experimental limit on $\mathrm{BR}(Z \to NN \to 2\nu + 2\gamma)$ as discussed in Sec. III, which restricts the choice of α_{HN}. Hence the expected cross section from this mode is significantly low and cannot be used to do meaningful phenomenological analysis. On the other hand the situation is relatively better in case of W-boson decay.

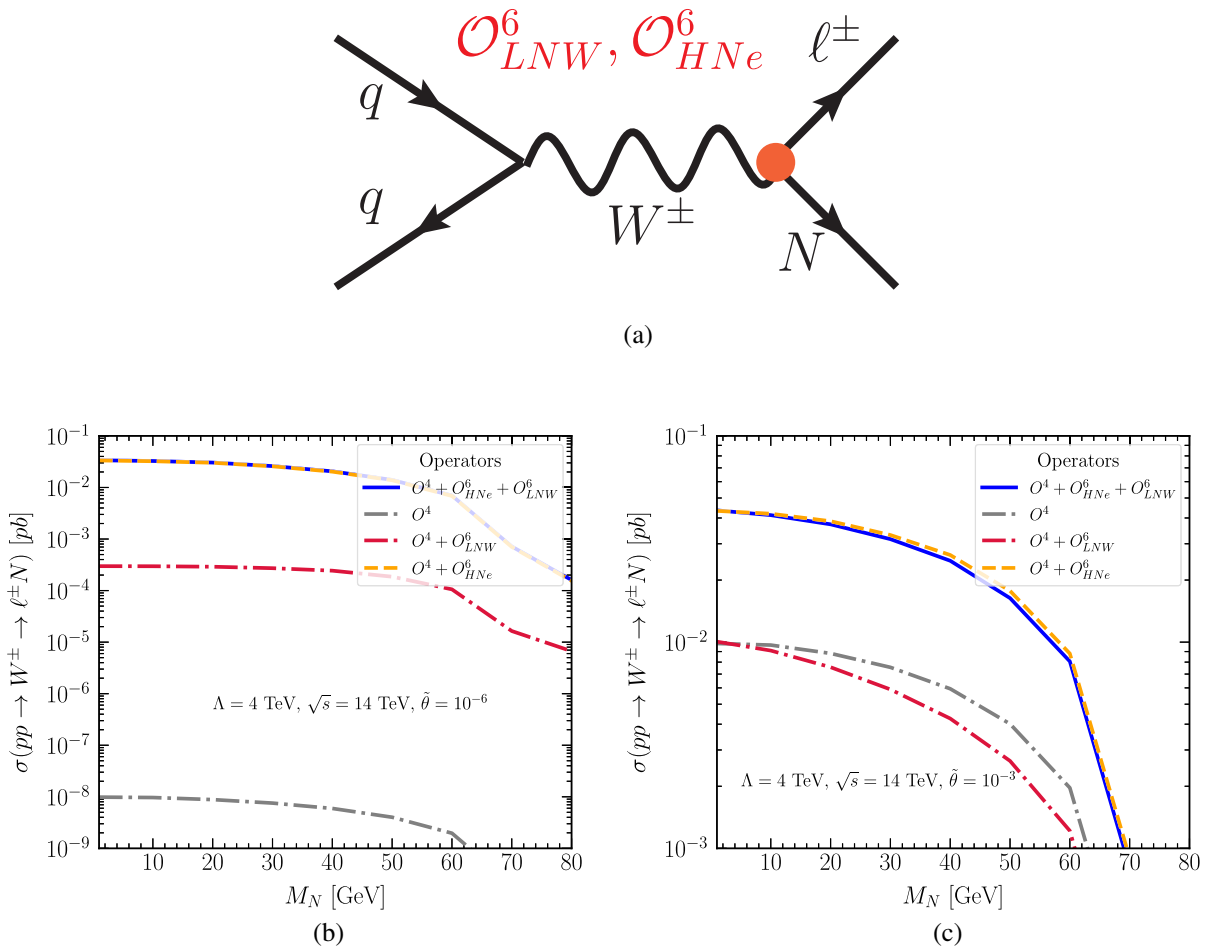

FIG. 6. (a) Feynman diagram and relevant operators for the process $pp \to W^\pm \to \ell^\pm N$. (b) and (c) are variations of $\sigma(pp \to W^\pm \to \ell^\pm N)$ with M_N for $\tilde{\theta} = 10^{-6}$ and 10^{-3}, respectively. In each panel the gray dot-dashed, red dot-dashed, orange dashed, and thick blue line stand for the contribution to this cross section coming from mixing only, mixing + $\mathcal{O}_{LNW}$, mixing + $\mathcal{O}_{HNe}$, and combining all the operators.

In Fig. 6(a), we present the relevant Feynman diagram for $pp \to W^* \to \ell N$ that arises from the operators, $\mathcal{O}_{HNe}$, $\mathcal{O}_{LNW}$ as well as the $d = 4$ charge current operator. The individual effects of these operators are illustrated in Figs. 6(b) and 6(c). We show the cross section for two values of $\tilde{\theta} = 10^{-6}$ [Fig. 6(b)], 10^{-3} [Fig. 6(c)]. For $\tilde{\theta} = 10^{-6}$, the effect of the $d = 4$ operator is suppressed. However, for $\tilde{\theta} = 10^{-3}$ it has notable contribution, which enhances the cross section as evident from Fig. 6(c). As we include $\mathcal{O}_{LNW}$, the relative sign difference between $\mathcal{O}^4$ and $\mathcal{O}_{LNW}$ coupling leads to a destructive interference, which is shown by the red dot-dashed line. For $\tilde{\theta} = 10^{-3}$ it is more prominent as the contribution of $\mathcal{O}^4$ become comparable to that of $\mathcal{O}_{LNW}$. Finally, the total contribution from all the three operators has been indicated by the blue line. It is evident from Figs. 6(b) and 6(c) that the operator $\mathcal{O}_{HNe}$ primarily controls the total cross section. For $\tilde{\theta} = 10^{-3}$, the total contribution is slightly lower than that for $\mathcal{O}_{HNe} + \mathcal{O}^4$ due to the relative sign difference in the effective coupling.

B. Electron proton collider

We consider the proposed $e^- p$ collider, FCC-eh [74], which will operate with a 60 GeV e^- beam and 50 TeV proton beam providing a c.m. energy 3.46 TeV. Here we set the cutoff scale as $\Lambda = 1.5$ TeV.

1. $e^- p \to jN$

Production of RHN in association with a jet arises via two channels. One is the four Fermi interaction and the other is W mediated process. Thus cross section for this process is governed by the $d = 4$ operator and as well as $d = 6$ operators such as $\mathcal{O}^6_{duNe}$, $\mathcal{O}^6_{QuNL}$,$\mathcal{O}^6_{LNQd}$,$\mathcal{O}^6_{LdQN}$, $\mathcal{O}^6_{HNe}$, and $\mathcal{O}^6_{LNW}$, which are shown in Figs. 7(a) and 7(b). In Fig. 7(c), the gray dot-dashed line indicates the $d = 4$ contribution which is mixing suppressed ($\tilde{\theta} = 10^{-3}$). The red dotted line shows the contribution from the W mediated process including the effect of $\mathcal{O}^6_{HNe}$ and $\mathcal{O}^6_{LNW}$. The blue line represents the total contribution after

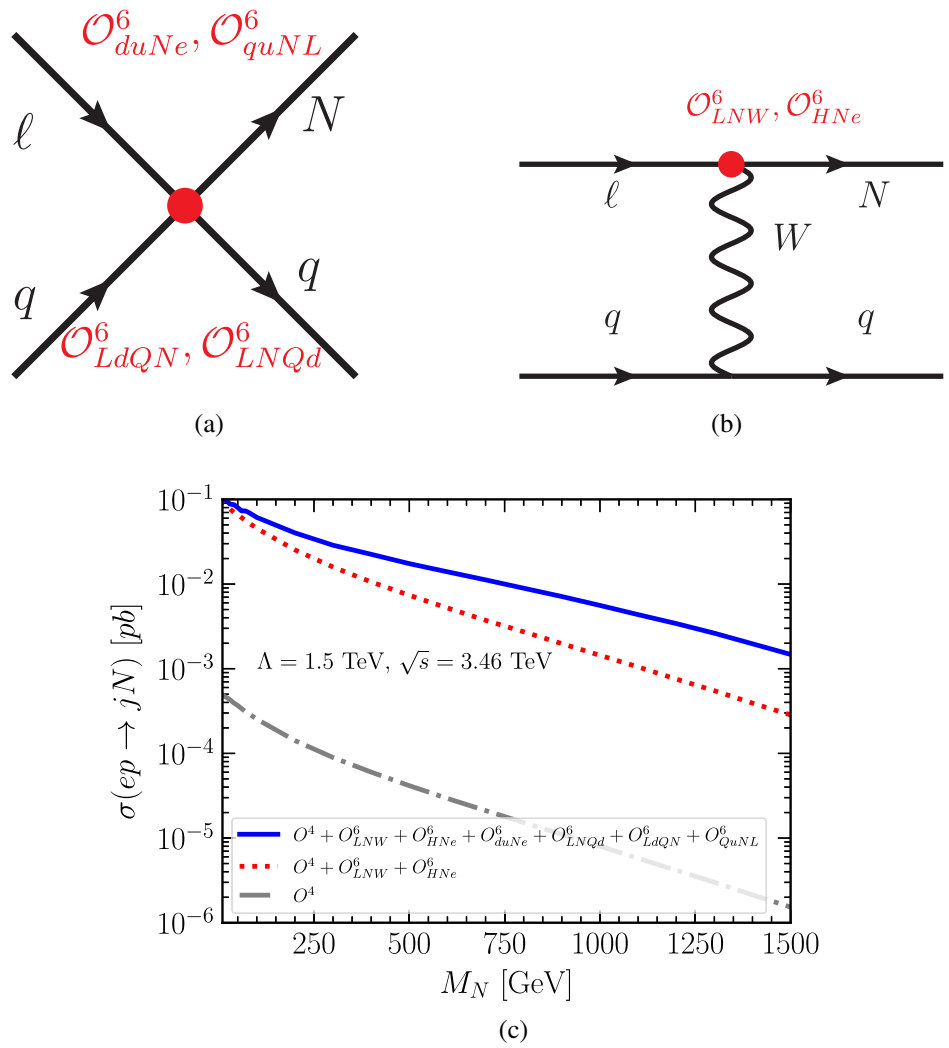

FIG. 7. Upper panel: the Feynman diagram and the relevant operators for the process $e^- p \to jN$. Bottom panel: variation of cross section for the process $e^- p \to jN$ as a function of the sterile neutrino mass M_N. The gray dot-dashed, red dotted, and blue thick lines stand for the contribution to the cross section coming from mixing only, mixing + $\mathcal{O}_{LNW} + \mathcal{O}_{HNe}$, and combination of all the operators, respectively.

including four Fermi interaction. As can be seen, large a cross section $\sim\mathcal{O}(100$ fb) is possible to obtain for $M_N \sim 50$ GeV.

2. $e^- p \to j + 3N/j + 2N + \nu$

Production of h/Z with $j + N$ can take place via the two diagrams shown in Figs. 8(a) and 8(b). These diagrams involve the $d = 6$ operator at two vertices, which can lead to $1/\Lambda^x$ with $x > 4$ term in cross section, which can also arise at the $d > 6$ level. However, we restrict our calculation up to the $1/\Lambda^4$ term in the cross section and ignore the higher power. The cross section for $e^- p \to j + 3N$ can be around 0.1 fb, which yields $\sim$100 events with 1000 fb^{-1} luminosity. However, for $e^- p \to j + 2N + \nu$ at most one event can be achieved with 1000 fb^{-1} luminosity. In this scenario, the Higgs mediated process is dominant over the Z-boson mediated process. Upon production the Higgs field further decays to $N\nu$. The relevant coupling corresponding to $h \to \nu N$ is dependent on the mixing angle $\tilde{\theta}$, which suppresses the total cross section of the $e^- p \to j + 2N + \nu$ channel.

C. Electron positron collider

We now discuss a different production mechanism of the N fields for the future electron positron collider. We choose two different c.m. energies $\sqrt{s} = 91$ GeV and 3 TeV, where the corresponding cutoff scales Λ are set to be 500 GeV and 4 TeV, respectively.

1. $e^+ e^- \to NN$

The four Fermi interaction, s-channel $Z/h/\gamma$ mediated diagram, and t-channel $W^\pm$ mediated diagram lead to pair

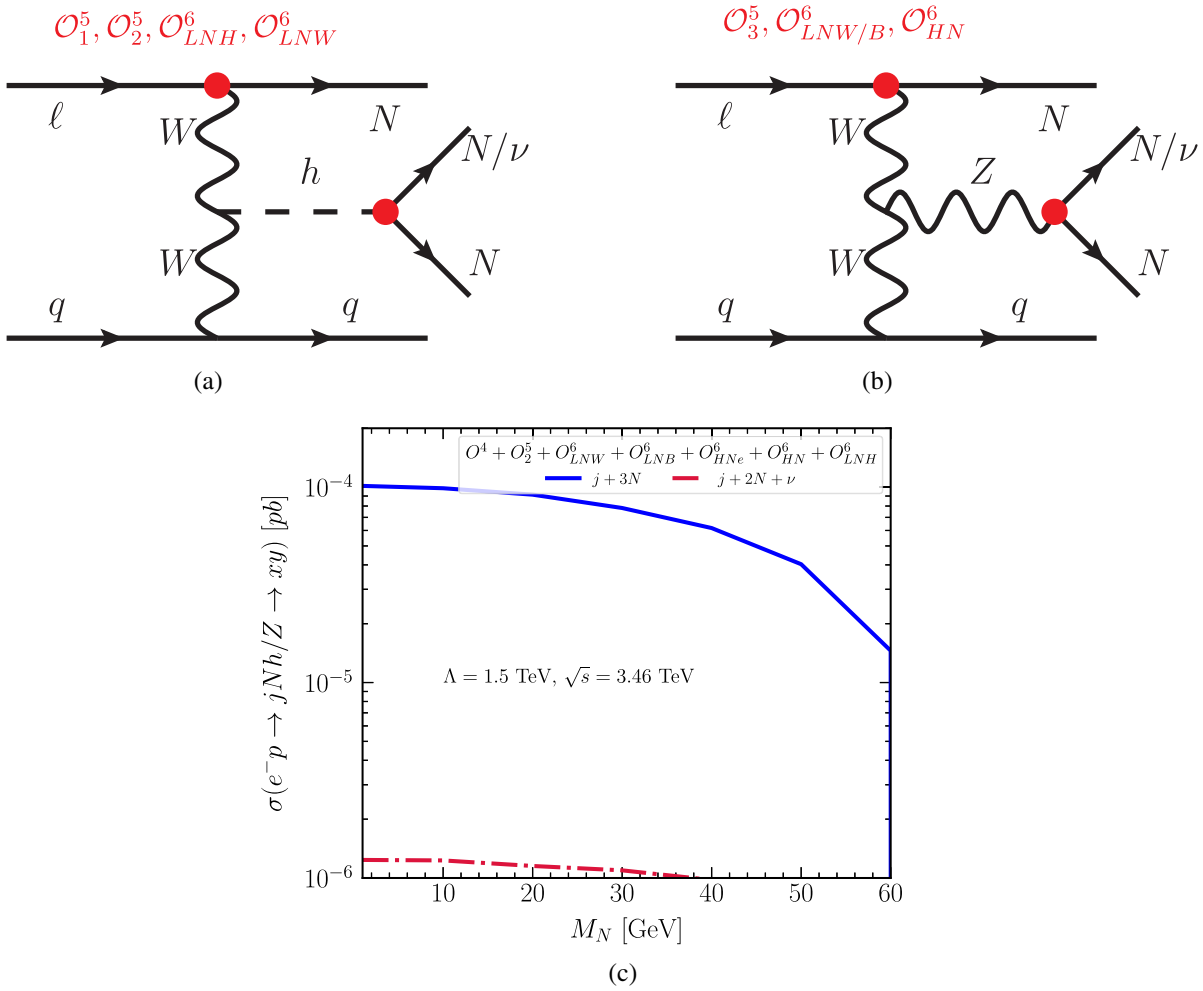

FIG. 8. Upper panel: the Feynman diagram and the relevant operators for the process $e^- p \to (j + 3N)/(j + 2N + \nu)$. The cross section for the process $e^- p \to j + 3N$. Bottom panel: variation of cross section corresponding to these processes as a function of the RHN mass M_N. The blue thick and red dot-dashed lines signify the cross section corresponding to the process $e^- p \to j + 3N$ and $e^- p \to j + 2N + \nu$, respectively. The cross section is evaluated while taking into account all relevant operators.

production of RHN at e^+e^- collider. The $W^\pm$ mediated diagram receives extra $1/\Lambda^2$ suppression as it has two EFT vertices and hence it is ignored. On the other hand, the contribution coming from the s-channel Higgs mediated process can also be ignored due to the smallness of $\mathcal{C}^h_{e^+e^-}$ coupling. Production cross section for this process is governed by the operators $\mathcal{O}^6_{eN}$, $\mathcal{O}^6_{LN}$, $\mathcal{O}^6_{LNW/B}$, $\mathcal{O}^{(5)}_3$, and $\mathcal{O}^6_{HN}$, which is shown in Figs. 9(a) and 9(b). In Figs. 9(c) and 9(d) we illustrate the cross section for two different c.m. energies $\sqrt{s} = 91$ GeV and $\sqrt{s} = 3$ TeV, the corresponding cutoff scales are $\Lambda = 500$ GeV and $\Lambda = 4$ TeV. Active sterile mixing is set to be $\tilde{\theta} = 10^{-3}$, which makes the contributions of the renormalizable interaction terms (denoted by $\mathcal{O}^4$) suppressed.

For $\sqrt{s} = 91$ GeV, Z-mediated process is dominant where the contribution from the operator $\mathcal{O}^6_{HN}$ plays a major role for $e^-e^+ \to NN$, as this interaction is not $\tilde{\theta}$ suppressed. Whereas, $\mathcal{O}^6_{LNW}$ and $\mathcal{O}^6_{LNB}$ involve $\tilde{\theta}$ dependency. Contrary to that, for $e^-e^+ \to N\nu$, the contribution from $\mathcal{O}^6_{HN}$ is $\tilde{\theta}$ suppressed and from the other two $d = 6$ operators are independent of $\tilde{\theta}$. The contribution from four Fermi operators are $\simeq 1$ pb. For $\sqrt{s} = 3$ TeV, Contribution from four Fermi operators are dominant.

2. $e^+e^- \to 2N + 2\nu/3N + \nu$

Figure 10(a) shows the Feynman diagram and corresponding operators for this process. As this diagram involves more than one $d = 6$ vertex, in the amplitude level there exist terms with $1/\Lambda^n$, $n \geq 3$. However, for simplicity we assume such a contribution to be zero [75]. Figure 10(b) shows the production rate for the processes $e^+e^- \to 2N + 2\nu$ and $e^+e^- \to 3N + \nu$ by the blue and red dashed lines, respectively. For $2N + 2\nu$, $\mathcal{C}^W_{\ell\nu}$ coupling is involved in two vertices and for $3N + \nu$, one $\mathcal{C}^W_{\ell\nu}$ and one

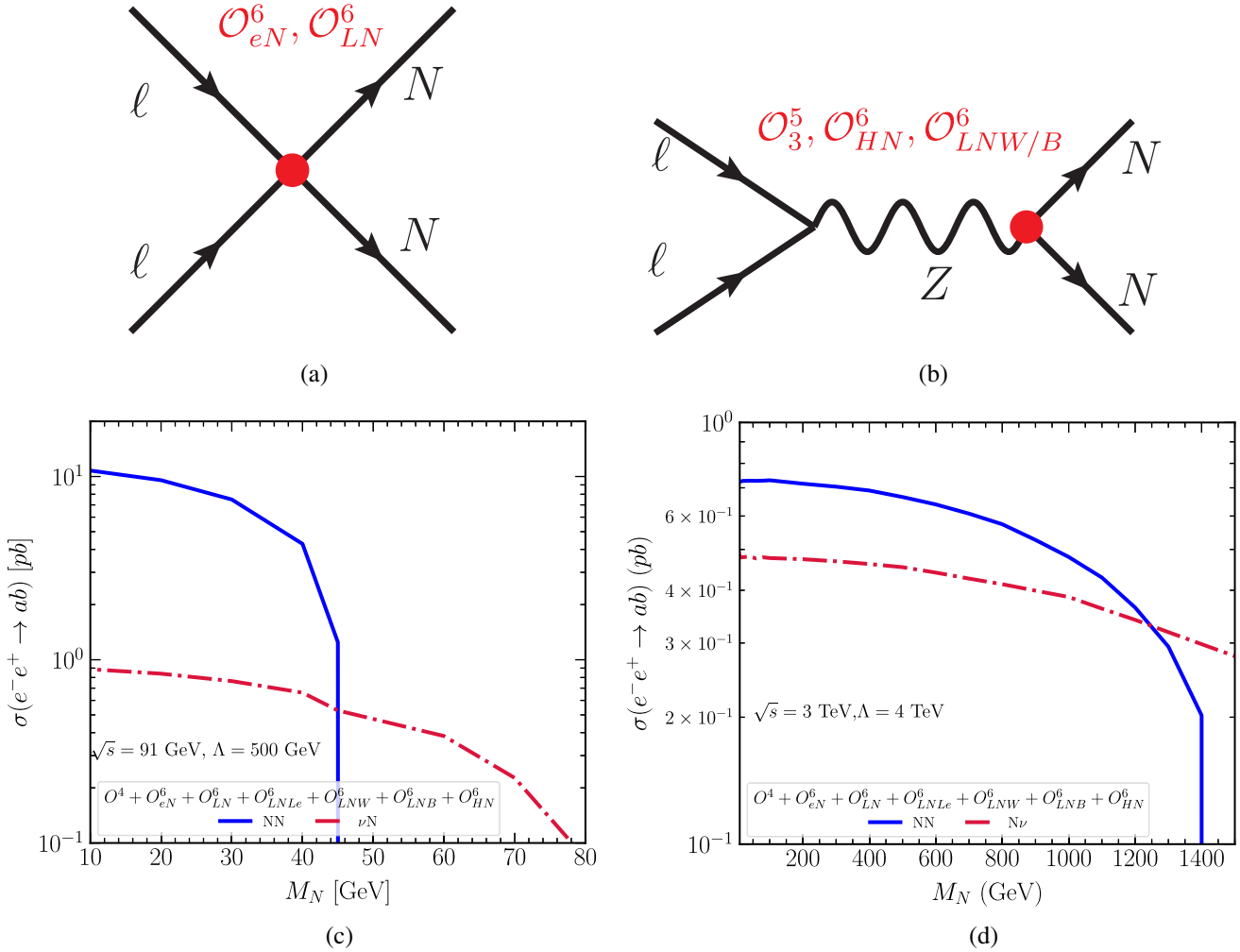

FIG. 9. In the upper panel we present the Feynman diagram and the relevant operators for the process $e^+e^- \to NN/N\nu$. In the lower panel we show the cross section for the process $e^+e^- \to NN/N\nu$ with $\sqrt{s} = 91$ GeV (c) and $\sqrt{s} = 3$ TeV (d). The blue thick line and red dot-dashed lines represent the process $e^+e^- \to NN$ and $e^+e^- \to N\nu$, respectively.

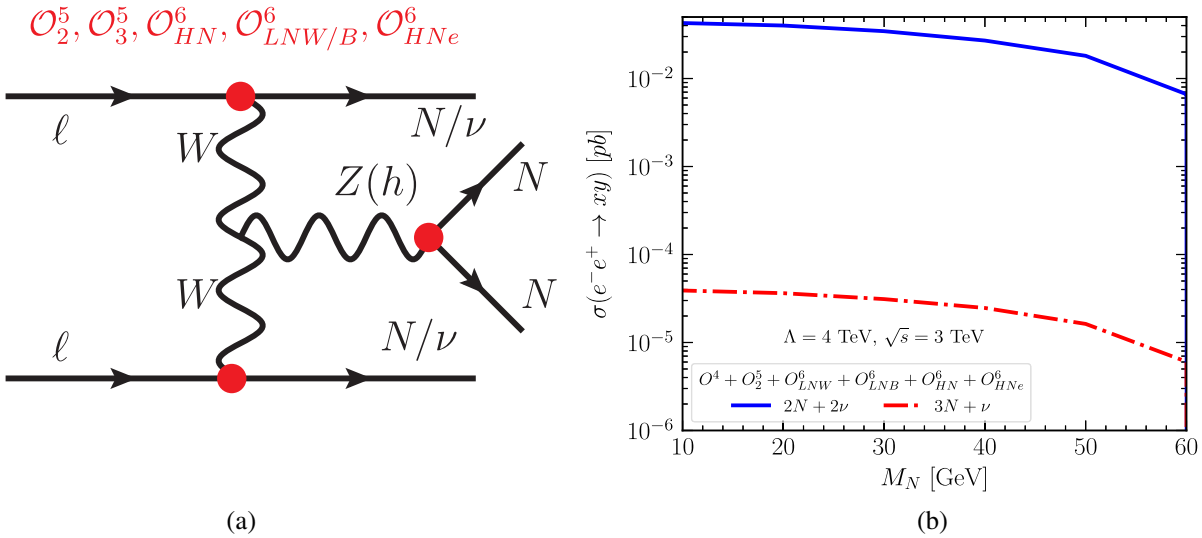

FIG. 10. In (a) we show the Feynman diagram and in (b) the cross section for the process $e^+e^- \to 2N + 2\nu$ and $e^+e^- \to 3N + \nu$. The blue thick and red dot dashed lines represent $e^+e^- \to 2N + 2\nu$ and $e^+e^- \to 3N + \nu$ processes, respectively.

$\mathcal{C}^W_{\ell N}$ couplings are involved. For $\mathcal{C}^W_{\ell\nu}$ coupling, the $\mathcal{O}^4$ contribution, which is independent of $\tilde{\theta}$, is dominant compared to the $\mathcal{O}^6$ contribution. The presence of extra $\mathcal{C}^W_{\ell\nu}$ coupling at one vertex makes the cross section for the $2N + 2\nu$ final state larger compared to that of $3N + \nu$.

V. THE RIGHT-HANDED NEUTRINO DECAY MODES

Depending on the mass, the sterile neutrino can decay either via two body or three body modes. If we only consider the renormalizable part of the effective Lagrangian heavy neutrinos decays to $W\ell$, νZ, and νh modes through the active-sterile mixing if it has sufficient mass. These decay modes receive additional contributions if we take into account the dimension five and dimension six operators. In Table VIII, we present various two body decay modes as well as the operators that would contributes to each of these modes. In principle, $N_i \to N_j h/N_j Z/N_j\gamma$ (where $i \neq j$) mode is also possible. But for simplicity we have chosen degenerate mass values for all the RHNs. Hence, those decay modes are kinematically disallowed. For the decay modes such as $N_i \to \nu_j Z/\nu_j h/\nu_j\gamma$ both $i = j$ and $i \neq j$ scenarios are possible and the operators that would contribute to these modes are mentioned in Table VIII. However, it is important to point out that the $\mathcal{O}^{(3)}_5$ operator is antisymmetric in flavor space. Hence it would not contribute to $N_i \to \nu_i Z/\nu_i\gamma$ modes. All the other operators are symmetric in the flavor space and participate in both the $i = j$ and $i \neq j$ scenarios. There exists a great volume of work that has studied possible phenomenological aspects of these decay modes, and interested readers can consult this in Ref. [35] for more comprehensive discussions. For completeness, here we briefly discuss the two body decay width and what role the different operators play in the corresponding decay width calculation.

A. $\Gamma(N_i \to \ell_j W)$

We begin our discussion with the $N_i \to \ell_j W$ channel, which gets contributions from the standard renormalizable charged current interaction and which depends on active-sterile mixing as well as dimension six operators $\mathcal{O}_{HNe}$ and $\mathcal{O}_{LNW}$. From our discussion on Sec. II B, one can see that the coupling $\mathcal{C}^{W_\mu}_{\ell N}$ does not receive any modification from dimension five operators. On the other hand in dimension six this coupling does alter and one can find the explicit form of this coupling in Table IV. However, in general the operator $\mathcal{O}_{LNW}$ is a loop mediated operator and the Wilson coefficient corresponding to this is suppressed by $\frac{1}{16\pi^2}$. Hence the contribution coming from this is very minimal with respect to both the $\mathcal{O}_{HNe}$ and $\tilde{\theta}$. Hence we can safely ignore its effect. With this assumption, the partial decay width of the above mentioned process is

$$\begin{aligned}\Gamma(N_i \to \ell_j W) = \frac{g^2}{64\pi M_N M_W^2}\{&(|A|^2 + |B|^2)(M_W^2(M_{\ell_j}^2 + M_N^2) \\ &+ (M_{\ell_j}^2 - M_N^2)^2 - 2M_W^4) \\ &- 12\mathrm{Re}[A^* B] M_{\ell_j} M_N M_W^2\} \\ &\times \lambda^{\frac{1}{2}}\left(1, \frac{M_{\ell_j}^2}{M_N^2}, \frac{M_W^2}{M_N^2}\right),\end{aligned} \tag{5.1}$$

where parameter A and B is defined in the following fashion

$$A = \tilde{\theta}, \qquad B = \frac{v^2 \alpha_{HNe}}{\Lambda^2}.$$

The left panel of Fig. 11 shows the decay width as a function of sterile neutrino mass M_N. For plotting purpose we fixed the cutoff scale at 4 TeV and chose the range of M_N from 200 GeV to 1 TeV. The red dashed line and the brown dotted line represents sole contributions from renormalizable charged current interaction with $\tilde{\theta} = 10^{-6}$ and $\tilde{\theta} = 10^{-3}$, respectively. On the other hand the black dashed-dotted curve highlight the effect of $\mathcal{O}_{HNe}$. The blue thick line shows the decay width when one accounts both the renormalizable part ($\tilde{\theta} = 10^{-3}$) and dimension six operator. From the left panel of Fig. 11, one can see the dominant contribution comes from the dimension six operator.

TABLE VIII. Different possible two body decay modes along with the operators that can contribute to these decays.

Decay	Contributing operators
$\Gamma(N_i \to \ell_j W) :=$	$\mathcal{L}_{CC}$, $\mathcal{O}_{HNe}$, $\mathcal{O}_{LNW}$
$\Gamma(N_i \to \nu_j Z) :=$	$\mathcal{L}_{NC}$, $\mathcal{O}^{(5)}_3$, $\mathcal{O}_{HN}$, $\mathcal{O}_{LNB}$, $\mathcal{O}_{LNW}$
$\Gamma(N_i \to \nu_j h) :=$	$\mathcal{L}_{yuk}$, $\mathcal{O}^{(5)}_1$, $\mathcal{O}^{(5)}_2$, $\mathcal{O}_{LNH}$
$\Gamma(N_i \to \nu_j\gamma) :=$	$\mathcal{O}^{(5)}_3$, $\mathcal{O}_{LNW}$, $\mathcal{O}_{LNB}$

B. $\Gamma(N_i \to \nu_j h)$

In case of N decaying to the νh mode, the partial width is dependent on the mixing angle between active and sterile neutrinos and also on the dimension six operator $\mathcal{O}_{LNH}$. In principle the operators $\mathcal{O}^{(5)}_1$ and $\mathcal{O}^{(5)}_2$ can also contribute to this decay mode. However, from Table II one can notice that the relevant coupling coming from these operators are $\tilde{\theta}$ suppressed. Hence we can ignore their effects. The definition of the mixing angle varies with the mass dimension of underlying EFT. For a better understanding, remember that, up to dimension five, the mixing angle is defined as $M_N^{-1}\frac{Y_\nu v}{\sqrt{2}}$ which is independent of EFT parameters. In dimension six the operator $\mathcal{O}_{LNH}$ modifies the

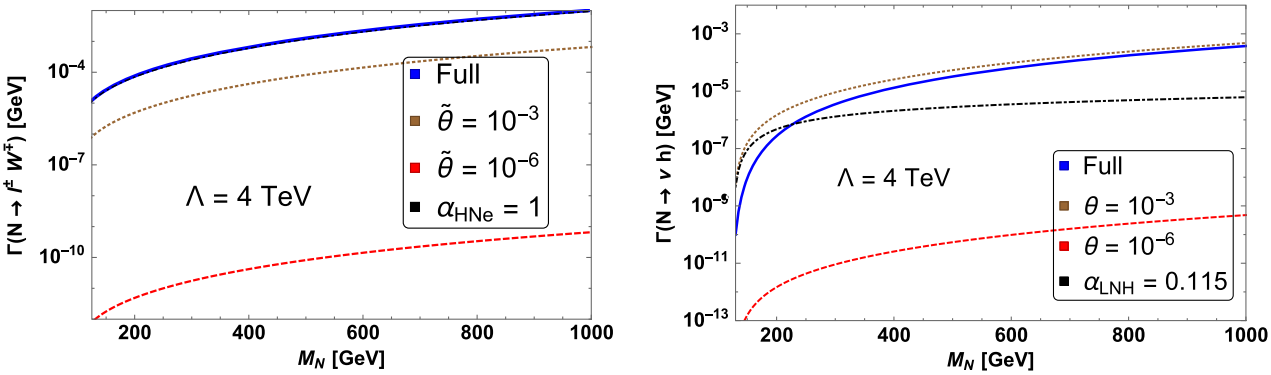

FIG. 11. The partial decay width correspond to $\Gamma(N \to \ell^{\pm} W^{\mp})$ (left) and $\Gamma(N \to \nu h)$ (right) respectively. For both these cases the cutoff scale is set at 4 TeV. See text for details.

definition of the mixing angle as discussed in Eq. (2.12) and the mixing angle θ is replaced with $\tilde{\theta}$. To make a suitable comparison between the two different dimensions, here we write down the explicit part of $\tilde{\theta}$, where θ to be $M_N^{-1}\frac{Y_\nu v}{\sqrt{2}}$ and the additional part arises from $\mathcal{O}_{LNH}$. The partial decay width for the process can be written in the following fashion:

$$\Gamma(N_i \to \nu_j h) = \frac{|A|^2}{32\pi M_N^3}(M_N^2 - M_h^2)^2, \tag{5.2}$$

where the coefficient A is expressed as

$$A = \left(\frac{3v^2}{2\sqrt{2}\Lambda^2}\alpha_{LNH} - \frac{\theta M_N}{v}\right). \tag{5.3}$$

To realize the effect of individual parameters we refer to the right panel of Fig. 11. The brown dotted and the black dash-dotted lines represent the effects of θ and α_{LNH}, respectively. The red dashed line shows the partial decay width if the mixing angle is 10^{-6}. The relative minus sign in the definition of A can be understood as the apparent destructive interference that appears in the full decay width calculation and is represented as the thick blue curve in Fig. 11 (right-hand side), which accounts for both the renormalizable part ($\theta = 10^{-3}$) and dimension six operator α_{LNH}.

C. $\Gamma(N_i \to \nu_i Z)$ & $\Gamma(N_i \to \nu_i \gamma)$

We now turn our attention to RHN decays to νZ and $\nu\gamma$ modes. In the absence of the EFT operators it can only decay to the νZ channel, and the partial width corresponding to this is regulated by the mixing angle. In the dimension five scenario the operator $\mathcal{O}_3^{(5)}$ invokes a new decay mode involving a photon besides modifying the coupling $\mathcal{C}^{Z_\mu}_{(\bar{\nu}N+\bar{\nu}N)}$. However, this operator is antisymmetric in the flavor space and does not participate in the N_R decay into the same flavor SM neutrino. For different flavor SM neutrino, the operator $\mathcal{O}_3^{(5)}$ does contribute, but the relevant coupling is mixing angle suppressed (see Table II for details.) Hence we can ignore this operator for present calculation. At the dimension six level, νZ receives a contribution from the operators $\mathcal{O}_{HN}$, $\mathcal{O}_{LNB}$, $\mathcal{O}_{LNW}$. But one can safely ignore $\mathcal{O}_{HN}$ as its effect in $\mathcal{C}^6_{Z_\mu(\bar{\nu}N+\bar{N}\nu)}$ coupling is negligible due to small mixing angle and $\frac{1}{\Lambda^2}$ factor. The other two operators can provide appreciable contribution in the decay width and in the following we present the definite formula for this case

$$\begin{aligned}\Gamma(N_i \to \nu_j Z) = \frac{(M_N^2 - M_Z^2)^2}{128\pi c_w^2 M_Z^2 M_N^3}\{&g^2|\tilde{\theta}|^2(M_N^2 + 2M_Z^2) \\ &+ 64c_w^2 M_Z^2|A|^2 + (M_Z^2 + 2M_N^2) \\ &+ 48gc_w M_N M_Z^2 \mathrm{Re}[\tilde{\theta}^* A]\}.\end{aligned} \tag{5.4}$$

The dimension six part is expressed by introducing the new parameter A, which is defined as

$$A = \frac{c_w \alpha_{LNW} v}{\sqrt{2}\Lambda^2} - \frac{s_w \alpha_{LNB} v}{\sqrt{2}\Lambda^2}.$$

The relative minus sign in the above expression can be understood from the mass basis definition of the Z boson and photon. In the SM, the $Z_\mu = c_w W_\mu^3 - s_w B_\mu$ and $A_\mu = s_w W_\mu^3 + c_w B_\mu$ where W_μ^3 and B_μ are fields correspond to T_3 and Y generators. The relative minus sign in the mass relation is responsible for the minus sign in A. Similarly, for the $\nu\gamma$ mode we present the explicit dependence of dimension five and dimension six operators in Eq. (5.5).

$$\Gamma(N_i \to \nu_j \gamma) = \frac{M_N^3}{\pi}(|A|^2 + |B|^2), \tag{5.5}$$

where $A = -\frac{c_w}{\Lambda}(\tilde{\theta}\alpha_3^{(5)}) + \frac{c_w v}{\sqrt{2}\Lambda^2}\alpha_{LNB} + \frac{s_w v}{\sqrt{2}\Lambda^2}\alpha_{LNW}$,

$B = \frac{c_w}{\Lambda}(\tilde{\theta}^* \alpha_5^{(3)})$.

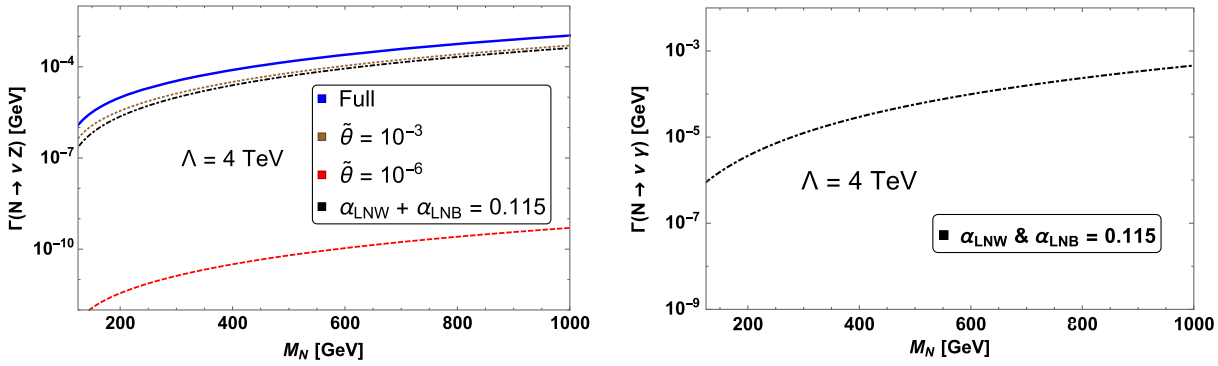

FIG. 12. The partial decay width correspond to $\Gamma(N \to \nu Z)$ (left) and $\Gamma(N \to \nu\gamma)$ (right), respectively. For both these cases the cutoff scale is set at 4 TeV. The value for α_{LNW} and α_{LNB} is consistent with the current experimental limits.

Here also, we set $\alpha_5^{(3)}$ to b1e zero for the reason discussed above. In Fig. 12, we represent the upshot of each operators and mixing angle along with their combine role. In left panel of Fig. 12 we plot the partial decay width of $N \to \nu Z$ mode. The red dashed line shows the contributions coming from $\tilde{\theta} = 10^{-6}$. The mixing angle 10^{-3}, which is shown as a brown dotted line in this figure, has the dominant contribution over the entire range of the chosen M_N. The effects of dimension six terms shown as a dot-dashed black curve are subdominant but have the same order of magnitude as with the mixing angle 10^{-3}. The blue line shows the full width for $N \to \nu Z$, which is calculated while taking into account both dimension six and mixing angle ($\tilde{\theta} = 10^{-3}$) contributions. The plot on the right side of Fig. 12 shows the decay width for $N \to \nu\gamma$ channel and it is entirely dependent on the operators $\mathcal{O}_{LNW}$ and $\mathcal{O}_{LNB}$. In both cases the cutoff scale is at 4 TeV.

We conclude our discussion on the two body decay modes while presenting the corresponding branching ratio in Fig. 13 (left panel). As expected the ℓW mode, which is represented by the thick blue line, is dominated in the entire range of mass. The νZ and $\nu\gamma$ channels are shown as red dashed and black dot-dashed lines, respectively, and their corresponding BR is less than 10%. Furthermore the BR of νZ is always greater than $\nu\gamma$ as it receives additional contribution from mixing angle $\tilde{\theta}$. The BR of νh, which is shown as a gray dotted line, remains the minimum for the entire mass range. For comparison, in the right panel of Fig. 13, we present the branching ratio corresponding to the only renormalizable part of the Lagrangian. We have considered two values of mixing angle $\tilde{\theta} = 10^{-3}$ and 10^{-6}. The pattern of the plot remain unaffected for the choice of mixing angle as the BR of each individual modes solely depend on their respective kinematic factor. Here also, the ℓW mode, which is illustrated as a blue thick line, is dominated in the entire range of RHN mass. However with respect to the EFT counterpart, the BR of the $N \to \ell W$ channel is relatively small. As a consequence the BR of νh and νZ mode can achieve around 20% value for $M_N \gtrsim 500$ GeV. The $\nu\gamma$ curve is absent in this plot as the N field cannot decay into this mode as it only arises in the EFT framework.

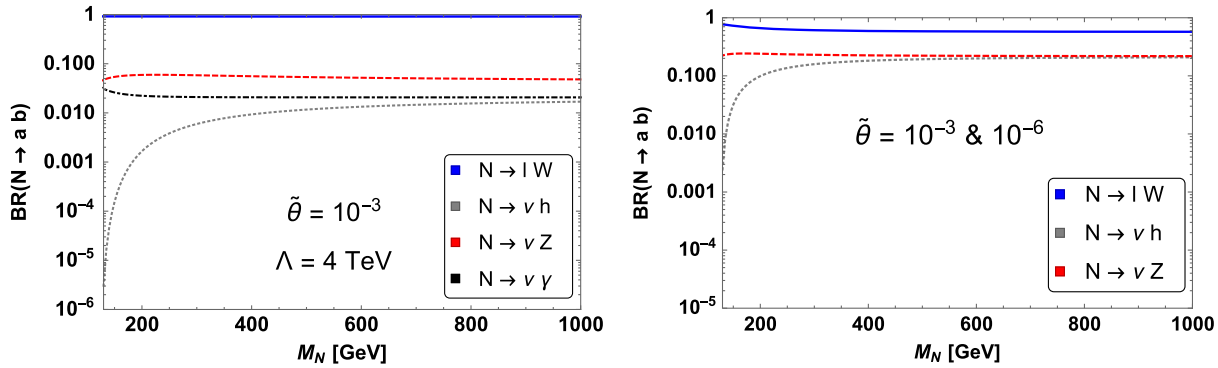

FIG. 13. The branching ratio corresponding to different two body decay modes for the M_N mass range from 200 GeV to 1 TeV. In the left panel, we show branching ratio correspond to N_R-EFT framework up to $d = 6$ where the cutoff scale Λ is set to be 4 TeV and the mixing angle $\tilde{\theta} = 10^{-3}$. In the right panel we show the branching ratio of possible two body decay modes if we only consider the renormalizable part of the Lagrangian. This plot correspond to both the mixing angle $\tilde{\theta} = 10^{-3}$ and 10^{-6}, respectively. See text for details.

D. Three body decay modes

Now we turn our attention to the mass range where $M_N \leq M_W$. Hence the only allowed two body decay mode is $\Gamma(N_i \to \nu_j \gamma)$. Having said that, the operators that control this process are loop suppressed. As a result the width corresponding to this channel is understandably low, and we safely choose the corresponding BR value to be 5% in the mass range $10\,\text{GeV} \leq M_N \leq 80\,\text{GeV}$. Instead, this particular mass range motivates us to consider different three body decay modes that can be perpetrated either via off shell decay of different SM states or via contact interactions. In the following we would discuss this in more detail.

Considering operators up to $d = 5$ the three body decay modes are primarily mediated via the off shell decay of SM electroweak gauge bosons. In principle the RHN field can also decay into three body modes via off shell Higgs boson decay $N_i \to \nu_j h^*$. Upon production, this off shell Higgs boson h^* can decay into SM light fermions. However the couplings between the Higgs boson and SM fermions are dependent on the light fermion masses, which have negligible values. As a result, the partial width corresponds to N field decay via off shell Higgs boson is minuscule and can be neglected in practical calculation. In the case of dimension six one can write different four Fermi operators. The contact interaction coming from these operators would significantly modify various three body decays. In Table IX, we illustrate these decay modes along with the Lagrangian term that will contribute to those processes. The latin indices i, j, and k denote the flavor of the daughter leptons and the greek indices α, β, and γ are restricted for quark labels. The term $\mathcal{L}_{CC}$ stands for the W-boson mediated decay and $\mathcal{L}_{NC}$ denotes the decay via Z boson. In contrast to Tables II, IV, and V, one can notice that we have only shown certain operators responsible for these decay modes. The rationale behind this choice will be argued for individual scenarios in the subsequent discussion.

TABLE IX. Various three body decay modes along with the operators that contribute to the process. Depending upon the final state flavor label of the particles, the operators might vary.

Decay	Contributing operators
$\Gamma(N_i \to \ell_j \ell_k \nu_k; j \neq k) :=$	$\mathcal{L}_{CC}$, $\mathcal{O}_{HNe}$, $\mathcal{O}_{LNLe}$
$\Gamma(N_i \to \nu_j \ell_k \ell_k; j = k) :=$	$\mathcal{L}_{CC}$, $\mathcal{L}_{NC}$, $\mathcal{O}_{HNe}$, $\mathcal{O}_{LNLe}$
$\Gamma(N_i \to \nu_j \ell_k \ell_k; j \neq k) :=$	$\mathcal{L}_{NC}$, $\mathcal{O}_{LNLe}$
$\Gamma(N_i \to \ell_j u_\alpha \bar{d}_\beta; \alpha \neq \beta) :=$	$\mathcal{L}_{CC}$, $\mathcal{O}_{HNe}$, $\mathcal{O}_{QuNL}$, $\mathcal{O}_{Nedu}$, $\mathcal{O}_{LNq}$, $\mathcal{O}_{LdqN}$
$\Gamma(N_i \to \nu_j u_\alpha \bar{u}_\alpha) :=$	$\mathcal{L}_{NC}$, $\mathcal{O}_{QuNL}$
$\Gamma(N_i \to \nu_j d_\alpha \bar{d}_\alpha) :=$	$\mathcal{L}_{NC}$, $\mathcal{O}_{LdqN}$
$\Gamma(N_i \to \nu_j \nu \bar{\nu}) :=$	$\mathcal{L}_{NC}$

E. $\Gamma(N_i \to \ell_j \ell_k \nu_k; j \neq k)$

This decay is mediated either via W-boson off shell decay, dimension six operator $\mathcal{O}_{HNe}$ or via four Fermi decay operator $\mathcal{O}_{LNLe}$. The diagram that involves the W boson can get contributions from $\mathcal{O}_{HNe}$ and $\mathcal{O}_{LNW}$ on top of the tree level charged current $\mathcal{L}_{CC}$. However we have discussed before that the vertex corresponding to the $\mathcal{O}_{LNW}$ operator is loop suppressed. Hence the effect of this is not sizeable enough with respect to the other operators for our choice of parameters and will be ignored hereafter. The matrix element corresponding to the W mediated processes can be expressed in the following fashion:

$$\begin{aligned}\mathcal{M}_W &= \mathcal{M}_{CC} + \mathcal{M}^{(6)}_{HNe} \\ &= -\frac{g^2}{2M_W^2}\bar{u}(k_1)\gamma^\mu\left(\tilde{\theta}^{ji}P_L + \frac{v^2}{\Lambda^2}\alpha^{ij}_{HNe}P_R\right) \\ &\quad \times u(p)\bar{u}(k_2)\gamma_\mu P_L v(k_3), \end{aligned} \tag{5.6}$$

where p is the momentum of decaying right-handed neutrinos and k_1, k_2, k_3 are the momentums of the outgoing leptons (k_1, k_3 correspond to singly charged leptons and k_2 corresponds to light neutrino), respectively. Along with that, the four Fermi operator $\mathcal{O}_{LNLe}$ will participate in this process and the scattering matrix can be expressed as

$$\begin{aligned}\mathcal{M}^{(6)}_{LNLe} &= -\frac{\alpha^{jikk}}{2\Lambda^2}\bar{u}(k_1)P_R u(p)\bar{u}(k_2)P_R v(k_3) \\ &\quad + \frac{\alpha^{jikk}}{8\Lambda^2}\bar{u}(k_1)\sigma_{\mu\nu}u(p)\bar{u}(k_2)\sigma^{\mu\nu}v(k_3). \end{aligned} \tag{5.7}$$

In a more general setup the dimension six operators $\mathcal{O}_{eN}$ and $\mathcal{O}_{LN}$ grant nonzero effects. However the coupling associated with these operators are proportionate with the mixing angle in addition to the quadratic cutoff scale suppression. As an outcome, one can safely ignore their effect while calculating the partial decay width. Adding Eqs. (5.6) and (5.7) one can find the total amplitude associated with the process $\Gamma(N_i \to \ell_j \ell_k \nu_k; j \neq k)$ is

$$\mathcal{M}_{\text{total}}(\Gamma(N_i \to \ell_j \ell_k \nu_k; j \neq k)) = \mathcal{M}_W + \mathcal{M}^{(6)}_{LNLe}. \tag{5.8}$$

Taking square of this total amplitude and performing the full phase space integral one can obtain the partial decay width for this process. The final form of this can be explicitly expressed as

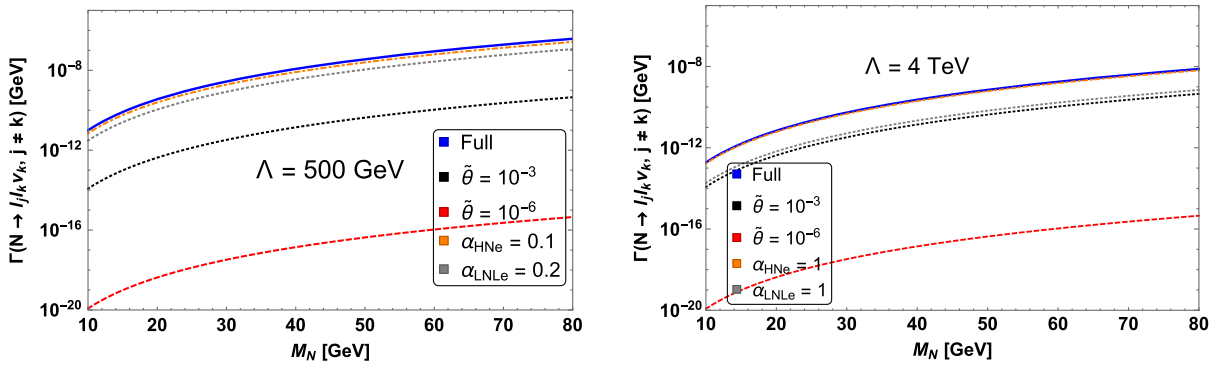

FIG. 14. Partial decay width corresponds to the decay mode $\Gamma(N_i \to \ell_j \ell_k \nu_k; j \neq k)$ for RHN mass ranging from 10 to 80 GeV. The orange dot-dashed, black dotted (red dashed), and gray dotted lines stand for the individual contribution coming from $\mathcal{O}_{HNe}$, $\mathcal{L}_{CC}$ with $\tilde{\theta} = 10^{-3}$ ($\tilde{\theta} = 10^{-6}$), and $\mathcal{O}_{LNLe}$, respectively. The blue thick line denotes the total decay taking into account all the contributions. The left panel is for cutoff scale $\Lambda = 500$ GeV and 4 TeV, respectively.

$$\Gamma(N_i \to \ell_j \ell_k \nu_k; j \neq k) = \frac{M_N^5}{512\pi^3}\left\{\left(\frac{g^4}{M_W^4}(|A|^2+|B|^2)+\frac{7}{4}|C|^2\right)\mathcal{I}_1(x_{\nu_k},x_{\ell_k},x_{\ell_j})+6|C|^2\mathcal{I}_5(x_{\nu_k},x_{\ell_k},x_{\ell_j})\right.$$
$$\left.+\frac{2g^4\mathrm{Re}[A^*B]}{M_W^4}\mathcal{I}_2(x_{\nu_k},x_{\ell_k},x_{\ell_j})+\frac{g^2\mathrm{Re}[A^*C]}{M_W^2}\mathcal{I}_3(x_{\nu_k},x_{\ell_k},x_{\ell_j})+\frac{g^2\mathrm{Re}[B^*C]}{M_W^2}\mathcal{I}_4(x_{\nu_k},x_{\ell_k},x_{\ell_j})\right\}, \quad (5.9)$$

where the coefficients A, B, and C stand for

$$A = \frac{v^2\alpha_{HNe}}{\Lambda^2}, \qquad B = \tilde{\theta}, \qquad C = \frac{\alpha_{LNLe}}{\Lambda^2}.$$

The explicit form of the integrals $\mathcal{I}_i (i = 1 \text{ to } 5)$ are given in Appendix D. From Eq. (5.7) one can notice that the operator $\mathcal{O}_{LNLe}$ has two distinct Lorentz structure, one is independent of γ^μ matrices and the other is dependent of $\sigma^{\mu\nu}$. As a result, one can see the pure terms arise from this operator is dependent on two integrals $\mathcal{I}_1$ and $\mathcal{I}_2$, respectively. The other three integrals $\mathcal{I}_i$ ($i = 2$ to 4) arise due respective interference terms between A, B, and C. To realize the impact of each of these terms one needs to diagrammatically express this for different values of mixing angle and the cutoff scale Λ. In Fig. 14, we have shown the partial decay width of this channel where we take the mixing angle and relevant Wilson coefficients consistent with the experimental bounds. In each panel of Fig. 14 the orange dot-dashed, black dotted (red dashed), and gray dotted lines represent the individual effect of $\mathcal{O}_{HNe}$, $\mathcal{L}_{CC}$ with $\tilde{\theta} = 10^{-3}$ ($\tilde{\theta} = 10^{-6}$), and $\mathcal{O}_{LNLe}$, respectively. The blue thick line denotes the total decay width which consists of individual operator contribution as well as the corresponding interference term. Note that when we are showing the total decay width we choose the value of mixing angle as $\tilde{\theta} = 10^{-3}$. The difference between the left and right panel of Fig. 14 is the cutoff scale and different Wilson coefficient consistent with the experimental constraint for that cutoff scale. From this figure, one can see the dominant contributions are usually coming from the dimension six operators. One can obtain a rough estimate of the significance of these operator while calculating the ratio between A, B, and C.

F. $\Gamma(N_i \to \nu_j \ell_k \ell_k; j = k)$

In this case as the flavor labels j and k are same, in addition to the operators such as $\mathcal{L}_{CC}$, $\mathcal{O}_{HNe}$, $\mathcal{O}_{LNLe}$, one needs to add the neutral current contribution that mediates via the Z-boson propagation. If we only consider the renormalizable part of the Lagrangian, then the coupling $\mathcal{C}^{Z_\mu}_{\bar{\nu}N+\bar{N}\nu}$ is dependent on the active sterile mixing angle. Moreover in case of N_R-EFT this coupling gets modification both from dimension five as well as dimension six operators. In dimension five, the operator $\mathcal{O}_3^{(5)}$ and in dimension six, three operators $\mathcal{O}_{HN}$, $\mathcal{O}_{NB}$, and $\mathcal{O}_{LNW}$ give some contributions that might not be tangible for the present calculation. For example, the relevant coupling coming from $\mathcal{O}_{HN}$ operator is proportional to the mixing angle as well as the $\frac{\alpha_{HN}}{\Lambda^2}$, which suggests that one can ignore this term. On the other hand, the rest of these three EFT operators are loop suppressed. So like the charged current, one can avoid its inclusion into the calculation. Bringing all these points together, one can write down the matrix element for the Z-boson mediated diagram in the following manner[4]:

[4]We define $g_L = 2\sin^2\theta_w - 1$ and $g_R = 2\sin^2\theta_w$ and $\sin^2\theta_w$ as the Weinberg angle.

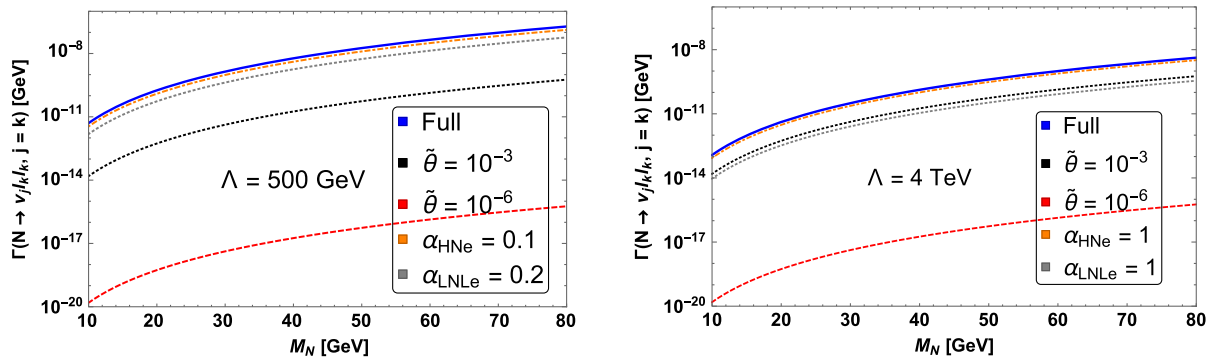

FIG. 15. Partial decay width corresponds to the decay mode $\Gamma(N_i \to \nu_j \ell_k \ell_k; j = k)$ for RHN mass ranging from 10 to 80 GeV. The meaning of color code is same as in Fig. 14.

$$\mathcal{M}_Z = -\frac{g^2}{2M_W^2}\bar{u}(k_1)\gamma^\mu \theta^{ki} P_L u(p)\bar{u}(k_2)\gamma_\mu(g_L P_L + g_R P_R)v(k_3). \tag{5.10}$$

Along with the $\mathcal{M}_Z$ one should take into account the $\mathcal{M}_W$ and $\mathcal{M}_{LNLe}$, which are illustrated in Eqs. (5.6) and (5.7), respectively. The total scattering matrix for this process is

$$\mathcal{M}_{\text{total}}((N_i \to \nu_j \ell_k \ell_k; j = k)) = \mathcal{M}_Z + \mathcal{M}_W + \mathcal{M}_{LNLe}. \tag{5.11}$$

Using this one can compute the partial decay width of this process, which takes the subsequent analytic structure:

$$\begin{aligned}\Gamma(N_i \to \ell_k \ell_k \nu_k) = \frac{M_N^5}{512\pi^3}\Bigg\{ &\left(\frac{g^4}{M_W^4}(|A|^2 + |B|^2(g_R^2 + (g_L - 1)^2)) + \frac{7}{4}|C|^2\right)\mathcal{I}_1(x_{\ell_k}, x_{\ell_k}, x_{\nu_k}) + 6|C|^2\mathcal{I}_5(x_{\ell_k}, x_{\ell_k}, x_{\nu_k}) \\ &+ \frac{3g^2\text{Re}[A^*C]}{M_W^2}\mathcal{I}_2(x_{\ell_k}, x_{\ell_k, x_{\nu_k}}) + \left(\frac{2g^2\text{Re}[A^*C]}{M_W^2} + \frac{2|B|^2 g^4}{M_W^4} g_R(g_L - 1)\right)\mathcal{H}_1(x_{\nu_k}, x_{\ell_k}) \\ &+ \left(\frac{g^4\text{Re}[A^*B]}{M_W^4}(g_L - g_R - 1) + \frac{g^2\text{Re}[B^*C]}{M_W^2}(2(g_L - 1) - g_R)\right)\mathcal{H}_2(x_{\nu_k}, x_{\ell_k}) \\ &+ \frac{3\text{Re}[B^*C]}{2M_W^2} g^2(g_L - 1)\mathcal{H}_3(x_{\nu_k}, x_{\ell_k})\Bigg\},\end{aligned} \tag{5.12}$$

where the coefficients A, B, and C signify

$$A = \frac{v^2\alpha_{HNe}}{\Lambda^2}, \qquad B = \tilde{\theta}, \qquad C = \frac{\alpha_{LNLe}}{\Lambda^2}.$$

The explicit form of the integrals $\mathcal{H}_i$ (where $i = 1$ to 3) is given in Appendix D. The Z-boson couplings to SM fermions do vary depending upon the chirality. As a result in Eq. (5.12), the term corresponding to $|B|^2$ has both g_L and g_R dependence. The dependence on the active-sterile mixing angle also come from W-boson mediated processes that justify the $(g_L - 1)$ factor in that term. It is important to highlight that the existing SM couplings receive some alteration in the EFT setup—examples include $g_{Z\nu\bar{\nu}}$ or $g_{W\ell\nu}$. However, we have assumed all those correction to be negligible as they are both cutoff scale and mixing suppressed. As expected, the pure term coming from A and C remains same as that of Eq. (5.9), but the interference effects do vary due to the emergence of Z-propagating decay mode. In Fig. 15, we illustrate the effect of these operators to this decay mode and the color code is same as in Fig. 14.

G. $\Gamma(N_i \to \nu_j \ell_k \ell_k; j \neq k)$

Apart from these modes the RHNs can potentially decay via another leptonic mode, i.e., $N_i \to \nu_j \ell_k \ell_k$; $j \neq k$. The assigned flavor label suggests that the charged leptons in this three body mode should have same flavor as opposed to the active neutrino. Invoking the idea of electromagnetic charge conservation one can see that a process like this can only appear via Z-boson off shell decay along with the four Fermi operator $\mathcal{O}_{LNLe}$. The matrix element for this process should not contain the $\mathcal{M}_W$ term and it can be written as

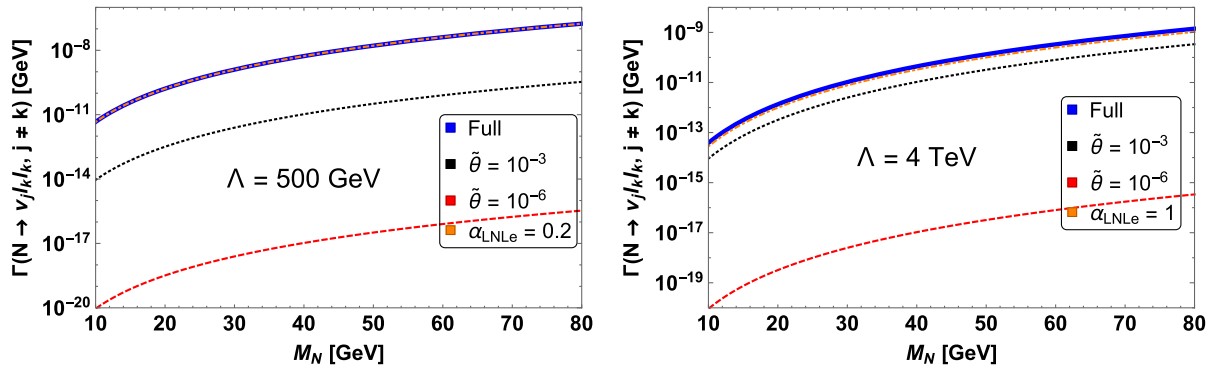

FIG. 16. Partial decay width corresponds to the decay mode $\Gamma(N_i \to \nu_j \ell_k \ell_k; j \neq k)$ for RHN mass ranging from 10 GeV to 80 GeV. The orange dot-dashed, black dotted (red dashed) line stands for the contribution coming from $\mathcal{O}_{LNLe}$ and mixing angle $\tilde{\theta} = 10^{-3}$ ($\tilde{\theta} = 10^{-6}$). The blue thick line represents the total contribution with the assumption of $\tilde{\theta} = 10^{-3}$. Left and right panel are for cutoff scales $\Lambda = 500$ GeV and 4 TeV, respectively.

$$\mathcal{M}_{\text{total}}(N_i \to \nu_j \ell_k \ell_k; j \neq k) = \mathcal{M}_Z + \mathcal{M}_{LNLe}. \quad (5.13)$$

Adopting the explicit form $\mathcal{M}_Z$ and $\mathcal{M}_{LNLe}$ as described in Eqs. (5.10) and (5.7), one can determine the analytic from of this decay width, which can be written as

$$\begin{aligned}\Gamma(N_i \to \nu_j \ell_k \ell_k) &= \frac{M_N^5}{512\pi^3}\left\{\left(\frac{g^4|B|^2}{M_W^4}(g_L^2+g_R^2)+\frac{7}{4}|C|^2\right)\mathcal{I}_1(x_{\ell_k},x_{\ell_k},x_{\nu_j})\right.\\ &+\frac{2|B|^2g^4}{M_W^4}g_Lg_R\mathcal{H}_1(x_{\nu_j},x_{\ell_k})+6|C|^2\mathcal{I}_5(x_{\ell_k},x_{\ell_k},x_{\nu_j})\\ &+\frac{\text{Re}(B^*C)}{M_W^2}g^2(2g_L+g_R)\mathcal{H}_2(x_{\nu_j},x_{\ell_k})\\ &\left.+\frac{3\text{Re}(B^*C)}{2M_W^2}g^2g_L\mathcal{H}_3(x_{\nu_j},x_{\ell_k})\right\}, \quad (5.14)\end{aligned}$$

where B, C stand for

$$B = \tilde{\theta}, \qquad C = \frac{\alpha_{LNLe}}{\Lambda^2}.$$

In Fig. 16, we illustrate the effects of various operators to this decay mode. The orange dot-dashed line represents the impact of $\mathcal{O}_{LNLe}$ operator whereas the black dotted (red dashed) line shows the effect of mixing angle $\tilde{\theta} = 10^{-3}$ ($\tilde{\theta} = 10^{-6}$) that is coming from Z-boson mediated decay. We see that the dominating contribution comes from the operator $\mathcal{O}_{LNLe}$. The blue thick line stands for the total contribution taking into account both the mixing part ($\tilde{\theta} = 10^{-3}$) and dimension six operator. The left and right panels are for two different cutoff scales, $\Lambda = 500$ GeV and 4 TeV, respectively.

H. $\Gamma(N_i \to \ell_j u_\alpha \bar{d}_\beta; \alpha \neq \beta)$

So far we have discussed the RHN decays via pure leptonic modes. The RHN can also decay via hadronic modes along with either a charged leptons or a light neutrino. We begin our discussion about RHN decay to a semileptonic final state: $N_i \to \ell_j u_\alpha \bar{d}_\beta$; $\alpha \neq \beta$. The presence of both up and down type quark along with charged leptons indicates a charge current mediated process. Hence, in evaluating this contribution, we consider the standard renormalizable charge current interaction part. There will be also contribution from dimension six operators such as α_{HNe} and α_{LNW}. Similar to before we consider α_{LNW} to be zero due to loop suppression. In addition to that, a tower of four Fermi operators would give appreciable contribution in this process. From Table III, one can see that these operators are $\mathcal{O}_{QuNL}$, $\mathcal{O}_{duNe}$, $\mathcal{O}_{LNqd}$, and $\mathcal{O}_{LdqN}$. Their contribution to this decay width is given as

$$\begin{aligned}\mathcal{M}^{(6)}_{QuNL} &= \frac{\alpha^{*\beta\alpha ij}_{QuNL}}{\Lambda^2}\bar{u}(k_1)P_Ru(p)\bar{u}(k_2)P_Lv(k_3),\\ \mathcal{M}^{(6)}_{duNe} &= \frac{\alpha^{*ij\beta\alpha}_{duNe}}{\Lambda^2}\bar{u}(k_1)\gamma^\mu P_Ru(p)\bar{u}(k_2)\gamma_\mu P_Rv(k_3),\\ \mathcal{M}^{(6)}_{LNqd} &= -\frac{\alpha^{ij\alpha\beta}_{LNqd}}{\Lambda^2}\bar{u}(k_1)P_Ru(p)\bar{u}(k_2)P_Rv(k_3),\\ \mathcal{M}^{(6)}_{LdqN} &= -\frac{\alpha^{j\beta\alpha i}_{LdqN}}{2\Lambda^2}\bar{u}(k_1)P_Ru(p)\bar{u}(k_2)P_Rv(k_3)\\ &\quad -\frac{\alpha^{j\beta\alpha i}_{LdqN}}{8\Lambda^2}\bar{u}(k_1)\sigma_{\mu\nu}u(p)\bar{u}(k_2)\sigma^{\mu\nu}v(k_3). \quad (5.15)\end{aligned}$$

Considering the chirality of the fermion fields as well as the intrinsic space-time transformation properties one can identify the distinction among each of these operator. For example, both the matrix elements $\mathcal{M}_{QuNL}$ and $\mathcal{M}_{LNqd}$ correspond to charged scalar mediated graph in high scale UV complete model. On the other hand, the

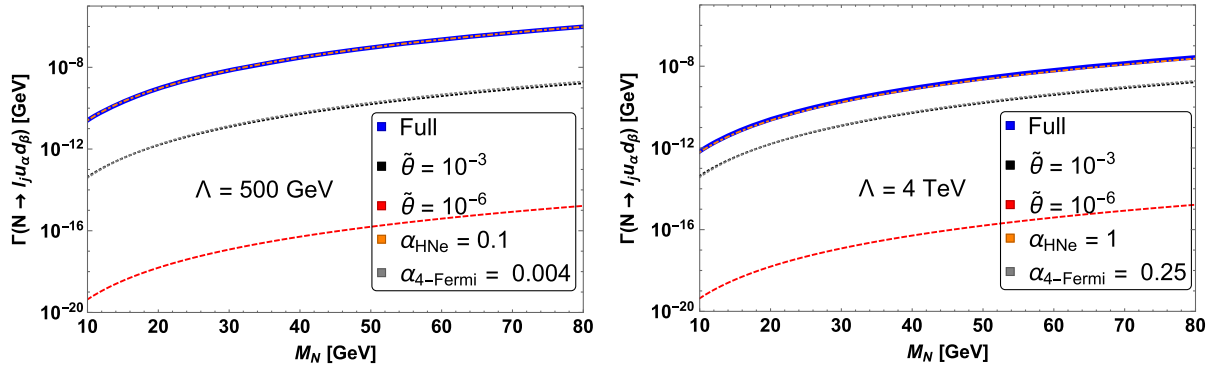

FIG. 17. Partial decay width corresponds to the decay mode $\Gamma(N_i \to \ell_j u_\alpha \bar{d}_\beta; \alpha \neq \beta)$ for RHN masses ranging from 10 to 80 GeV. In each panel, the black dotted or red dashed, orange dot-dashed, and gray lines stand for the contribution coming from the mixing angle, $\mathcal{O}_{HNe}$, and from combination of four Fermi operator. The blue thick line represents the total contribution with the assumption of $\tilde{\theta} = 10^{-3}$, and the left and right panels are for two different cutoff scale.

matrix element $\mathcal{M}_{duNe}$ hints upon a vectorlike charged currents that one can realize in BSM theories with $SU(2)_R$ extensions. The operator $\mathcal{O}_{LdqN}$ contains two separate Lorentz structures similar to $\mathcal{O}_{LNLe}$. Using appropriate Fierz transformation one can separate the $\mathcal{M}^{(6)}_{LdqN}$ matrix into a scalar as well as tensor objects. Adding the matrix elements that are mentioned in Eq. (5.15) with $\mathcal{M}_W$ and performing the full phase space integrals one can obtain the partial decay width for this channel. In Eq. (5.16), we write down its explicit form

$$\begin{aligned}\Gamma(N_i \to \ell_j u_\alpha \bar{d}_\beta) = \frac{M_N^5 N_c}{512\pi^3}\Bigg\{ & \left(\frac{g^4|V_{\rm CKM}|^2}{M_W^4}(|A|^2+|B|^2)+4|C_2|^2+|C_1|^2+|C_3|^2+\frac{3}{2}|C_4|^2\right)\mathcal{I}_1(x_u,x_d,x_{\ell_j}) \\ & +\frac{2{\rm Re}[A^*B]g^4}{M_W^4}\mathcal{I}_2(x_u,x_d,x_{\ell_j})+\left(3|C_4|^2-\frac{8g^2{\rm Re}[A^*C_2]}{M_W^2}\right)\mathcal{I}_5(x_u,x_d,x_{\ell_j}) \\ & +\left(\frac{3g^2{\rm Re}[B^*C_4]}{2M_W^2}-\frac{g^2{\rm Re}[A^*C_1]}{M_W^2}\right)\mathcal{G}_1(x_u,x_d,x_{\ell_j})+\left(\frac{3g^2{\rm Re}[A^*C_4]}{2M_W^2}-\frac{g^2{\rm Re}[A^*C_3]}{M_W^2}-3{\rm Re}[C_2^*C_4]\right)\mathcal{G}_1(x_d,x_u,x_{\ell_j}) \\ & +\left(\frac{3g^2{\rm Re}[A^*C_4]}{2M_W^2}+\frac{g^2{\rm Re}[B^*C_1]}{M_W^2}+2{\rm Re}[C_2^*C_3]-3{\rm Re}[C_2^*C_4]\right)\mathcal{G}_2(x_u,x_d,x_{\ell_j}) \\ & +\left(\frac{g^2{\rm Re}[B^*C_3]}{M_W^2}+\frac{3g^2{\rm Re}[B^*C_4]}{2M_W^2}+2{\rm Re}[C_1^*C_2]\right)\mathcal{G}_2(x_d,x_u,x_{\ell_j}) \\ & +\left(\frac{4g^2{\rm Re}[B^*C_2]}{M_W^2}-4{\rm Re}[C_1^*C_3]\right)\mathcal{G}_3(x_u,x_d,x_{\ell_j})\Bigg\}, \end{aligned} \tag{5.16}$$

where different vertex factors are defined as

$$A=\tilde{\theta},\quad B=\frac{v^2\alpha_{HNe}}{\Lambda^2},\quad C_1=\frac{\alpha_{QuNL}}{\Lambda^2},$$
$$C_2=\frac{\alpha_{Nedu}}{\Lambda^2},\quad C_3=\left(\frac{\alpha_{LNqd}}{\Lambda^2}+\frac{\alpha_{LdqN}}{\Lambda^2}\right),\quad C_4=\frac{\alpha_{LdqN}}{\Lambda^2},$$

and $N_c = 3$ is the color factor. The integrals $\mathcal{G}_i$ (where $i = 1$ to 3) are given in Appendix D. The scalar piece of operator $\mathcal{O}_{LNqd}$ contributes to coefficient C_3 along with $\mathcal{O}_{LdqN}$, whereas the tensorial part is treated as a separate coefficient C_4. Without loss of generality, one can choose the value of both these coefficients are in the same order while understanding their role in the decay width formula. In Fig. 17, we display the decay width as a function of mass M_N. As before, the black dotted (red dashed) line corresponds to the mixing angle $\tilde{\theta} = 10^{-3}$ ($\tilde{\theta} = 10^{-6}$) and the orange dot-dashed line corresponds to $\mathcal{O}_{HNe}$, respectively. The gray dotted lines show the combined effects of different four Fermi operators. The blue thick line stands for the total contribution taking into account both the mixing part ($\tilde{\theta} = 10^{-3}$) and dimension six operators. The left and right panel is for two different cutoff scale $\Lambda = 500$ GeV and 4 TeV, respectively. For these two cutoff scales we set the Wilson coefficient correspond to

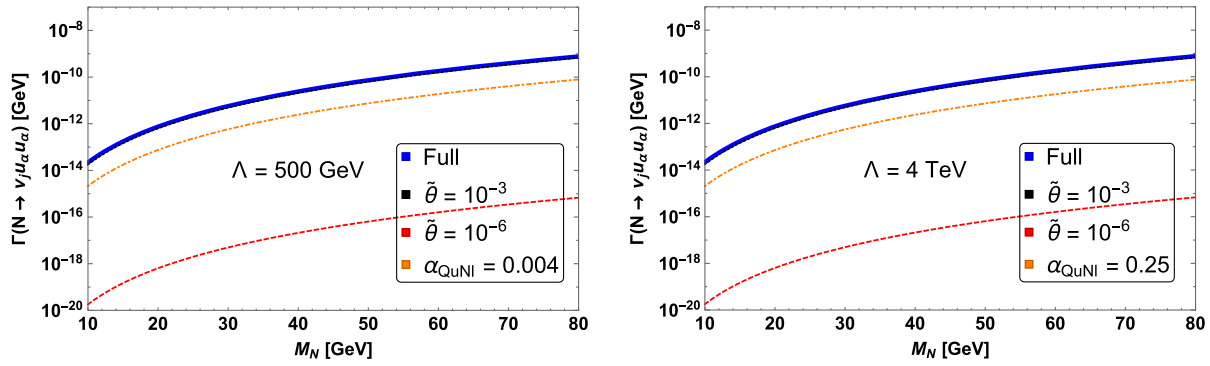

FIG. 18. Partial decay width corresponds to the decay mode $\Gamma(N_i \to \nu_j u_\alpha \bar{u}_\alpha)$ of RHN having mass in the range of 10 to 80 GeV. In each panel, the black dotted or red dashed and orange dot-dashed line stands for the contribution coming from the mixing angle and $\mathcal{O}_{QuNl}$. The blue thick line represents the total contribution with the assumption of $\tilde{\theta} = 10^{-3}$, and the left and right panels are for two different cutoff scales.

four Fermi operators to be $\alpha_{4-\text{Fermi}} = 0.004$ and 0.25, respectively, which is consistent with the current experimental bounds.

I. $\Gamma(N_i \to \nu_j u_\alpha \bar{u}_\alpha)$ & $\Gamma(N_i \to \nu_j d_\alpha \bar{d}_\alpha)$

The RHN can also decay via the same flavor hadronic modes along with missing energy. The flavor neutrality in the final states suggest that the decay can occur due to the Z-boson mediation at a renormalizable level Lagrangian. Furthermore, depending upon the quark flavor, different four Fermi operators would participate in it. In case of up-type quarks these operators are $\mathcal{O}_{uN}$, $\mathcal{O}_{QN}$, and $\mathcal{O}_{QuNL}$. However, out of these three operators the first two are mixing suppressed, hence they do not play much role in the decay mode $\Gamma(N_i \to \nu_j u_\alpha \bar{u}_\alpha)$. For the current calculation we add the matrix elements $\mathcal{M}_Z$ and $\mathcal{M}_{QuNL}$ and the total matrix element of the process takes the following form:

$$\mathcal{M}_{\text{total}}(N_i \to \nu_j u_\alpha \bar{u}_\alpha) = \mathcal{M}_Z + \mathcal{M}_{QuNL}. \tag{5.17}$$

Taking the explicit form of $\mathcal{M}_Z$ and $\mathcal{M}_{QuNL}$ from Eqs. (5.10) and (5.15) one can obtain the corresponding partial decay width of this channel

$$\Gamma(N_i \to \nu_j u_\alpha \bar{u}_\alpha) = \frac{M_N^5 N_c}{512\pi^3}\left\{\left(|B|^2 + \frac{g^4|A|^2}{M_W^4}(g_L^2 + g_R^2)\right)\mathcal{I}_1(x_u, x_u, x_{\nu_j}) - \frac{2|A|^2 g^2}{M_W^2} g_L g_R \mathcal{G}_3(x_u, x_u, x_{\nu_j}) + \frac{\text{Re}[A^* B] g^2}{M_W^2}(g_R - g_L)\mathcal{G}_1(x_u, x_u, x_{\nu_j})\right\}, \tag{5.18}$$

where A and B are

$$A = \tilde{\theta}, \qquad B = \frac{\alpha_{QuNL}}{\Lambda^2}.$$

Similar to previous cases, we have only considered the renormalizable neutral current interaction for the diagram correspond to $\mathcal{M}_Z$. In Fig. 18, we illustrate the effects of these operators for this decay mode. The black dotted (red dashed) line corresponds to the mixing angle $\tilde{\theta} = 10^{-3}$ ($\tilde{\theta} = 10^{-6}$) and the orange dot-dashed line corresponds to $\mathcal{O}_{QuNL}$, respectively. The blue thick line stands for the total contribution taking into account both the mixing part ($\tilde{\theta} = 10^{-3}$) and dimension six operator $\mathcal{O}_{QuNL}$. We see that the contribution coming from renormalizable part (Z-mediated case) dominates over the dimension six contribution when the mixing angle is $\tilde{\theta} = 10^{-3}$. The blue thick line denotes the full decay width with the assumption on the mixing angle as $\tilde{\theta} = 10^{-3}$. In case of a down type quark the underlying calculation has an additional complication. As mentioned before, the decay receives substantial contribution from the Z-boson propagation. Along with that, the operators, $\mathcal{O}_{dN}$, $\mathcal{O}_{QN}$, $\mathcal{O}_{LNQd}$, and $\mathcal{O}_{LdqN}$ gives sufficient contributions. But the effects coming from the operators $\mathcal{O}_{dN}$ and $\mathcal{O}_{QN}$ are in general mixing dependent and one can safely ignore these for practical purpose. On the other hand the operators $\mathcal{O}_{LNQd}$ and $\mathcal{O}_{LdqN}$ do play a role here. Taking into account all of these operators, one can obtain the following form of partial decay width:

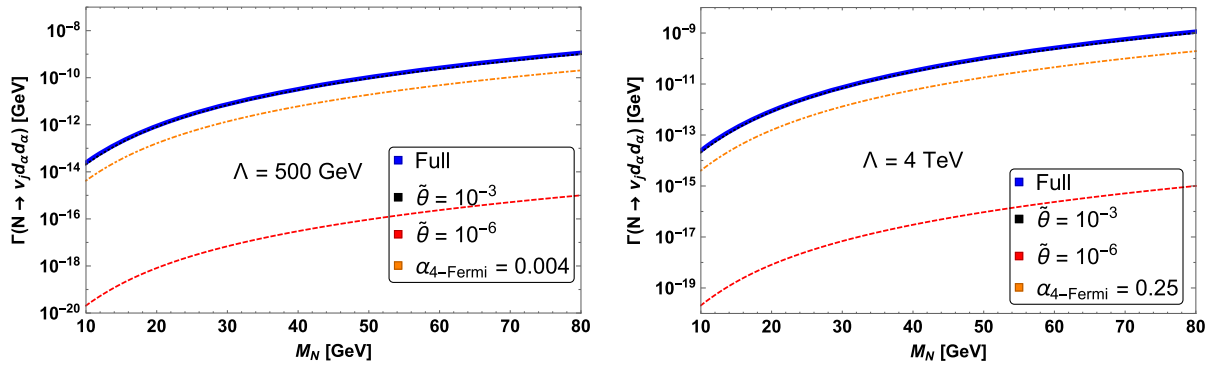

FIG. 19. Partial decay width corresponds to the decay mode $\Gamma(N_i \to \nu_j d_\alpha \bar{d}_\alpha)$ of RHN mass ranging from 10 to 80 GeV. The color code is same as in Fig. 18 except the orange dot-dashed line now stands for four Fermi operators.

$$\Gamma(N_i \to \nu_j d_\alpha \bar{d}_\alpha) = \frac{M_N^5 N_c}{512\pi^3}\left\{\frac{2|A|^2}{M_W^4} g^4 g_L g_R \mathcal{H}_1(x_{\nu_j}, x_{d_\alpha}) + \left(\frac{|A|^2}{M_W^4} g^4 (g_L^2 + g_R^2) + \frac{|B|^2}{4} + \frac{3}{4}|C|^2\right)\mathcal{I}_1(x_{d_\alpha}, x_{d_\alpha}, x_{\nu_j}) \right.$$
$$+ 3|C|^2 \mathcal{I}_5(x_{d_\alpha}, x_{d_\alpha}, x_{\nu_j}) + \frac{g^2}{2M_W^2}[(g_L - g_R)\mathrm{Re}[A^* B] - 3(g_L + g_R)\mathrm{Re}[A^* C]]\mathcal{G}_1(x_{d_\alpha}, x_{d_\alpha}, x_{\nu_j})$$
$$\left. - \frac{3g^2 \mathrm{Re}[A^* C]}{2M_W^2}(g_L + g_R)\mathcal{H}_3(x_{\nu_j}, x_{d_\alpha})\right\}, \tag{5.19}$$

where the coefficients A, B, and C are

$$A = \tilde{\theta}, \qquad B = \frac{\alpha_{LNQd}}{\Lambda^2} + \frac{\alpha_{LdqN}}{\Lambda^2}, \qquad C = \frac{\alpha_{LdqN}}{\Lambda^2}.$$

In Fig. 19, we illustrate the participation of these operators in the decay width for mass value 10 to 80 GeV. The black dotted and red dashed lines denote the contribution from a renormalizable neutral current process for $\tilde{\theta} = 10^{-3}$ and $\tilde{\theta} = 10^{-6}$, respectively. The orange dot-dashed line shows the subdominant contribution coming from the combination of four Fermi operators. The blue thick line shows the overall effect coming from mixing ($\tilde{\theta} = 10^{-3}$) and four Fermi operators. We see that the contribution coming from renormalizable part (Z-mediated case) dominates over the dimension six contribution when the mixing angle is $\tilde{\theta} = 10^{-3}$, and because of this the black dotted and thick blue lines coincide in each panel.

J. $\Gamma(N_i \to \nu_j \nu \bar{\nu})$

The RHNs can also decay to pure active neutrino states. The decay can be mediated either via off shell Z decay or via four Fermi operators $\mathcal{O}_{NN}$ and $\mathcal{O}_{NNNN}$ that arise in the dimension six setup. However the relevant terms coming from these dimension six operators are proportional to the cubic power of the mixing angle along with the inverse of the quadratic Λ suppression. Hence, once we can ignore those terms for practical purposes. The partial decay is then written as

$$\Gamma(N_i \to \nu_j \nu \bar{\nu}) = \frac{G_F^2 M_N^5}{96\pi^3}|\tilde{\theta}|^2. \tag{5.20}$$

In Fig. 20, we present the corresponding decay width for different choices of mixing angles. As the EFT operators do not participate in the process the change in the cutoff scale is irrelevant in this calculation. In Fig. 21 we illustrate the total decay width of the RHN fields while taking into account all possible decay modes in the mass range 10 GeV $< M_N <$ 80 GeV. The red dot dashed line and the blue dashed line correspond to mixing angle $\tilde{\theta} = 10^{-6}$

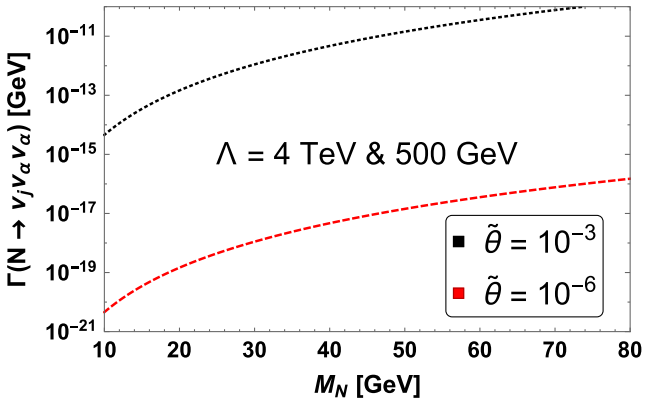

FIG. 20. Partial decay width corresponds to the decay mode $\Gamma(N_i \to \nu_j \nu \bar{\nu})$ of RHN mass ranging from 10 to 80 GeV. The black dotted and red dashed lines stand for mixing angles $\tilde{\theta} = 10^{-3}$ and $\tilde{\theta} = 10^{-6}$, respectively.

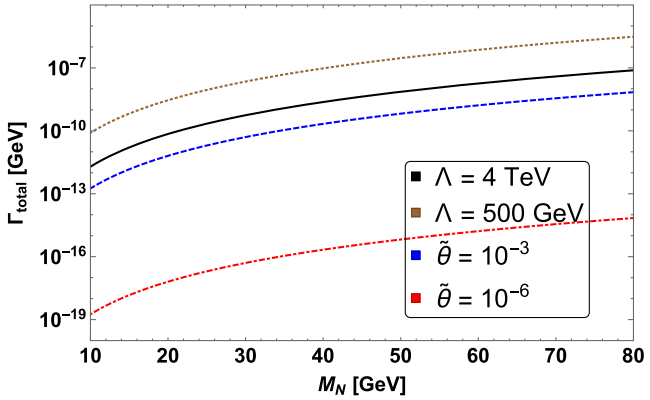

FIG. 21. The total decay width correspond to RHN field where the M_N is ranging from 10 to 80 GeV. The blue dashed and red dot-dashed line stands for the mixing angle $\tilde{\theta} = 10^{-3}$ and $\tilde{\theta} = 10^{-6}$, respectively. The black solid line represents the total decay width of the N field under full $d = 6$ N_R-EFT where the cutoff scale Λ is set to be 4 TeV. Similarly the brown dotted line stands for the total decay width of the N field with cutoff scale $\Lambda = 500$ GeV.

and $\tilde{\theta} = 10^{-3}$, respectively. On the other hand, the black thick and the brown dotted lines signify the total decay width corresponding to full $d = 6$ N_R-EFT, where the cutoff scale $\Lambda = 4$ TeV and 500 GeV, respectively. In the EFT calculation we set the active-sterile mixing angle to be $\tilde{\theta} = 10^{-3}$. The value of the total decay width suggests that the RHN field would behave as a prompt particle in both the EFT benchmark points as well as $\tilde{\theta} = 10^{-3}$ case for entire range of 10 GeV $< M_N <$ 80 GeV.

We now present the branching ratio for the benchmark points BP1 ($\Lambda = 500$ GeV) and BP2 ($\Lambda = 4$ TeV) while setting active-sterile mixing angle to be $\tilde{\theta} = 10^{-3}$. In upper panel of Fig. 22, we present the corresponding plots for these scenarios. For both these cases the BR value for the $\ell_j ud$ channel will be maximum for the entire mass range as shown by the black dotted curve. Similarly, the BR value for the $\nu_j \nu \bar{\nu}$ mode is minimum. But the relative difference between the other possible channels vary depending on the underlying benchmark choice. For comparison purpose we also present the branching ratio in the lower panel of Fig. 22 while considering only the renormalizable part of the EFT Lagrangian. The important change in dimension six N_R-EFT is the enhancement of the BR value of pure leptonic three body modes. In a renormalizable level, the BR for $N_i \to \nu_j q_\alpha \bar{q}_\alpha$ channels dominate over leptonic channels for the entire range of 10 GeV $< M_N < M_W$. However, the interplay between the operators $\mathcal{O}_{LNLe}$ and $\mathcal{O}_{HNe}$ alter these result and BR of $N_i \to \ell_k \ell_k \nu_k / \ell_j \ell_k \nu_k$ (gray solid and brown dotted) dominates over $N_j \to \nu_j q_\alpha q_\alpha$ mode for both the benchmark scenarios.

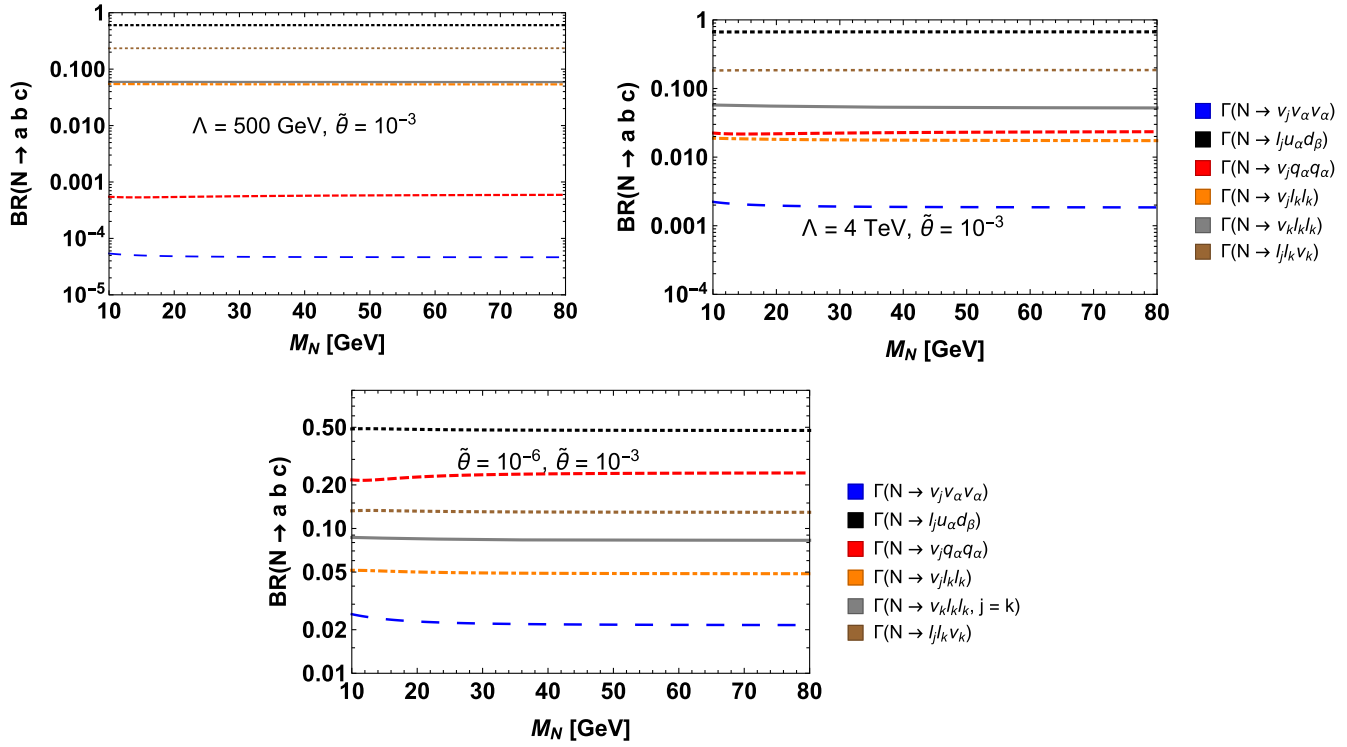

FIG. 22. Upper panel: the branching ratios of RHN mass ranging from 10 to 80 GeV in various three body modes for the benchmark points BP1 ($\Lambda = 500$ GeV) and BP2 ($\Lambda = 4$ TeV). In both cases, we have considered the active sterile mixing angle $\tilde{\theta} = 10^{-3}$. Lower panel: we calculate the branching ratio of the RHN mass ranging from 10 to 80 GeV in different three body decay modes while considering the renormalizable part of the Lagrangian.

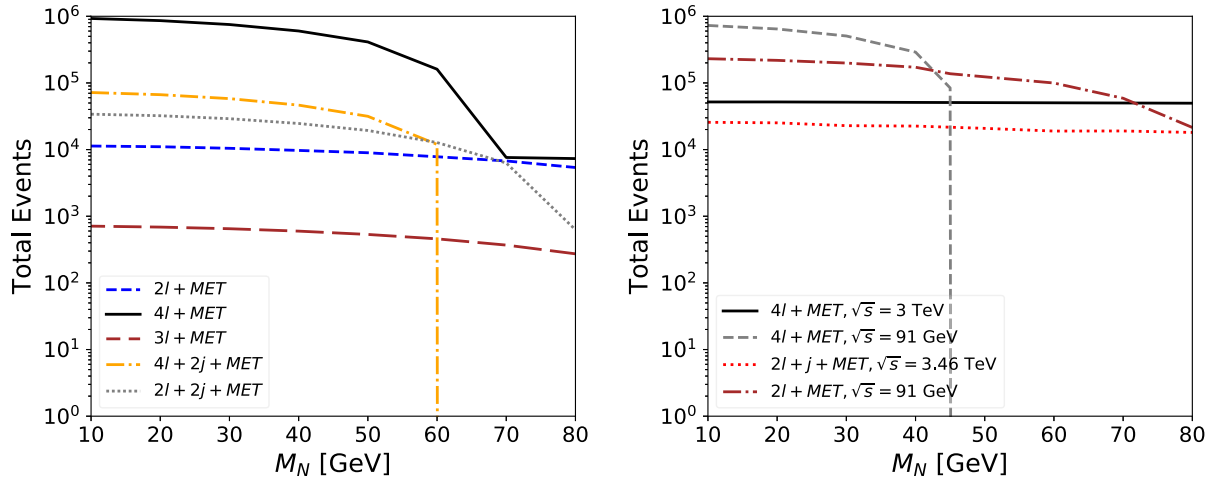

FIG. 23. The left panel denotes the number of events that can be obtained at HL-LHC with c.m. energy 14 TeV and $\mathcal{L} = 3000$ fb^{-1}. The right panel shows achievable number events that can be obtained at e^+e^- and e^-p colliders for different c.m. energies.

VI. PROSPECTIVE MULTILEPTON FINAL STATES

We focus on producing multilepton final states that arise from single/pair production of RHN fields and their subsequent decays. We have calculated various three body decay modes of the RHNs. In Fig. 22, we show that the N decaying to purely leptonic final states have branching ratios of 20% to 25%, depending on the cutoff scale $\Lambda =$ 500 GeV and 4 TeV. With these results, one can estimate the expected number of events in the heavy neutrino production processes at pp, ep, and e^+e^- colliders, which we show in Fig. 23. We assume in all these cases that the RHN decays purely leptonically.

Figure 23(a) shows the number of events expected at the HL-LHC with c.m. energy $\sqrt{s} = 14$ TeV and $\mathcal{L} = 3000$ fb^{-1}. The solid black line represents the number of events for the $4\ell + MET$ final state, which results from the pair-production of Ns and their subsequent decay to leptonic final states. N-pair production is either mediated via Higgs decay, where the Higgs boson is produced through gluon fusion, or via four Fermi operators. The Z boson, produced via the Drell-Yan process, can give rise to the same final state. However, this process is suppressed by the mixing angle $\tilde{\theta}$ and fails to provide any appreciable contribution. As seen from the figure, the total number of events for this channel is as large as $\mathcal{O}(10^6)$.

Instead, the blue dashed line shows the $2\ell + MET$ final state, resulting from single N production and its subsequent leptonic decay. Similar to the previous channel, the N in this case can be produced either via Higgs decay or via four Fermi operators. Additionally, there is a Drell-Yan contribution via Z-mediated process. These production modes, however, depend on the active-sterile mixing angle. Hence, the total number of events for this process is small compared to the $4\ell + MET$ final state, where the four Fermi and $\mathcal{O}_2^5$ operators can give mixing angle independent, unsuppressed contributions.

The $4\ell + 2j + MET$ and $2\ell + 2j + MET$ final states are represented by the orange dot-dashed line and the gray dotted line, respectively. These final states are produced via Higgs and Z-boson-mediated VBF production modes. The above two final states can appear depending on the rates for the decay $h/Z \to \nu N/NN$ and subsequent leptonic decay of N. Amongst these two processes, the former is dominant, and many signal events can be expected $\sim\mathcal{O}(10^5)$.

The $3\ell + MET$ final state, shown as a red dashed line in Fig. 23(a), which arises from the $qq' \to W \to \ell N$ production mode can provide signal events ranging between $\mathcal{O}(10^4)$ to $\mathcal{O}(10^3)$.

In Fig. 23(b) we present the number of signal events one can obtain at e^+e^- and e^-p colliders. For the e^+e^- collider, we consider a c.m. energy of 91 GeV and 3 TeV, respectively. On the other hand, for e^-p colliders, the c.m. energy has been chosen to be 3.46 TeV. In all these cases, we have considered the luminosity $\mathcal{L} = 1$ ab^{-1}. The gray dashed line denotes the $4\ell + MET$ final state for $\sqrt{s} = 91$ GeV. There can be different processes contributing to the final state, among which the Z mediated diagram generating two Ns followed by $N \to \ell\ell\nu$ decay give rise to a significant number of events $N \sim \mathcal{O}(10^5)$. One can obtain $2\ell + MET$ final states via Z-boson decay or four Fermi operators. Although, the relevant production vertex is suppressed by the mixing angle $\tilde{\theta}$, the presence of Z-pole leads to substantial number of signal events.

The number of signal events associated with $4\ell + MET$ final state is shown for e^+e^- collider with c.m. energy of 3 TeV. This process can arise via VBF production or four

fermion contact operators, which give rise to a sizeable number of events $N \sim \mathcal{O}(10^4)$.

For $e^- p$ colliders, the only process which can generate a significant number of signal events is the $e^- p \to jN \to 2l + j + MET$ channel. The number of signal events corresponding to this channel is represented by the red dotted curve and is $N_{\text{Signal}} \sim \mathcal{O}(10^4)$.

VII. SUMMARY AND CONCLUSION

The N_R-EFT framework can provide a suitable phenomenological description of the BSM physics. In this work we have systematically established this EFT up to dimension six level and shown the detailed construction of all possible operators that one can construct at $d = 5$ and $d = 6$, respectively. At each order these higher dimensional operators either modify different $d = 4$ couplings involving RHN field or introduce new set of interactions relevant to neutrino phenomenology.

The interaction of the RHN with SM fields leads to new decay modes and hence modifies the decay width of $h/W/Z$. However, the existing experimental observations restrict such modifications and impose meaningful bounds on mixing angle $\tilde{\theta}$, Wilson coefficients and the associated cutoff scale Λ. One can further tighten these constraints while incorporating different direct search limits and determine allowed range of EFT parameters. Our analysis deduces that, in the case of cutoff $\Lambda = 4$ TeV, one is allowed to fix the mixing angle $\tilde{\theta} = 10^{-3}$ and that the Wilson coefficients $\alpha_2^{(5)} \leq 0.1$ α_{HN}, $\alpha_{HNe} \leq 1$, $\alpha_{LNW/B} \leq 0.1$, and coefficients correspond to four Fermi operators to be $\alpha_{\text{four Fermi}} \leq 0.5$. Similarly, for the cutoff scale $\Lambda = 500$ GeV one needs to rescale these Wilson coefficients accordingly.

We have presented the viable production mode of the RHN fields at 14 TeV pp, as well as future e^+e^- and $e^- p$ colliders. In case of pp collider pair production of N field via $gg \to h \to NN$ mode remains dominant production mode for the mass range $M_N < \frac{m_h}{2}$ with the cross section roughly around $\mathcal{O}(10)$ pb. Above this mass range RHN pair production through four Fermi contact interaction serves as a dominant production mode with the cross section ranging between $\mathcal{O}(10^{-1})$ to $\mathcal{O}(10^{-3})$ pb for the mass range 100 GeV $< M_N <$ 1 TeV. All the operators which can generate NN pair can also invoke single N production. However the cross section correspond to single RHN field production is comparatively low with respect to RHN pair production as this is active-sterile mixing suppressed. For completeness we also present RHN production through VBF as well as Drell-Yan mechanism. Apart from RHN production via W-boson decay (where W is produced via Drell-Yan process), for all other cases the cross section is significantly low. The cross section for RHN production via Drell-Yan W mode is large [roughly around $\mathcal{O}(10^{-1})$ pb to $\mathcal{O}(10^{-3})$ pb] due to the significant contribution coming from $d = 6$ operator $\mathcal{O}_{HNe}$. In case of ep collider $ep \to jN$ mode stands as a viable production channel for the RHN field. This process can occur either via t-channel W-mediated process or via contact interaction through different four Fermi operators and corresponding cross section lies within the range $\mathcal{O}(10^{-1})$ to $\mathcal{O}(10^{-3})$ pb. In the case of the e^+e^- collider we have studied the feasible production modes for c.m. energies $\sqrt{s} = 91$ GeV and 3 TeV, respectively. For $\sqrt{s} = 91$ GeV, RHN pair production via an s-channel Z boson is the dominant production mode. The presence of a Z pole in the underlying process significantly increases the production cross section to 10 pb. In contrast to that for $\sqrt{s} = 3$ TeV, this process is primarily governed by different four Fermi operators ($\mathcal{O}_{eN}$, $\mathcal{O}_{LN}$ etc.) and the corresponding cross section lies roughly around $\mathcal{O}(0.5)$ pb for M_N ranging between 100 GeV to 1 TeV.

Apart from the production mechanism, we evaluate the decay width as well as branching ratio of RHN fields while considering both renormalizable part of effective Lagrangian as well as relevant higher dimension operators. Depending upon RHN masses it can either decay via two body or three body decay modes where we assume decay among RHN fields are forbidden due to mass degeneracy. In case of two body decay calculation, the N fields can decay into νh, νZ, and ℓW modes if we only consider the $d = 4$ Lagrangian. The presence of EFT operators $\mathcal{O}_3^{(5)}$, $\mathcal{O}_{LNB}$, and $\mathcal{O}_{LNW}$ invoke an additional decay mode $\nu\gamma$ for the RHN field. The branching ratio correspond to $N \to \ell W$ mode remains dominant for entire M_N mass range in both the $d = 4$ as well as the $d = 6$ setup and the contributions from $\mathcal{O}_{HNe}$ significantly enhance $\text{BR}(N \to \ell W)$ with respect to the $d = 4$ result. The BR corresponding to the $N \to \nu h$ mode remains minimum for entire RHN mass range in both of these setups.

In the case of $M_N < M_W$, the RHN fields can decay via different leptonic as well as semileptonic three body modes in addition to the two body $\nu\gamma$ mode. Up to dimension five these three body decay modes can only occur due to the off shell decay of W and Z bosons. In dimension six the presence of different four Fermi operators significantly alters this situation. These four Fermi operators can contribute to the three body modes through contact interaction and enhance the corresponding partial width. For example, operator $\mathcal{O}_{LNLe}$ would participate in different leptonic channels $N_i \to \ell_j \ell_k \nu_k / \ell_k \ell_k \nu_k / \nu_j \ell_k \ell_k$ and increases partial width. The $d = 6$ operator $\mathcal{O}_{HNe}$ noticeably increases off shell W mediated contribution but the off shell Z-boson decay does not receive any significant enhancement from the EFT operators as the relevant couplings are either mixing angle $\tilde{\theta}$ suppressed or loop suppressed. We also present comparative analysis between the branching ratio for two EFT benchmark scenarios ($\Lambda = 500$ GeV, 4 TeV) as well as renormalizable level Lagrangian. Our analysis dictates that the BR value for

$\ell_j u_\alpha d_\beta$ mode is maximum and BR value for $\nu_j \nu_\alpha \nu_\alpha$ remains minimum in all these scenarios. The important aspect of dimension six N_R-EFT is the enhancement of the BR value of pure leptonic three body modes. In renormalizable level the BR for $N_i \to \nu_j q_\alpha \bar{q}_\alpha$ channels dominate over leptonic modes for entire range of 10 GeV $< M_N < M_W$. However, the interplay between the operators $\mathcal{O}_{LNLe}$ and $\mathcal{O}_{HNe}$ alter these result and BR of $N_i \to \ell_j \ell_k \nu_k / \ell_k \ell_k \nu_k$ dominates over $N_j \to \nu_j q_\alpha q_\alpha$ mode for both the benchmark scenarios.

The major advantage of the N_R-EFT setup is the enhancement in the BR value for different three body pure leptonic decay modes. This motivates us to propose few golden channel signatures for the RHN field in multileptonic final states. Our study suggest $4\ell + MET$ channel can serve as an optimal discovery mode for the RHN field at both 14 TeV HL-LHC and future e^+e^- (with c.m. $\sqrt{s} =$ 91 GeV and 3 TeV) machine. In case of ep collider the viable discovery mode would be $2\ell + j + MET$ final state. We will investigate these channels for a detailed cut-based analysis in our future studies.

ACKNOWLEDGMENTS

The work of S. M. is supported by KIAS Individual Grants (Grant No. PG086001) at Korea Institute for Advanced Study. M. M. and A. S. acknowledge the support from the Indo-French Centre for the Promotion of Advanced Research (Grant No. 6304-2). M. M. acknowledges the support from IPPP DIVA Programme. R. P. acknowledges the support of Fulbright-Nehru Doctoral Research Fellowship, 2022–2023.

APPENDIX A: USEFUL TRANSFORMATION RULES BETWEEN FLAVOR AND MASS BASIS

In Eqs. (2.8) and (2.13) we established the relation between the gauge basis $\{\nu_L, N_R^c\}$ and the mass basis $\{\nu_{L,m}, N_{R,m}^c\}$ in dimension five and dimension six frameworks, respectively. Furthermore, for the explicit coupling extraction one needs other possible gauge basis definitions like ν_L^c, N_R etc. In Eqs. (A1) and (A2) we illustrate a different relationship between the gauge basis and the mass basis states of both the active and sterile neutrinos.

$$\begin{aligned} \nu_L &\simeq U_{\rm PMNS}\nu_{L,m} + \theta N_{R,m}^c, \quad \overline{\nu_L} \simeq \bar{\nu}_{L,m} U_{\rm PMNS}^\dagger + \overline{N}_{R,m}^c \theta^\dagger \\ \nu_L^c &\simeq U_{\rm PMNS}^* \nu_{L,m}^c + \theta^* N_{R,m}, \quad \bar{\nu}_L^c \simeq \bar{\nu}_{L,m}^c U_{\rm PMNS}^\dagger + \overline{N}_{R,m} \theta^T. \end{aligned} \tag{A1}$$

$$\begin{aligned} N_R^c &\simeq -\theta^T \nu_{L,m} + \kappa N_{R,m}^c, \quad \overline{N_R}^c \simeq -\theta^* \bar{\nu}_{L,m} + \kappa^\dagger \overline{N}_{R,m}^c \\ N_R &\simeq -\theta^\dagger \nu_{L,m}^c + \kappa^* N_{R,m}, \quad \overline{N}_R \simeq -\theta \bar{\nu}_{L,m}^c + \kappa^T \overline{N}_{R,m}. \end{aligned} \tag{A2}$$

In the above we present all these relations for dimension five setup. At dimension six, one should replace the mixing angle θ with $\tilde{\theta}$.

APPENDIX B: EVALUATING COUPLINGS UP TO DIMENSION FIVE SETUP

The RHN fields couple to different SM fields even in the minimal seesaw Lagrangian. At renormalizable level these couplings are governed by the mixing angle between the active and sterile neutrinos. In $d = 5$ N_R-EFT one can write three more operators $\mathcal{O}_1^{(5)}$, $\mathcal{O}_2^{(5)}$, and $\mathcal{O}_3^{(5)}$, which can modify the existing couplings as well as introduce new couplings involving RHN fields. Here we present the explicit expansion correspond to the relevant part of the renormalizable Lagrangian as well as dimension five operators.

$$\begin{aligned} \bar{L}\gamma_\mu D_\mu L + \text{h.c.} &\subset \frac{g}{\sqrt{2}} \bar{\nu}_L \gamma^\mu W_\mu^+ \ell_L + \bar{\nu}_L \gamma^\mu \left(\frac{g}{2} W_\mu^3 - \frac{g'}{2} B_\mu \right) \nu_L + \text{H.c.} \\ &\subset \frac{g}{\sqrt{2}} \bar{\nu}_L \gamma^\mu W_\mu^+ \ell_L + \frac{g}{2c_w} \bar{\nu}_L \gamma^\mu W_\mu^+ \nu_L + \text{H.c.} \\ &\subset \frac{gU}{\sqrt{2}} [\bar{\nu}_m \gamma_\mu P_L + \bar{N}_m \gamma_\mu P_L] \ell_m + \frac{g}{2c_w} Z_\mu [U^\dagger U \bar{\nu}_m \gamma^\mu P_L \nu_m + U^\dagger \theta \bar{\nu}_m \gamma^\mu P_L N_m \\ &\quad + U\theta^\dagger \bar{N}_m \gamma^\mu P_L \nu_m + \theta^\dagger \theta \bar{N}_m \gamma^\mu P_L \nu_m] + \text{H.c.} \end{aligned} \tag{B1}$$

The lepton doublets are charged under the SM $SU(2)_L \times U(1)_Y$ gauge group. As a result the left-handed ν_L field couples to electroweak gauge bosons through the covariant derivative term as illustrated in Eq. (B1). Using the transformation rule as discussed in Appendix A one can rewrite the ν_L fields in terms of mass basis $\{\nu_m, N_m\}$. As a result one obtain different three point couplings between the RHN fields and SM electroweak gauge bosons. One can notice that the coupling involving RHN field is mixing angle suppressed as it does not directly couple to W/Z boson in the renormalizable Lagrangian.

$$Y_\nu \bar{L}\,\tilde{H}\,N_R = \frac{Y_\nu v}{\sqrt{2}}\bar{\nu}_\ell\left(1+\frac{h}{v}\right)N_R \subset \frac{Y_\nu}{\sqrt{2}}h\bar{\nu}_\ell N_R,$$
$$= \frac{Y_\nu}{\sqrt{2}}h[U^\dagger\theta^\dagger\bar{\nu}_m P_R\nu_m - U^\dagger\kappa^*\bar{\nu}_m P_R N_m + \theta^\dagger\theta^\dagger\bar{N}_m P_R\nu_m - \theta\kappa^*\bar{N}_m P_R N_m]. \quad \text{(B2)}$$

In the renormalizable part of the Lagrangian the neutrino fields can achieve mass through usual Yukawa term. This will invoke different couplings between both active, sterile neutrinos with Higgs boson. In Eq. (B2) we present the explicit structure of these couplings.

$$\mathcal{O}_1^{(5)} = \left(\frac{\alpha_1^{(5)}}{\Lambda}\right)(\bar{L}^c\tilde{H}^\dagger\tilde{H}L) = \left(\frac{\alpha_1^{(5)}}{\Lambda}\right)\bar{\nu_\ell}^c\frac{(v+h)^2}{2}\nu_\ell$$
$$\subset \left(\frac{\alpha_1^{(5)}v}{\Lambda}\right)h[U^T U\bar{\nu}_m P_L\nu_m + \theta^T U\bar{N}_m P_L\nu_m + U^T\theta\bar{\nu}_m P_L N_m + \theta^T\theta\bar{N}_m P_L N_m]. \quad \text{(B3)}$$

The Higgs-neutrino couplings receive further modification through the dimension five operators $\mathcal{O}_1^{(5)}$ and $\mathcal{O}_2^{(5)}$. In Eqs. (B3) and (B4) we present these corrections in detailed manner.

$$\mathcal{O}_2^{(5)} = \left(\frac{\alpha_2^{(5)}}{\Lambda}\right)(\overline{N_R}^c N_R)(H^\dagger H) = \left(\frac{\alpha_2^{(5)}}{\Lambda}\right)(\overline{N_R}^c N_R)\frac{(v+h)^2}{2}$$
$$\subset \left(\frac{\alpha_2^{(5)}v}{\Lambda}\right)h[\theta^*\theta^\dagger\bar{\nu}_m P_R\nu_m - \kappa^\dagger\theta^\dagger\bar{N}_m P_R\nu_m - \theta^*\kappa^*\bar{\nu}_m P_R N_m + \kappa^\dagger\kappa^*\bar{N}_m P_R N_m]. \quad \text{(B4)}$$

In the above, we only have presented the three point vertices involving RHN fields and the SM Higgs field. Apart from the operators involving Higgs field, one can write another operator $\mathcal{O}_3^{(5)}$ involving the $U(1)_Y$ field-strength tensor in $d=5$ N_R-EFT.

$$\mathcal{O}_3^{(5)} = \left(\frac{\alpha_3^{(5)}}{\Lambda}\right)(\overline{N_R}^c\sigma_{\mu\nu}N_R)B_{\mu\nu} = \left(\frac{\alpha_3^{(5)}}{\Lambda}\right)(\overline{N_R}^c\sigma_{\mu\nu}N_R)(\partial_\mu B_\nu - \partial_\nu B_\mu),$$
$$= \left(\frac{\alpha_3^{(5)}}{\Lambda}\right)(\overline{N_R}^c\sigma_{\mu\nu}N_R)(-\sin\theta_w\{\partial_\mu Z_\nu - \partial_\nu Z_\mu\} + \cos\theta_w\{\partial_\mu A_\nu - \partial_\nu A_\mu\}),$$
$$= c_w A_{\mu\nu}\left(\frac{\alpha_3^{(5)}}{\Lambda}\right)[\theta^*\theta^\dagger\bar{\nu}_m\sigma_{\mu\nu}P_R\nu_m - \kappa^\dagger\theta^\dagger\bar{N}_m\sigma_{\mu\nu}P_R\nu_m - \theta^*\kappa^*\bar{\nu}_m\sigma_{\mu\nu}P_R N_m + \kappa^\dagger\kappa^*\bar{N}_m\sigma_{\mu\nu}P_R N_m]$$
$$- s_w Z_{\mu\nu}\left(\frac{\alpha_3^{(5)}}{\Lambda}\right)[\theta^*\theta^\dagger\bar{\nu}_m\sigma_{\mu\nu}P_R\nu_m - \kappa^\dagger\theta^\dagger\bar{N}_m\sigma_{\mu\nu}P_R\nu_m - \theta^*\kappa^*\bar{\nu}_m\sigma_{\mu\nu}P_R N_m + \kappa^\dagger\kappa^*\bar{N}_m\sigma_{\mu\nu}P_R N_m]. \quad \text{(B5)}$$

Here we define $A_{\mu\nu} = \partial_\mu A_\nu - \partial_\nu A_\mu$ and $Z_{\mu\nu} = \partial_\mu Z_\nu - \partial_\nu Z_\mu$. In above equation, we present the explicit expansion of this operator. The B_μ field corresponding to the $U(1)_Y$ gauge group couples to the RHN field through this operator. One can redefine this B_μ field as a linear sum of the neutral gauge boson Z_μ and the photon field A_μ. As a consequence the RHN fields would couple to both the Z and γ. The coupling between the N fields and the photon is a direct consequence of the underlying N_R-EFT.

APPENDIX C: EVALUATING COUPLING USING DIMENSION SIX OPERATORS

In this section we present the explicit expansion of various operators, which leads to different couplings that involve RHN fields. The dimension six setup allows one to construct a different class of operators, which are ψ^2H^3, ψ^2H^2D, ψ^2H^2X, and four Fermi, respectively. The Higgs to neutrino couplings get substantial modification due to the operator $\mathcal{O}_{LNH}$ that comes under ψ^2H^3 class. The $\tilde{H}(H^\dagger H)$ part of the operator invokes sufficient change in the neutrino mass matrix once the Higgs field acquires vacuum expectation value (vev) and break the electroweak symmetry. As an outcome of the EWSB, this operator also introduces an Yukawa interaction between Higgs and neutral leptons. Transforming the gauge basis to a mass basis using the prescriptions mentioned in Appendix A, one can deduce the precise form of interaction terms. The parameter $\tilde{\theta}$ is the redefined active sterile mixing. In our presentation of different interaction terms involving Higgs field, we stick to three point vertices:

$$\mathcal{O}_{LNH} = \frac{\alpha_{LNH}}{\Lambda^2}(\bar{L}N_R)\tilde{H}(H^\dagger H) + \text{H.c.}$$
$$\subset \frac{3v^2\alpha_{LNH}}{2\sqrt{2}\Lambda^2}h[-U^\dagger\tilde{\theta}^\dagger\bar{\nu}_m P_R\nu_m - \tilde{\theta}^\dagger\tilde{\theta}^\dagger\bar{N}_m P_R\nu_m + U^\dagger\kappa^*\bar{\nu}_m P_R N_m + \tilde{\theta}^\dagger\kappa^*\bar{N}_m P_R N_m] + \text{H.c.} \quad \text{(C1)}$$

In Eq. (C1), we present the precise form of $\mathcal{C}^{(6)}_{h\bar{\nu}\nu}$, $\mathcal{C}^{(6)}_{h\bar{N}N}$, and $\mathcal{C}^{(6)}_{h(\bar{\nu}N+\bar{N}\nu)}$ couplings, respectively. Under the class of ψ^2H^2D there are two operators $\mathcal{O}_{HNe}$ and $\mathcal{O}_{HN}$. Here also

we focus only on the three point vertices involving gauge boson fields. The operator $\mathcal{O}_{HNe}$ invokes coupling between the W boson and the heavy neutrinos.

$$\begin{aligned}\mathcal{O}_{HNe} &= \frac{\alpha_{HNe}}{\Lambda^2}(\bar{N}_R\gamma^\mu e_R)(\tilde{H}^\dagger iD_\mu H) + \text{H.c.} \\ &\subset \frac{\sqrt{2}\alpha_{HNe}M_W^2}{g\Lambda^2}W_\mu^+[\bar{N}_R\gamma^\mu P_R e_R] + \text{H.c.} \\ &= \frac{\sqrt{2}\alpha_{HNe}M_W^2}{g\Lambda^2}W_\mu^+[-\tilde{\theta}\bar{\nu}_m\gamma^\mu P_R e_m \\ &\quad + \kappa^T\bar{N}_m\gamma^\mu P_R e_m] + \text{H.c.} \end{aligned} \tag{C2}$$

In addition to that, this operator also generates additional term to the charged gauge boson and SM leptons. The presence of a right-handed chiral matrix suggests a non-standard interaction, which indicates a distinct deviation from the SM $SU(2)_L$ gauge properties. Using explicit definition of the $H^\dagger \overleftrightarrow{D} H$, i.e., $H^\dagger D_\mu H - (D_\mu H)^\dagger H$ one can see that the RHN fields only couple the neutral gauge bosons via three point interactions.

$$\begin{aligned}\mathcal{O}_{HN} &= \frac{\alpha_{HN}}{\Lambda^2}(\bar{N}_R\gamma^\mu N_R)(iH^\dagger \overleftrightarrow{D}_\mu H) \\ &= -\left(\frac{M_Z v\alpha_{HN}}{\Lambda^2}\right)(\bar{N}_R\gamma^\mu N_R)Z_\mu[v+h]^2 \\ &\subset -\left(\frac{M_Z\alpha_{HN}v}{\Lambda^2}\right)Z_\mu[\tilde{\theta}\tilde{\theta}^\dagger\bar{\nu}_m\gamma^\mu P_R\nu_m - \kappa^T\tilde{\theta}^\dagger\bar{N}_m\gamma^\mu P_R\nu_m \\ &\quad - \tilde{\theta}\kappa^*\bar{\nu}_m\gamma^\mu P_R N_m + \kappa^T\kappa^*\bar{N}_m\gamma^\mu P_R N_m]. \end{aligned} \tag{C3}$$

In Eq. (C3), we present the explicit form of these couplings. One can notice that this operator modifies the coupling between the Z boson and active neutrino pair. This coupling substantially changes the total decay width of the Z boson, which is precisely measured. However, apart from the dimension six operator coefficient this coupling is also dependent on the square of the mixing angle. Hence the bounds coming from the EWPO can be evaded by suitably fixing the value of $\frac{\alpha_{HN}}{\Lambda^2}$ and $\tilde{\theta}$. Similar to dimension five one can write down two more operators that include stress-energy tensors. We begin with the operator that considers the $B_{\mu\nu}$ tensor associated with the Abelian $U(1)_Y$ group. In Eq. (C4), we present the explicit form of this operator:

$$\begin{aligned}\mathcal{O}_{NB} &= \frac{\alpha_{LNB}}{\Lambda^2}\bar{L}\sigma_{\mu\nu}N_R\tilde{H}B_{\mu\nu} + \text{H.c.} \\ &\subset \frac{\alpha_{LNB}v}{\sqrt{2}\Lambda^2}[c_w A_{\mu\nu} - s_w Z_{\mu\nu}](\bar{\nu}_L\sigma_{\mu\nu}N_R) + \text{H.c.} \\ &\subset \frac{\alpha_{LNB}v}{\sqrt{2}\Lambda^2}[c_w A_{\mu\nu} - s_w Z_{\mu\nu}] \\ &\quad \times [-U^\dagger\tilde{\theta}^\dagger\bar{\nu}_m\sigma_{\mu\nu}P_R\nu_m - \tilde{\theta}^\dagger\tilde{\theta}^\dagger\bar{N}_m\sigma_{\mu\nu}P_R\nu_m \\ &\quad + U^\dagger\kappa^*\bar{\nu}_m\sigma_{\mu\nu}P_R N_m + \tilde{\theta}^\dagger\kappa^*\bar{N}_m\sigma_{\mu\nu}P_R N_m]. \end{aligned} \tag{C4}$$

From the SM, one can rewrite the gauge field as the linear sum of photon and Z-boson fields. Using that one can express $B_{\mu\nu}$ as $[c_w A_{\mu\nu} - s_w Z_{\mu\nu}]$. Hence this operator generates different three point vertices between the leptons and the neutral gauge bosons both massless and massive. The dimension six also allows us to build an operator that involves a non-Abelian stress energy tensor. Depending on the generators the operator $\mathcal{O}_{NW}$ can be reexpressed as the sum of $\mathcal{O}_{NW}^\pm$ and $\mathcal{O}_{NW}^0$:

$$\mathcal{O}_{NW} = \mathcal{O}_{NW}^\pm + \mathcal{O}_{NW}^0 = \left(\frac{\alpha_{LNW}}{\Lambda^2}\right)(\bar{L}\sigma_{\mu\nu}N_R)\tau^I\tilde{H}W_{\mu\nu}^I + \text{H.c.}, \tag{C5}$$

$$\mathcal{O}_{NW}^\pm = \frac{v\alpha_{LNW}}{\sqrt{2}\Lambda^2}W_{\mu\nu}^\pm[-\tilde{\theta}^\dagger\bar{e}_m\sigma_{\mu\nu}P_R\nu_m + \kappa^*\bar{e}_m\sigma_{\mu\nu}P_R N_m] + \text{H.c.}, \tag{C6}$$

$$\begin{aligned}\mathcal{O}_{NW}^0 &= \frac{v\alpha_{LNW}}{\sqrt{2}\Lambda^2}[s_w A_{\mu\nu} + c_w Z_{\mu\nu}] \\ &\quad \times [-U^\dagger\tilde{\theta}^\dagger\bar{\nu}_m\sigma_{\mu\nu}P_R\nu_m - \tilde{\theta}^\dagger\tilde{\theta}^\dagger\bar{N}_m\sigma_{\mu\nu}P_R\nu_m \\ &\quad + U^\dagger\kappa^*\bar{\nu}_m\sigma_{\mu\nu}P_R N_m + \tilde{\theta}\kappa^*\bar{N}_m\sigma_{\mu\nu}P_R N_m]. \end{aligned} \tag{C7}$$

In Eqs. (C5) and (C7) we present the analytic form of these operators in the mass basis.

Now we turn our discussion to different four Fermi operators. The operator $\mathcal{O}_{QuNL}$ comes under the class of $(\bar{L}R)(\bar{R}L)$:

$$\begin{aligned}\mathcal{O}_{QuNL} &= \frac{\alpha_{LNQ}}{\Lambda^2}(\bar{Q}u_R)(\bar{N}_R L) + \text{H.c.} \\ &= \frac{\alpha_{LNQ}}{\Lambda^2}\begin{bmatrix}\bar{u}_L u_R & \bar{d}_L u_R\end{bmatrix}\begin{bmatrix}\bar{N}_R\nu_\ell \\ \bar{N}_R e_L\end{bmatrix} + \text{H.c.}, \\ &= \frac{\alpha_{LNQ}}{\Lambda^2}(\bar{u}_m P_R u_m)(-\tilde{\theta}U\bar{\nu}_m P_L\nu_m + \kappa^T U\bar{N}_m P_L\nu_m \\ &\quad - \tilde{\theta}\,\tilde{\theta}\,\bar{\nu}_m P_L N_m + \kappa^T\tilde{\theta}\bar{N}_m P_L N_m) \\ &\quad + \frac{\alpha_{LNQ}}{\Lambda^2}(\bar{d}_m P_R u_m)(-\tilde{\theta}\bar{\nu}_m P_L e_m + \kappa^T\bar{N}_m P_L e_m) \\ &\quad + \text{H.c.} \end{aligned} \tag{C8}$$

The operator $\mathcal{O}_{fN}$ that comes under the $(\bar{R}R)(\bar{R}R)$ class signifies a different scenario for different f. The label f stands for various right-handed gauge singlet SM quarks or charged leptons:

$$(\bar{R}R)(\bar{R}R) \subset \mathcal{O}_{fN} = \frac{\alpha_{fN}}{\Lambda^2}(\bar{f}_R\gamma^\mu f_R)(\bar{N}_R\gamma_\mu N_R),$$
$$= \frac{\alpha_{fN}}{\Lambda^2}(\bar{f}_m\gamma^\mu P_R f_m)\{\tilde{\theta}\tilde{\theta}^\dagger\bar{\nu}_m\gamma^\mu P_R\nu_m - \kappa^T\tilde{\theta}\bar{N}_m\gamma^\mu P_R\nu_m - \tilde{\theta}\kappa^*\bar{\nu}_m\gamma^\mu P_R N_m + \kappa^T\kappa^*\bar{N}_m\gamma^\mu P_R N_m\}. \quad \text{(C9)}$$

In addition to that, one can construct another operator $\mathcal{O}_{duNe}$, which comes under $(\bar{R}R)(\bar{R}R)$ and which takes the following explicit form:

$$\mathcal{O}_{duNe} = \frac{\alpha_{duNe}}{\Lambda^2}(\bar{d}_R\gamma^\mu u_R)(\bar{N}_R\gamma_\mu e_R) + \text{H.c.},$$
$$= \frac{\alpha_{duNe}}{\Lambda^2}(\bar{d}_m\gamma^\mu P_R u_m)[-\tilde{\theta}\bar{\nu}_m\gamma_\mu P_R e_m + \kappa^T\bar{N}_m\gamma^\mu P_R e_m] + \text{H.c.} \quad \text{(C10)}$$

The $\mathcal{O}_{FN}$ stands for two different operators that take the generic form $(\bar{L}L)(\bar{R}R)$. The F represents various SM-like quarks and lepton fields that transform as a doublet under the $SU(2)_L$ gauge group.

$$(\bar{L}L)(\bar{R}R) \subset \mathcal{O}_{FN} = \frac{\alpha_{FN}}{\Lambda^2}(\bar{f}_L^{(1)}\gamma^\mu f_L^{(1)} + \bar{f}_L^{(2)}\gamma^\mu f_L^{(2)})(\bar{N}_R\gamma_\mu N_R),$$
$$= \frac{\alpha_{FN}}{\Lambda^2}(\bar{f}_m^{(1)}\gamma^\mu P_L f_m^{(1)} + \bar{f}_m^{(2)}\gamma^\mu P_L f_m^{(2)})\{\tilde{\theta}\tilde{\theta}^\dagger\bar{\nu}_m\gamma^\mu P_R\nu_m - \kappa^T\tilde{\theta}\bar{N}_m\gamma^\mu P_R\nu_m - \tilde{\theta}\kappa^*\bar{\nu}_m\gamma^\mu P_R N_m + \kappa^T\kappa^*\bar{N}_m\gamma^\mu P_R N_m\}. \quad \text{(C11)}$$

The $f_L^{(1)}$ and $f_L^{(2)}$ denotes the up and down components of the left-handed doublet fermions. We conclude this section with the remaining three operators that comes under $(\bar{L}R)(\bar{L}R)$. The ϵ_{ij} in Eq. (C12)–(C14) is the 2×2 matrix, which is equal to $i\sigma_2$, where σ_2 is the second Pauli matrix. The operator $\mathcal{O}_{LNLe}$ is constructed only with the lepton fields, whereas the other two take both quarks and leptons into account.

$$\mathcal{O}_{LNLe} = \left(\frac{\alpha_{LNLe}}{\Lambda^2}\right)[\bar{L}_i N_R]\epsilon_{ij}[\bar{L}_j e_R] + \text{H.c.},$$
$$= \left(\frac{\alpha_{LNLe}}{\Lambda^2}\right)[\bar{\nu}_L N_R][\bar{e}_L e_R] - \left(\frac{\alpha_{LNLe}}{\Lambda^2}\right)[\bar{e}_L N_R][\bar{\nu}_L e_R] + \text{H.c.},$$
$$= \left(\frac{\alpha_{LNLe}}{\Lambda^2}\right)[-U^\dagger\tilde{\theta}^\dagger\bar{\nu}_m P_R\nu_m - \tilde{\theta}\,\tilde{\theta}\,\bar{N}_m P_R\nu_m + U^\dagger\kappa^*\bar{\nu}_m P_R N_m + \tilde{\theta}\kappa^*\bar{N}_m P_R N_m](\bar{e}_m P_R e_m)$$
$$- \left(\frac{\alpha_{LNLe}}{\Lambda^2}\right)[-\tilde{\theta}^\dagger\bar{e}_m P_R\nu_m + \kappa^*\bar{e}_m P_R N_m][U^\dagger\bar{\nu}_m P_R e_m + \tilde{\theta}\bar{N}_m P_R e_m] + \text{H.c.}, \quad \text{(C12)}$$

$$\mathcal{O}_{LNQd} = \left(\frac{\alpha_{LNQd}}{\Lambda^2}\right)[\bar{L}_i N_R]\epsilon_{ij}[\bar{Q}_j d_R] + \text{H.c.},$$
$$= \left(\frac{\alpha_{LNQd}}{\Lambda^2}\right)[\bar{\nu}_L N_R][\bar{d}_L d_R] - \left(\frac{\alpha_{LNQd}}{\Lambda^2}\right)[\bar{e}_L N_R][\bar{u}_L d_R] + \text{H.c.},$$
$$= \left(\frac{\alpha_{LNQd}}{\Lambda^2}\right)[-U^\dagger\tilde{\theta}\bar{\nu}_m P_R\nu_m - \tilde{\theta}^\dagger\tilde{\theta}^\dagger\bar{N}_m P_R\nu_m + U^\dagger\kappa^*\bar{\nu}_m P_R N_m + \tilde{\theta}\kappa^*\bar{N}_m P_R N_m](\bar{d}_m P_R d_m)$$
$$- \left(\frac{\alpha_{LNQd}}{\Lambda^2}\right)[\kappa^*\bar{e}_m P_R e_m - \tilde{\theta}\bar{e}_m P_R e_m](\bar{u}_m P_R d_m), \quad \text{(C13)}$$

$$\mathcal{O}_{LdQN} = \left(\frac{\alpha_{LdQN}}{\Lambda^2}\right)[\bar{L}_i d_R]\epsilon_{ij}[\bar{Q}_j N_R] + \text{H.c.},$$
$$= \left(\frac{\alpha_{LdQN}}{\Lambda^2}\right)[\bar{\nu}_L d_R][\bar{d}_L N_R] - \left(\frac{\alpha_{LdQN}}{\Lambda^2}\right)[\bar{e}_L d_R][\bar{u}_L N_R] + \text{H.c.},$$
$$= \left(\frac{\alpha_{LdQN}}{\Lambda^2}\right)[U^\dagger\bar{\nu}_m P_R d_m + \tilde{\theta}^\dagger\bar{N}_m P_R d_m][-\tilde{\theta}\bar{d}_m P_R\nu_m + \kappa^*\bar{d}_m P_R N_m]$$
$$- \left(\frac{\alpha_{LdQN}}{\Lambda^2}\right)[\bar{e}_m P_R d_m][-\tilde{\theta}^\dagger\bar{u}_m P_R\nu_m + \kappa^*\bar{u}_m P_R N_m]. \quad \text{(C14)}$$

APPENDIX D: INTEGRATION FORMULA

Following are the phase space integrals that are required to evaluate the three body decay modes of the RHN field. The λ here stands for the usual Kellen function of the form $\lambda(x,y,z) = x^2 + y^2 + z^2 - 2xy - 2yz - 2xz$:

$$\mathcal{I}_1(x_a,x_b,x_c) = \int_{(x_a+x_b)^2}^{(1-x_c)^2} \frac{dz}{z}(z - x_a^2 - x_b^2)(1 + x_c^2 - z)\lambda^{\frac{1}{2}}(1,z,x_c^2)\lambda^{\frac{1}{2}}(1,x_a^2,x_b^2),$$

$$\mathcal{I}_2(x_a,x_b,x_c) = -\int_{(x_a+x_b)^2}^{(1-x_c)^2} \frac{dz}{z} x_c(z - x_a^2 - x_b^2)\lambda^{\frac{1}{2}}(1,z,x_c^2)\lambda^{\frac{1}{2}}(1,x_a^2,x_b^2),$$

$$\mathcal{I}_3(x_a,x_b,x_c) = \int_{(x_a+x_b)^2}^{(1-x_c)^2} \frac{dz}{z^2}\left\{x_b x_c(z + x_a^2 - x_b^2)(1 - x_c^2 + z) - \frac{3}{2}x_a x_a(z - x_a^2 + x_b^2)(1 - x_c^2 - z)\right\} \times \lambda^{\frac{1}{2}}(1,z,x_c^2)\lambda^{\frac{1}{2}}(1,x_a^2,x_b^2),$$

$$\mathcal{I}_4(x_a,x_b,x_c) = \int_{(x_a+x_b)^2}^{(1-x_c)^2} \frac{dz}{z^2}\left\{\frac{3}{2}x_c x_a(z + x_b^2 - x_a^2)(1 - x_c^2 + z) - 2x_b(z + x_a^2 - x_b^2)(1 - x_c^2 - z)\right\} \times \lambda^{\frac{1}{2}}(1,z,x_c^2)\lambda^{\frac{1}{2}}(1,x_a^2,x_b^2),$$

$$\mathcal{I}_5(x_a,x_b,x_c) = -\int_{(x_a+x_b)^2}^{(1-x_c)^2} \frac{dz}{z} x_c x_a x_b \lambda^{\frac{1}{2}}(1,z,x_c^2)\lambda^{\frac{1}{2}}(1,x_a^2,x_b^2),$$

$$\mathcal{H}_1(x_a,x_b) = \int_{(1-x_a)^2}^{4x_b^2} \frac{dz}{z} x_b^2(1 + x_a^2 - z)\lambda^{\frac{1}{2}}(1,x_a^2,z)\lambda^{\frac{1}{2}}(z,x_b^2,x_b^2),$$

$$\mathcal{H}_2(x_a,x_b) = \int_{(1-x_a)^2}^{4x_b^2} \frac{dz}{z} x_b(1 - x_a^2 - z)\lambda^{\frac{1}{2}}(1,x_a^2,z)\lambda^{\frac{1}{2}}(z,x_b^2,x_b^2),$$

$$\mathcal{H}_3(x_a,x_b) = -\int_{(1-x_a)^2}^{4x_b^2} \frac{dz}{z} x_a x_b(1 - x_a^2 + z)\lambda^{\frac{1}{2}}(1,x_a^2,z)\lambda^{\frac{1}{2}}(z,x_b^2,x_b^2),$$

$$\mathcal{G}_1(x_a,x_b,x_c) = \int_{(x_a+x_b)^2}^{(1-x_c)^2} \frac{dz}{z^2} x_a(1 - x_c^2 - z)(z - x_a^2 + x_b^2)\lambda^{\frac{1}{2}}(1,x_c^2,z)\lambda^{\frac{1}{2}}(z,x_a^2,x_b^2),$$

$$\mathcal{G}_2(x_a,x_b,x_c) = -\int_{(x_a+x_b)^2}^{(1-x_c)^2} \frac{dz}{z^2} x_c x_a(1 - x_c^2 + z)(z - x_a^2 + x_b^2)\lambda^{\frac{1}{2}}(1,x_c^2,z)\lambda^{\frac{1}{2}}(z,x_a^2,x_b^2),$$

$$\mathcal{G}_3(x_a,x_b,x_c) = -\int_{(x_a+x_b)^2}^{(1-x_c)^2} \frac{dz}{z} x_a x_b(1 + x_c^2 - z)\lambda^{\frac{1}{2}}(1,x_c^2,z)\lambda^{\frac{1}{2}}(z,x_a^2,x_b^2).$$

APPENDIX E: COLLIDER SIGNATURES FOR RHN FIELDS

In this appendix we will present different possible signatures involving RHN field for pp, e^+e^-, and e^-p colliders. In Sec. VI, we discussed few of the multilepton final states where the RHN fields produce either via single or via pair production mechanism and then subsequently decay to three body pure leptonic channels. In addition to those channels one can also look for the RHN fields in other final states. In Table X, we present different production mode for the RHN fields for pp colliders. The first row and first column of the Table X illustrate the flavor label of the final state leptons and quarks.

Similarly in Table XI we tabulate different single production of N fields at e^+e^- colliders. The commonalities between Tables X and XI is that we only highlight the single N field production. The majority of the channels that are presented in these two tables can serve as the pair production mode for the RHN fields. For example, in the case of pp collider apart from VBF $\to Wqq' \to \ell_\delta N_i qq'$ and Drell-Yan $qq' \to W \to \ell_\delta N_i$ process, all the other modes can potentially produce pair of RHN fields. On other hand in case of e^+e^- collider apart from the t-channel W-boson mediated process all the other process can generate pair of N fields. Using Table XII, one can evaluate the final state signature for these modes. In Table XII we only illustrate the final states that can arise due to the

TABLE X. Different collider signatures for the single RHN production at pp collider. Apart from the VBF $\to Wqq' \to \ell_\delta N_i qq'$ and Drell-Yan $qq' \to W \to \ell_\delta N_i$ process all the other channels can be used for the pair production of the RHN fields. For details regarding the final states correspond to N-pair production, see the text.

	Decay					
Production	$N_i \to \ell_j \ell_k \nu_k$	$N_i \to \ell_k \ell_k \nu_k$	$N_i \to \nu_j \ell_k \ell_k$	$N_i \to \ell_j u_\alpha d_\beta$	$N_i \to \nu_j q_\alpha q_\alpha$	$N_i \to \nu_j \nu_k \nu_k$
$gg \to h \to \nu_\delta N_i$	$2\ell + \not{E}_T$	$2\ell + \not{E}_T$	$2\ell + \not{E}_T$	$\ell + 2q + \not{E}_T$	$2q + \not{E}_T$	$\not{E}_T$
$qq' \to W \to \ell_\delta N_i$	$3\ell + \not{E}_T$	$3\ell + \not{E}_T$	$3\ell + \not{E}_T$	$2\ell + 2q$	$\ell + 2q + \not{E}_T$	$\ell + \not{E}_T$
$q\bar{q} \to Z \to \nu_\delta N_i$	$2\ell + \not{E}_T$	$2\ell + \not{E}_T$	$2\ell + \not{E}_T$	$\ell + 2q + \not{E}_T$	$2q + \not{E}_T$	$\not{E}_T$
$pp \to Zh \to \ell_\rho \ell_\rho \nu_\delta N_i$	$4\ell + \not{E}_T$	$4\ell + \not{E}_T$	$4\ell + \not{E}_T$	$3\ell + 2q + \not{E}_T$	$2\ell + 2q + \not{E}_T$	$2\ell + \not{E}_T$
$pp \to Zh \to \nu_\delta N_i 2b$	$2\ell + 2b + \not{E}_T$	$2\ell + 2b + \not{E}_T$	$2\ell + 2b + \not{E}_T$	$\ell + 2b + 2q + \not{E}_T$	$2b + 2q + \not{E}_T$	$2b + \not{E}_T$
$pp \to \nu_\delta N_i$ via four Fermi	$2\ell + \not{E}_T$	$2\ell + \not{E}_T$	$2\ell + \not{E}_T$	$\ell + 2q + \not{E}_T$	$2q + \not{E}_T$	$\ell + \not{E}_T$
VBF $\to Wqq' \to \ell_\delta N_i qq'$	$3\ell + 2q + \not{E}_T$	$3\ell + 2q + \not{E}_T$	$3\ell + 2q + \not{E}_T$	$2\ell + 4q$	$\ell + 4q + \not{E}_T$	$\ell + 2q + \not{E}_T$
VBF $\to Zqq' \to \nu_\delta N_i qq'$	$2\ell + 2q + \not{E}_T$	$2\ell + 2q + \not{E}_T$	$2\ell + 2q + \not{E}_T$	$\ell + 4q + \not{E}_T$	$4q + \not{E}_T$	$2q + \not{E}_T$
VBF $\to hqq' \to \nu_\delta N_i qq'$	$2\ell + 2q + \not{E}_T$	$2\ell + 2q + \not{E}_T$	$2\ell + 2q + \not{E}_T$	$\ell + 4q + \not{E}_T$	$4q + \not{E}_T$	$2q + \not{E}_T$

TABLE XI. Different collider signatures for the single RHN production at e^+e^- collider. Apart from the t-channel W-boson mediated process all the other modes can serve as the pair production mode for RHN fields. For details regarding the final states correspond to N-pair production see the text.

	Decay					
Production	$N_i \to \ell_j \ell_k \nu_k$	$N_i \to \ell_k \ell_k \nu_k$	$N_i \to \nu_j \ell_k \ell_k$	$N_i \to \ell_j u_\alpha d_\beta$	$N_i \to \nu_j q_\alpha q_\alpha$	$N_i \to \nu_j \nu_k \nu_k$
$e^+e^- \to \nu_\delta N_i$ via Four Fermi	$2\ell + \not{E}_T$	$2\ell + \not{E}_T$	$2\ell + \not{E}_T$	$\ell + 2q + \not{E}_T$	$2q + \not{E}_T$	$\ell + \not{E}_T$
$e^+e^- \to Zh \to \ell_\rho \ell_\rho \nu_\delta N_i$	$4\ell + \not{E}_T$	$4\ell + \not{E}_T$	$4\ell + \not{E}_T$	$3\ell + 2q + \not{E}_T$	$+2\ell + 2q + \not{E}_T$	$2\ell + \not{E}_T$
$e^+e^- \to Zh \to \nu_\delta N_i 2b$	$2\ell + 2b + \not{E}_T$	$2\ell + 2b + \not{E}_T$	$2\ell + 2b + \not{E}_T$	$\ell + 2b + 2q + \not{E}_T$	$2b + 2q + \not{E}_T$	$2b + \not{E}_T$
$e^+e^- \to Z \to \nu_\delta N_i$	$2\ell + \not{E}_T$	$2\ell + \not{E}_T$	$2\ell + \not{E}_T$	$\ell + 2q + \not{E}_T$	$2q + \not{E}_T$	$\not{E}_T$
VBF $\to Z\nu_\rho \nu_\delta \to N_i \nu_\sigma \nu_\rho \nu_\delta$	$2\ell + \not{E}_T$	$2\ell + \not{E}_T$	$2\ell + \not{E}_T$	$\ell + 2q + \not{E}_T$	$2q + \not{E}_T$	$\not{E}_T$
VBF $\to W\ell_\delta \nu_\rho \to \ell_\delta \nu_\rho N_i \ell_\sigma$	$4\ell + \not{E}_T$	$4\ell + \not{E}_T$	$4\ell + \not{E}_T$	$3\ell + 2q + \not{E}_T$	$2\ell + 2q + \not{E}_T$	$2\ell + \not{E}_T$
$e^+e^- \to W \to \ell_\delta N_i$ t channel	$3\ell + \not{E}_T$	$3\ell + \not{E}_T$	$3\ell + \not{E}_T$	$2\ell + 2q + \not{E}_T$	$\ell + 2q + \not{E}_T$	$\ell + \not{E}_T$

TABLE XII. Different possible final states that can arise due to the subsequent three body decays of RHN pair. The X in the first row signifies the SM fields that can generate due to the underlying production mechanism in association with the RHN pair. For explicit evaluation one should replace X with appropriate field content.

Possible production mode	$pp \to N_i N_j X$ and $e^+e^- \to N_i N_j X$					
	N_i decay					
N_j decay	$N_i \to \ell_j \ell_k \nu_k$	$N_i \to \ell_k \ell_k \nu_k$	$N_i \to \nu_j \ell_k \ell_k$	$N_i \to \ell_j u_\alpha d_\beta$	$N_i \to \nu_j q_\alpha q_\alpha$	$N_i \to \nu_j \nu_k \nu_k$
$N_j \to \ell_a \ell_b \nu_b$	$4\ell + \not{E}_T$	$4\ell + \not{E}_T$	$4\ell + \not{E}_T$	$3\ell + 2q + \not{E}_T$	$2\ell + 2q + \not{E}_T$	$2\ell + \not{E}_T$
$N_j \to \ell_b \ell_b \nu_b$	$4\ell + \not{E}_T$	$4\ell + \not{E}_T$	$4\ell + \not{E}_T$	$3\ell + 2q + \not{E}_T$	$2\ell + 2q + \not{E}_T$	$2\ell + \not{E}_T$
$N_j \to \ell_a \ell_a \nu_b$	$4\ell + \not{E}_T$	$4\ell + \not{E}_T$	$4\ell + \not{E}_T$	$3\ell + 2q + \not{E}_T$	$2\ell + 2q + \not{E}_T$	$2\ell + \not{E}_T$
$N_j \to \ell_a u_\rho d_\delta$	$3\ell + 2q + \not{E}_T$	$3\ell + 2q + \not{E}_T$	$3\ell + 2q + \not{E}_T$	$2\ell + 4q + \not{E}_T$	$\ell + 4q + \not{E}_T$	$\ell + 2q + \not{E}_T$
$N_j \to \nu_a q_\rho q_\rho$	$2\ell + 2q + \not{E}_T$	$2\ell + 2q + \not{E}_T$	$2\ell + 2q + \not{E}_T$	$\ell + 4q + \not{E}_T$	$4q + \not{E}_T$	$2q + \not{E}_T$
$N_j \to \nu_a \nu_b \nu_b$	$2\ell + \not{E}_T$	$2\ell + \not{E}_T$	$2\ell + \not{E}_T$	$\ell + 2q + \not{E}_T$	$2q + \not{E}_T$	$\not{E}_T$

TABLE XIII. Different collider signatures for the single RHN production at $e^- p$ collider.

	Decay					
Production	$N_i \to \ell_j \ell_k \nu_k$	$N_i \to \ell_k \ell_k \nu_k$	$N_i \to \nu_j \ell_k \ell_k$	$N_i \to \ell_j u_\alpha d_\beta$	$N_i \to \nu_j q_\alpha q_\alpha$	$N_i \to \nu_j \nu_k \nu_k$
$ep \to W \to q_\delta N_i$ via t channel	$2\ell + q + \not{E}_T$	$2\ell + q + \not{E}_T$	$2\ell + q + \not{E}_T$	$\ell + 3q$	$3q + \not{E}_T$	$q + \not{E}_T$
$ep \to q_\delta N_i$ via four Fermi	$2\ell + q + \not{E}_T$	$2\ell + q + \not{E}_T$	$2\ell + q + \not{E}_T$	$\ell + 3q$	$3q + \not{E}_T$	$q + \not{E}_T$
VBF $\to h\nu_\rho q_\delta \to \nu_\sigma N_i \nu_\rho q_\delta$	$2\ell + q + \not{E}_T$	$2\ell + q + \not{E}_T$	$2\ell + q + \not{E}_T$	$\ell + 3q + \not{E}_T$	$3q + \not{E}_T$	$q + \not{E}_T$
$ep \to tbN_i \to N_i + 2b + q_\delta + q_\sigma$	$2\ell + 2b + 2q + \not{E}_T$	$2\ell + 2b + 2q + \not{E}_T$	$2\ell + 2b + 2q + \not{E}_T$	$2\ell + 2b + 4q + \not{E}_T$	$\ell + 2b + 2q + \not{E}_T$	$\ell + 2b + \not{E}_T$
$ep \to tbN_i \to N_i + 2b + \ell_\delta \nu_\rho$	$3\ell + 2b + \not{E}_T$	$3\ell + 2b + \not{E}_T$	$3\ell + 2b + \not{E}_T$	$2\ell + 2q + 2b + \not{E}_T$	$\ell + 2q + 2b + \not{E}_T$	$\ell + 2b + \not{E}_T$

subsequent decay of both N_i and N_j. Moreover, at the production level other SM particles can arise in association with the RHN fields. Hence one need to put suitable particles in place of X as mentioned in the first row of Table XII.

We like to elaborate this point with two suitable examples. For the process $gg \to h \to N_i N_j$ the possible final states are the states that are mentioned in this table and one does not need to put any SM fields in place of X. On the other hand, in the case of $pp \to Zh \to \ell_\rho \ell_\rho N_i N_j$, the X would be replaced with $\ell_\rho \ell_\rho$ and to obtain the final states corresponding to this process one needs to add 2ℓ in each cell of Table XII. In Table XIII, we present different RHN production modes relevant for the $e^- p$ collider. Here we will restrict ourselves to single production of the N fields. In principle one can generate more than one RHN fields in this collider. However, the processes related to these would involve more than one EFT vertices. Hence the cross section would receive a higher order cutoff scale suppression [see Fig. 8(a) for details].

[1] G. Aad *et al.* (ATLAS Collaboration), Observation of a new particle in the search for the Standard Model Higgs boson with the ATLAS detector at the LHC, Phys. Lett. B **716**, 1 (2012).

[2] S. Chatrchyan *et al.* (CMS Collaboration), Observation of a new boson at a mass of 125 GeV with the CMS experiment at the LHC, Phys. Lett. B **716**, 30 (2012).

[3] W. Buchmuller and D. Wyler, Effective Lagrangian analysis of new interactions and flavor conservation, Nucl. Phys. **B268**, 621 (1986).

[4] C. G. Callan, Jr., S. R. Coleman, J. Wess, and B. Zumino, Structure of phenomenological Lagrangians. 2., Phys. Rev. **177**, 2247 (1969).

[5] S. Weinberg, Phenomenological Lagrangians, Physica (Amsterdam) **96A**, 327 (1979).

[6] I. Brivio and M. Trott, The standard model as an effective field theory, Phys. Rep. **793**, 1 (2019).

[7] A. Dobado, A. Gomez-Nicola, A. L. Maroto, and J. R. Pelaez, Effective lagrangians for the standard model. 1997.

[8] J. Preskill, Gauge anomalies in an effective field theory, Ann. Phys. (N.Y.) **210**, 323 (1991).

[9] T. Appelquist and J. Carazzone, Infrared singularities and massive fields, Phys. Rev. D **11**, 2856 (1975).

[10] S. Weinberg, Effective gauge theories, Phys. Lett. **91B**, 51 (1980).

[11] Y. Fukuda *et al.* (Super-Kamiokande Collaboration), Evidence for Oscillation of Atmospheric Neutrinos, Phys. Rev. Lett. **81**, 1562 (1998).

[12] S. Fukuda *et al.* (Super-Kamiokande Collaboration), Constraints on Neutrino Oscillations using 1258 Days of Super-Kamiokande Solar Neutrino Data, Phys. Rev. Lett. **86**, 5656 (2001).

[13] T. Toshito (Super-Kamiokande Collaboration), Super-Kamiokande atmospheric neutrino results, in *36th Rencontres de Moriond on Electroweak Interactions and Unified Theories* (2001), 5, arXiv:hep-ex/0105023.

[14] Q. R. Ahmad *et al.* (SNO Collaboration), Direct Evidence for Neutrino Flavor Transformation from Neutral Current Interactions in the Sudbury Neutrino Observatory, Phys. Rev. Lett. **89**, 011301 (2002).

[15] P. F. de Salas, D. V. Forero, S. Gariazzo, P. Martínez-Miravé, O. Mena, C. A. Ternes, M. Tórtola, and J. W. F. Valle, 2020 global reassessment of the neutrino oscillation picture, J. High Energy Phys. 02 (2021) 071.

[16] M. Gell-Mann, P. Ramond, and R. Slansky, Complex spinors and unified theories, Conf. Proc. C **790927**, 315 (1979),

[17] P. Minkowski, $\mu \to e\gamma$ at a rate of one out of 10^9 muon decays?, Phys. Lett. **67B**, 421 (1977).

[18] R. N. Mohapatra and G. Senjanovic, Neutrino Mass and Spontaneous Parity Nonconservation, Phys. Rev. Lett. **44**, 912 (1980).

[19] T. Yanagida, Horizontal gauge symmetry and masses of neutrinos, Conf. Proc. C **7902131**, 95 (1979).

[20] A. Pilaftsis, Radiatively induced neutrino masses and large Higgs neutrino couplings in the standard model with Majorana fields, Z. Phys. C **55**, 275 (1992).

[21] F. Borzumati and Y. Nomura, Low scale seesaw mechanisms for light neutrinos, Phys. Rev. D **64**, 053005 (2001).

[22] J. Kersten and A. Y. Smirnov, Right-handed neutrinos at CERN LHC and the mechanism of neutrino mass generation, Phys. Rev. D **76**, 073005 (2007).

[23] F. del Aguila, S. Bar-Shalom, A. Soni, and J. Wudka, Heavy Majorana neutrinos in the effective Lagrangian description: Application to hadron colliders, Phys. Lett. B **670**, 399 (2009).

[24] A. Aparici, K. Kim, A. Santamaria, and J. Wudka, Right-handed neutrino magnetic moments, Phys. Rev. D **80**, 013010 (2009).

[25] S. Bhattacharya and J. Wudka, Dimension-seven operators in the standard model with right handed neutrinos, Phys. Rev. D **94**, 055022 (2016); Erratum, Phys. Rev. D **95**, 039904 (2017).

[26] Y. Liao and X.-D. Ma, Operators up to dimension seven in standard model effective field theory extended with sterile neutrinos, Phys. Rev. D **96**, 015012 (2017).

[27] H.-L. Li, Z. Ren, M.-L. Xiao, J.-H. Yu, and Y.-H. Zheng, Operator bases in effective field theories with sterile neutrinos: d ≤ 9, J. High Energy Phys. 11 (2021) 003.

[28] D. Barducci, E. Bertuzzo, A. Caputo, P. Hernandez, and B. Mele, The see-saw portal at future Higgs Factories, J. High Energy Phys. 03 (2021) 117.

[29] A. Caputo, P. Hernandez, J. Lopez-Pavon, and J. Salvado, The seesaw portal in testable models of neutrino masses, J. High Energy Phys. 06 (2017) 112.

[30] F. Delgado, L. Duarte, J. Jones-Perez, C. Manrique-Chavil, and S. Peña, Assessment of the dimension-5 seesaw portal and impact of exotic Higgs decays on non-pointing photon searches, J. High Energy Phys. 09 (2022) 079.

[31] J. Jones-Pérez, J. Masias, and J. D. Ruiz-Álvarez, Search for long-lived heavy neutrinos at the LHC with a VBF trigger, Eur. Phys. J. C **80**, 642 (2020).

[32] J. Alcaide, S. Banerjee, M. Chala, and A. Titov, Probes of the standard model effective field theory extended with a right-handed neutrino, J. High Energy Phys. 08 (2019) 031.

[33] J. De Vries, H. K. Dreiner, J. Y. Günther, Z. S. Wang, and G. Zhou, Long-lived sterile neutrinos at the LHC in effective field theory, J. High Energy Phys. 03 (2021) 148.

[34] R. Beltrán, G. Cottin, J. C. Helo, M. Hirsch, A. Titov, and Z. S. Wang, Long-lived heavy neutral leptons from mesons in effective field theory, arXiv:2210.02461.

[35] L. Duarte, I. Romero, J. Peressutti, and O. A. Sampayo, Effective Majorana neutrino decay, Eur. Phys. J. C **76**, 453 (2016).

[36] M. Drewes and J. Hajer, Heavy Neutrinos in displaced vertex searches at the LHC and HL-LHC, J. High Energy Phys. 02 (2020) 070.

[37] G. Cottin, Searches for long-lived particles and heavy neutral leptons: Theory perspective, Proc. Sci., LHCP2021 (**2021**) 003.

[38] J. Liu, Z. Liu, L.-T. Wang, and X.-P. Wang, Seeking for sterile neutrinos with displaced leptons at the LHC, J. High Energy Phys. 07 (2019) 159.

[39] A. Abada, N. Bernal, M. Losada, and X. Marcano, Inclusive displaced vertex searches for heavy neutral leptons at the LHC, J. High Energy Phys. 01 (2019) 093.

[40] D. Barducci and E. Bertuzzo, The see-saw portal at future Higgs factories: The role of dimension six operators, J. High Energy Phys. 06 (2022) 077.

[41] G. Cottin, J. C. Helo, M. Hirsch, A. Titov, and Z. S. Wang, Heavy neutral leptons in effective field theory and the high-luminosity LHC, J. High Energy Phys. 09 (2021) 039.

[42] R. Beltrán, G. Cottin, J. C. Helo, M. Hirsch, A. Titov, and Z. S. Wang, Long-lived heavy neutral leptons at the LHC: four-fermion single-N_R operators, J. High Energy Phys. 01 (2022) 044.

[43] J. M. Butterworth, M. Chala, C. Englert, M. Spannowsky, and A. Titov, Higgs phenomenology as a probe of sterile neutrinos, Phys. Rev. D **100**, 115019 (2019).

[44] L. Duarte, G. Zapata, and O. A. Sampayo, Angular and polarization trails from effective interactions of Majorana neutrinos at the LHeC, Eur. Phys. J. C **78**, 352 (2018).

[45] G. Zapata, T. Urruzola, O. A. Sampayo, and L. Duarte, Lepton collider probes for Majorana neutrino effective interactions, Eur. Phys. J. C **82**, 544 (2022).

[46] S. Weinberg, Baryon and Lepton Nonconserving Processes, Phys. Rev. Lett. **43**, 1566 (1979).

[47] E. Ma, Pathways to Naturally Small Neutrino Masses, Phys. Rev. Lett. **81**, 1171 (1998).

[48] P.-H. Gu and H.-J. He, Neutrino mass and baryon asymmetry from Dirac seesaw, J. Cosmol. Astropart. Phys. 12 (2006) 010.

[49] S. Centelles Chuliá, R. Srivastava, and J. W. F. Valle, See-saw roadmap to neutrino mass and dark matter, Phys. Lett. B **781**, 122 (2018).

[50] F. Bonnet, M. Hirsch, T. Ota, and W. Winter, Systematic study of the d = 5 Weinberg operator at one-loop order, J. High Energy Phys. 07 (2012) 153.

[51] B. Fuks, J. Neundorf, K. Peters, R. Ruiz, and M. Saimpert, Probing the Weinberg operator at colliders, Phys. Rev. D **103**, 115014 (2021).

[52] C. Arzt, M. B. Einhorn, and J. Wudka, Patterns of deviation from the standard model, Nucl. Phys. **B433**, 41 (1995).

[53] A. Aparici, K. Kim, A. Santamaria, and J. Wudka, Right-handed neutrino magnetic moments, Phys. Rev. D **80**, 013010 (2009).

[54] J. Hashida, T. Morozumi, and A. Purwanto, Neutrino mixing in seesaw model, Prog. Theor. Phys. **103**, 379 (2000); Erratum, Prog. Theor. Phys. **103**, 865 (2000).

[55] O. G. Miranda, D. K. Papoulias, M. Tórtola, and J. W. F. Valle, XENON1T signal from transition neutrino magnetic moments, Phys. Lett. B **808**, 135685 (2020).

[56] S.-S. Xue, *W* boson mass tension caused by its right-handed gauge coupling at high energies?, Nucl. Phys. **B985**, 115992 (2022).

[57] T. Aaltonen *et al.* (CDF Collaboration), High-precision measurement of the W boson mass with the CDF II detector, Science **376**, 170 (2022).

[58] M. Tanabashi *et al.* (Particle Data Group Collaboration), Review of particle physics, Phys. Rev. D **98**, 030001 (2018).

[59] M. Z. Akrawy *et al.* (OPAL Collaboration), Limits on neutral heavy lepton production from Z0 decay, Phys. Lett. B **247**, 448 (1990).

[60] M. Acciarri *et al.* (L3 Collaboration), Search for new physics in energetic single photon production in e^+e^- annihilation at the Z resonance, Phys. Lett. B **412**, 201 (1997).

[61] ATLAS Collaboration, Search for invisible Higgs boson decays with vector boson fusion signatures with the ATLAS detector using an integrated luminosity of 139 fb^{-1}, J. High Energy Phys. 08 (2022) 104.

[62] A. M. Sirunyan *et al.* (CMS Collaboration), Search for heavy Majorana neutrinos in same-sign dilepton channels in proton-proton collisions at $\sqrt{s} = 13$ TeV, J. High Energy Phys. 01 (2019) 122.

[63] ATLAS Collaboration, Search for heavy neutral leptons in decays of W bosons using a dilepton displaced vertex in $\sqrt{s} = 13$ TeV pp collisions with the ATLAS detector, arXiv:2204.11988.

[64] A. M. Sirunyan *et al.* (CMS Collaboration), Search for supersymmetry in events with a photon, a lepton, and missing transverse momentum in proton-proton collisions at $\sqrt{s} = 13$ TeV, J. High Energy Phys. 01 (2019) 154.

[65] A. Biekötter, M. Chala, and M. Spannowsky, The effective field theory of low scale see-saw at colliders, Eur. Phys. J. C **80**, 743 (2020).

[66] A. M. Sirunyan *et al.* (CMS Collaboration), Search for supersymmetry in final states with photons and missing transverse momentum in proton-proton collisions at 13 TeV, J. High Energy Phys. 06 (2019) 143.

[67] A. M. Sirunyan *et al.* (CMS Collaboration), Search for new physics in final states with a single photon and missing transverse momentum in proton-proton collisions at $\sqrt{s} = 13$ TeV, J. High Energy Phys. 02 (2019) 074.

[68] A. Alloul, N. D. Christensen, C. Degrande, C. Duhr, and B. Fuks, FeynRules 2.0-A complete toolbox for tree-level phenomenology, Comput. Phys. Commun. **185**, 2250 (2014).

[69] J. Alwall, R. Frederix, S. Frixione, V. Hirschi, F. Maltoni, O. Mattelaer, H. S. Shao, T. Stelzer, P. Torrielli, and M. Zaro, The automated computation of tree-level and next-to-leading order differential cross sections, and their matching to parton shower simulations, J. High Energy Phys. 07 (2014) 079.

[70] C. Henderson (CMS Collaboration), Future physics prospects with the CMS detector at the high-luminosity LHC, SciPost Phys. Proc. **8**, 111 (2022).

[71] J. Nielsen (ATLAS Collaboration), Physics prospects for ATLAS at the HL-LHC, J. Phys. Conf. Ser. **1690**, 012156 (2020).

[72] G. Gustavino, Beyond-the-standard-model searches at HL-LHC, Proc. Sci., LHCP2019 (**2019**) 244.

[73] F. del Aguila, J. de Blas, and M. Perez-Victoria, Effects of new leptons in electroweak precision data, Phys. Rev. D **78**, 013010 (2008).

[74] R. G. Suarez, The Future Circular Collider (FCC) at CERN, Proc. Sci., DISCRETE2020-2021 (**2022**) 009,

[75] I. Brivio *et al.*, Truncation, validity, uncertainties, arXiv: 2201.04974.